Air Permeable Heat Exchanging Concrete

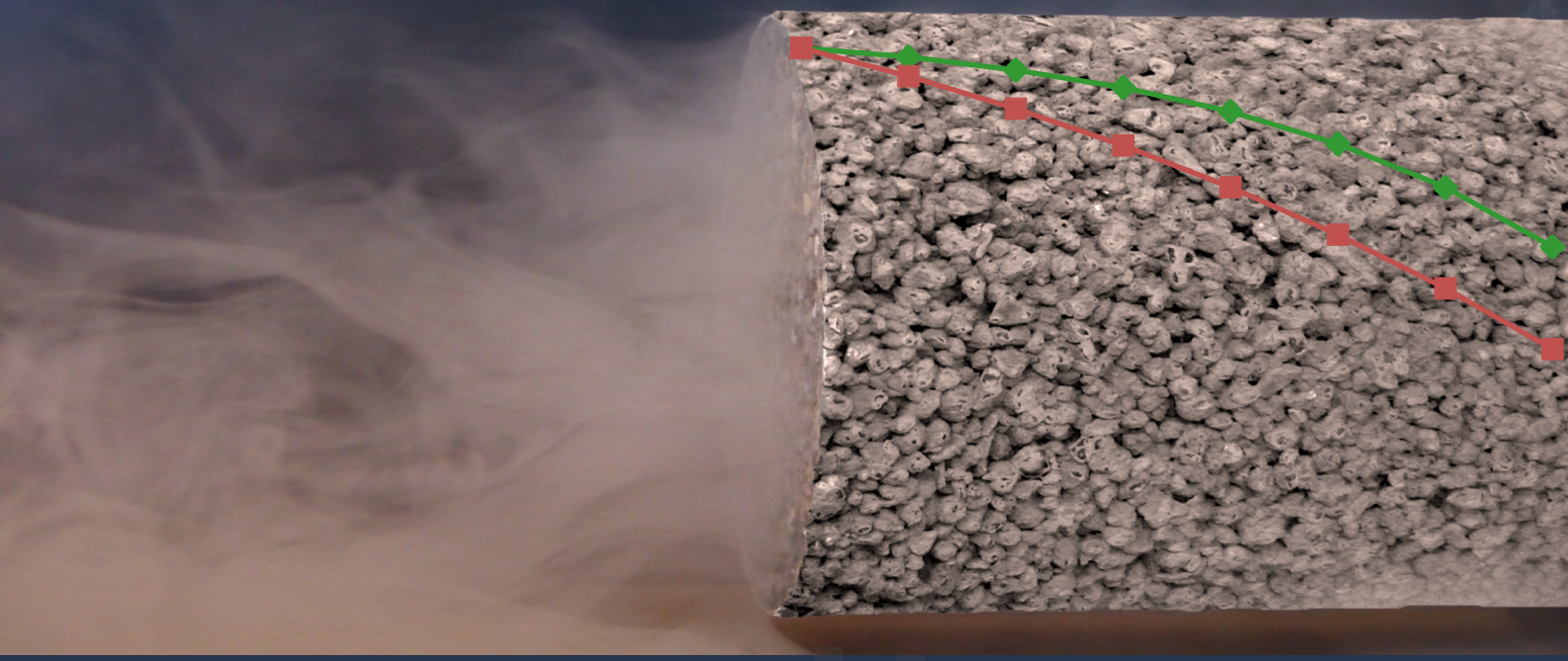

Master Thesis
Ole Daniels and Jesper Nørgaard
Indoor Environmental Engineering
Study Board of Civil Engineering
Aalborg University
June 9 2011

AALBORG UNIVERSITY
Students' report

The School of Engineering and Science
Study Board of Civil Engineering
Sohngårdsholmsvej 57, 9000 Aalborg
Phone 96 35 80 80
Fax 98 14 25 55
http://www.bsn.aau.dk

Title:

Air permeable heat exchanging concrete

Project:

Master Thesis,
Indoor Environmental Engineering

Project period:

September 2010 - June 2011

Project group:

B107a

Participants:

Ole Daniels

Jesper Nørgaard

Supervisors:

Per K. Heiselberg
Eigil V. Sørensen

Editions: 5
Report pages: 122
Appendix pages: 37
Completed 09-06-2011

Synopsis:

This master thesis deals with air permeable concrete as a promising passive cooling solution for office buildings, often requiring cooling in daytime and heating during night. Thermal mass can be used to equilize the loads, store heat and dampen temperature fluctuations, however traditional concrete not very efficiently due to poor heat transfer at the surface, poor heat conduction in the material and a short cycle period. Permitting air transport through the material is seen as a promising approach towards enhancing the heat transfer and utilising the entire thermal mass.

Measurement of fundamental properties were conducted on several concrete specimens with reference to a parameter variation - density, compressive strength and permeability. From the results two well-performing cases were subjected to energy performance measurements - thermal conductivity, specific heat capacity and heat exchanger efficiency. The main finding was the result of the heat exchanger efficiency, which states that this type of concrete is suitable for operating in daily cycles in an office building. A numerical model was developed to predict the temperatures profiles in the concrete over time and to compare with the measurements.

Preface

This report is the documentation of a long master thesis at Aalborg University as the final part of the master programme in Indoor Environmental Engineering. The report is composed in the period September 2010 - June 2011 and deals with permeable concrete with permitted air transport. The prerequisite for reading the report is academic knowledge within the fields of concrete and building energy physics.

The authors would like to address great thanks to the project supervisors Per K. Heiselberg and Eigil V. Sørensen for inspiring supervision and constructive criticism during the project period. Rasmus L. Jensen is thanked for answering questions and supervision of measurements and setups in the laboratory. Michal Pomianowski is thanked for measurement assistance and providing material properties. Finally, Morten Olsen, Jan Laursen and the additional laboratory staff are thanked for practical assistance and guidance.

The report is documented through calculations and argumentation and is divided into six parts. Part I contains an introduction with a literature review and a description of goals and phases. Part II contains concrete, phase change material and heat transport theory, an evaluation of performance potential and mathematical models for use in the subsequent parts. Part III deals with concrete casting and the basic material properties of air permeable concrete, measured and calculated from specimens based on a parameter variation. Part IV contains more advanced energy related measurements of a few selected specimens with suitable properties and comparison with dynamical mathematical models. Part V holds the conclusion and recommendations for future work.

Finally, at the back of the report, part VI holds the two appendices. These are thorough descriptions of the long process in the laboratory, where large amounts of time has been spent with casting and measuring. A collection of measurement setups, processes and corresponding experiences can be found, hopefully assisting others with similar challenges. Furthermore a CD with enclosures is attached. Here it will be possible to find simulation models, calculation programs, spread sheets and suchlike.

Plain, numbered citations are used in the report and listed at the back of the report in the order they appear (Vancouver style). If the reference is placed before a full stop, only the respective sentence is referred to. If the reference is placed after a full stop, the whole paragraph is referred to. References to the CD with enclosures will occur with the file name or folder in the form of [Enclosures-CD, File name/folder]. Figures and tables in the report are numbered according to the respective chapter. In this way the first figure in chapter 3 has number 3.1, the second number 3.2 and so on. Explanatory text is found under the given figures and tables. Figures without references are composed by the authors.

Danish summary

Dette afgangsprojekt ved kandidatuddannelsen i Indeklima og Energi på Aalborg Universitet omhandler optimering af betons evne til at lagre varmeenergi ved at tillade lufttransport gennem forsætligt skabte, forbundne kanaler i betonen samt iblande faseskiftende materialer (PCM). Ideen til en sådan permeabel beton stammer fra Imbabi et al. på Aberdeen Universitet i Skotland, som har udført eksperimentelle studier af materialets grundlæggende egenskaber og udgivet det i et patent [1].

Der er foretaget et litteraturstudie med henblik på at tilegne den nyeste viden indenfor området. Emnerne permeabel beton, dets anvendelse, varmeledning, varmestrøm, permeabilitet samt faseskiftende materialer har været i fokus. Dette har dannet baggrund for at kunne opstille kriterier for, funktionskrav til og ideer til praktisk implementering af permeabel beton.

Konceptideen er at implementere et separat system af permeabel beton som en passiv løsning til kontorbygninger, som i stigende grad kræver køling i dagtimerne og opvarmning om natten. Forsyningen af friskluft skal stadig leveres af den eksisterende ventilation. Løsningen består i at udnytte den termiske masse af det tunge materiale til at lagre den overskydende varme, udligne belastningerne og dæmpe temperatursvingninger. Traditionel beton er dog ikke særlig effektiv, hvilket skyldes en kombination af lille varmeovergangstal ved overfladen, lille varmeledning i materialet og en kort cyklus. Permeabel beton med lufttransport ses som en lovende metode til at hæve varmeovergangstallet og udnytte hele den termiske masse.

Princippet er konstant at cirkulere bygningens luft gennem betonen. Ved arbejdsdagens begyndelse er betonen nedkølet. Dagen igennem stiger lufttemperaturen løbende, som følge af sol- og intern belastning og denne energi udveksles med betonen, som løbende opvarmes, mens lufttemperaturen stabiliseres. Målet er en 12 timers periode med lagring, som ender med mættet beton og luft med temperaturer indenfor komfortkravet på typisk 26 °C. Herfra kan afladning begynde med kold udeluft eller energien kan frigives til bygningen som opvarmning om natten. Overordnede beregninger viser, at løsningen har potentiale.

Forud for støbningen af en række betonemner i en parametervariation er forskellige parametre blevet undersøgt i laboratoriet med henblik på at analysere deres indflydelse på støbningen, den endelige beton, evnen til at reproducere betonemner, indbyrdes korrelation og lignende. På baggrund af disse erfaringer blev den endelige parametervariation fastlagt og en række af cylindere støbt i ni forskellige cases. Permeabel beton fremstilles ved kun at fylde en fraktion af den tilgængelige porøsitet mellem tilslagspartiklerne med cementpasta, hvorved forbundne kanaler til lufttransport opstår.

I første del af afhandlingen er de grundlæggende egenskaber af alle emner blevet målt -

densitet, trykstyrke og permeabilitet. Interessante korrelationer er blevet analyseret og resultaterne sammenholdt med relevant teori samt matematiske modeller. For en stor del af prøverne viste det sig, at de ikke var komprimeret ordentligt da betonen blev støbt i forme, hvilket gjorde, at deres teoretiske densitet ikke passer sammen med den reelle. For de mest holdbare prøver, med styrker på op til 22 MPa, lå permeabiliteten på omkring $0.2\,\mathrm{m}^2$/Pa h, hvor den for de lave styrker på 2-8 MPa kom op på omkring $0.6\,\mathrm{m}^2$/Pa h. Ved tilføjelse af PCM sænkes trykstyrken på grund af en reduceret mængde af cement.

I anden del af afhandlingen er der fokus på den energimæssige ydeevne af permeabel beton. Her er der udvalgt to cases, som gennemgår måling af varmeledningsevne, specifik varmefylde og dynamisk varmevekslereffektivitet. Endvidere er der tilsat PCM i den ene case, som også bliver målt i denne anden del. Resultatet for varmevekslereffektiviteten var, for alle målte prøver og luftmængder, at efter ca. 6 timer var værdien faldet fra en startværdi på 1 til 0,2. Efter 12 timer var betonens varmelager udtømt i forhold til det fastsatte mål, hvilket kan omsættes til den konklusion, at denne type beton er egnet til at benytte i en daglig cyklus i et kontorbyggeri. COP-værdier på op til 380 blev målt for den mere permeable prøve ved en luftmængde på $8.5\,\mathrm{l/s\ m}^2$ og for samme luftmængde med den mindre permeable prøve blev en værdi på 170 målt. For alle prøver og luftmængder gælder det, at efter 9-11 timer er COP-værdien faldet til omkring 5, hvilket er sammenligneligt med en god varmepumpe. De beregnede dynamiske varmekapaciteter ligger mellem 70 og $115\,\mathrm{kJ/m}^2$ K.

En numerisk model er opbygget til at simulere temperaturen i betonprøven og luften igennem prøven baseret på en starttemperatur for dem begge og en fast indblæsningstemperatur. Endvidere behøver modellen en værdi for det konvektive overgangstal, hvilket bliver itereret indtil sluttemperaturen for modellen og de målte temperature passer sammen. Værdien blev 1.5 W/K for hele betonprøven (cylinder på $100\,\mathrm{mm} \times 200\,\mathrm{mm}$) som her er betragtet og grunden til at værdien er opgivet med denne enhed er at det indre overfladeareal, som er kontaktfladen imellem luften og betonen, ikke er kendt. Forskellen fra målingerne til modellens randbetingelser er, at indblæsningluften i modellen efter første tidsskridt falder til en fast værdi, hvor den ved forsøget falder løbende i de første 2 timer. Med værdien for det konvektive overgangstal, hvor temperaturene passer efter 12 timer, fås for den benyttede prøve en dynamisk varmekapacitet på $309\,\mathrm{kJ/m}^2$ K, som kan sammenlignes med $115\,\mathrm{kJ/m}^2$ K.

Table of contents

Part I

Introduction

1 Introduction

In these years massive focus is addressed CO_2 and global energy consumption due to its suspected role in global warming. A large part of the focus is levelled at the building sector, as it alone accounts for 40 % of EU's total energy consumption [2]. During the last decades, efforts regarding energy reductions have mainly been focused on reducing energy needs for heating. However, this is often at the expense of the need for cooling of the building in summer time due to the climatic season variations of the year.

At the same time, concurrently with the technological development and the growing wealth, increased expectations and demands regarding comfort, working environment and health have been observed. In order to respond to the increasing comfort and cooling demands, a trend towards increased use of active cooling solutions have been observed in commercial buildings to cope with overheating - the most commonly used parameter to evaluate thermal discomfort.

The need for cooling is further enhanced by a number of factors. The technological development has led to increased needs and requests for technical installations. Combined with the popularity of extensively glazed facades in commercial buildings, it will result in high internal and solar gains. Furthermore the cooling demands are enhanced by present and predicted climate changes. Although future climate models are subject to high uncertainties, a continuous increase in cooling degree days is believed to be very likely [3]. Finally the cooling demands are in large cities also enhanced by the urban heat island effect. The characteristics of this is a more densely populated and developed metropolitan area, which is significantly warmer than its surrounding rural areas due to heat retainment in materials, lack of evaporation and waste heat generation.

Hence, the task in designing buildings with low or zero energy needs overall, requires energy efficient cooling strategies. This can be achieved by implementing passive cooling solutions. Passive cooling refers to design features implemented to cool the building structure without consumption of energy. The basic principle is of course the reduction of internal and solar heat gains. The gains coming from solar radiation can be limited by effective, preferably exterior, solar shading devices. Internal gains in the form of people and equipment contribute as heat gains as well. Next to the direct energy savings, the application of energy efficient office equipment and using daylight instead of electric light helps to reduce the cooling energy demand.

1.1 Passive cooling

Besides the reduction of heat gains, passive cooling is based on the utilisation of natural heat sinks including the atmosphere, the sky and the earth. The most obvious design is natural ventilation, which is driven by natural forces (thermal buoyancy and wind). The cooling effect consists in removing heat gains during the day and if continued during night the building structure can be precooled to reduce temperature fluctuations. Heat transfer to the sky is solely by radiation and can be enhanced by exposing the thermal mass by night. The building can also exchange heat with the earth or a source of water (ground water, lakes and suchlike). This can be either directly linked or the supply air can be cooled by means of an earth-to-air heat exchanger.

Many of these passive strategies have a very long tradition. The warm and dry regions of southern Europe and the Middle East contain several ancient examples of very effective passive cooling systems. The famous Pantheon building in Rome has a dome-shaped roof with an incorporated air vent for natural ventilation. To increase ventilation effect wind towers and underground tunnels were applied. The utilisation of the thermal mass in massive, heavy structures to minimise daily internal temperature fluctuations was also very common. Finally architects and builders were fully aware of evaporative cooling for which reason damp walls, fountains or underground water streams would be implemented. Combining different methods yielded very effective cooling systems.

Passive cooling can also be combined with active cooling into hybrid cooling. Here the passive strategies will be utilised as long as the natural heat sinks are sufficient. When they are not sufficient, the active systems will activate. To power these, renewable energy sources should be considered over conventional sources. An assisting fan for ventilation can for example be powered by a solar power cell.

1.2 Night-time ventilation

One promising approach to reduce the energy needed for the cooling of commercial buildings without reducing comfort is passive cooling by night-time ventilation. Here the outdoor air is used as a natural heat sink. By day-time in the summer this is not suitable because it is often warmer than the indoor air and the building structure. But in the night-time it contains a cooling potential, being colder than the building structure and can be utilised as a heat sink. This can be used to discharge the heat in the building structure by night-time ventilation. As the heat gains occur only during the day, non-simultaneously with the ventilation, heat storage is an essential part of night-time ventilation. The basic principle is to accumulate the gains in the heavy building mass during the day and discharge the stored heat at night-time, where the cooling potential is greatest. This is shown in figure 1.1.

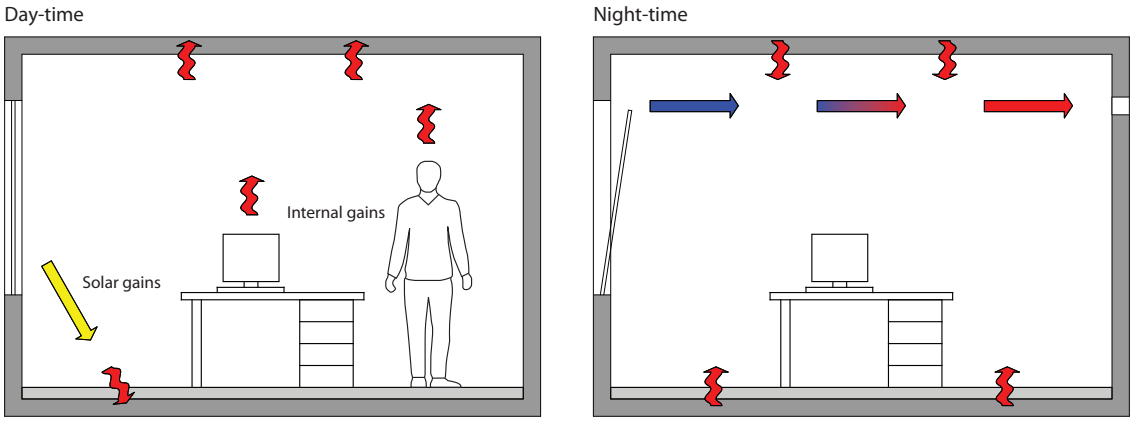

Fig. 1.1. Basic principle of night-time ventilation.

Night-time ventilation is of course highly dependent on climatic conditions, as a sufficiently high temperature difference between the outdoor air and the building structure is needed during the night to achieve efficient cooling of the building mass. To ensure effective convection, night ventilation is only applied if the difference between building and ambient temperature is greater than 3 K [4].

The principle of climatic cooling potential, CCP, is illustrated in green in figure 1.2, when the difference in outdoor temperature, T_o and building temperature, T_b exceeds 3 K. The building temperature is defined as a harmonic oscillation around 24.5 °C with an amplitude of 2.5 °C. It is assumed that night-time ventilation starts at t = 19 h and ends at t = 7 h.

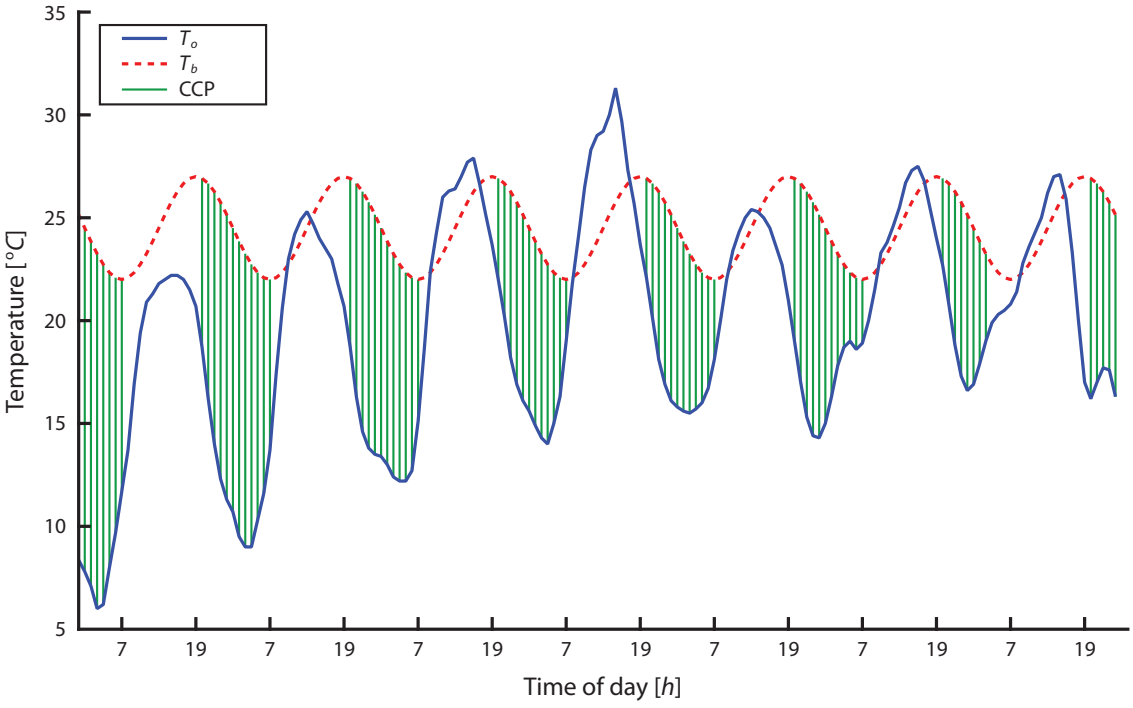

Fig. 1.2. Building temperature, T_b and outdoor temperature, T_o during a week in summer. Data extracted from the Danish DRY [5]. Areas in green graphically illustrate the CCP.

The figure should be seen as an illustration of the principle of CCP only. However, the outdoor temperature is extracted from Danish design reference year (DRY) data and thereby represents conditions as they could be expected to be measured. Artmann et al. [4] evaluated the potential for passive cooling of buildings by night time ventilation by analysing climatic data. They developed a method for calculation of CCP based on degree-hours of the difference between building and external air temperature. The study showed a very high night cooling potential over all of Northern Europe. In Central, Eastern and even in some regions of Southern Europe, the CCP is still significant. However, due to the inherent stochastic properties of weather patterns, a series of warmer nights may occur, possibly resulting in malfunction of the night cooling. In a continuous study, changes in CCP for the period 1990-2100 were evaluated [6]. The result was a considerable decrease of the CCP by the end of the present century. Night time ventilation will cease to be sufficient to ensure satisfactory thermal comfort in buildings in Southern and Central Europe. In Northern European buildings CCP was however found to remain at least for the next few decades.

1.3 Permeable concrete

The increasing cooling demand in non-residential buildings can be accommodated by the utilisation of thermal mass. A study made by Nikolai Artmann et al. [7] shows that the dynamic heat storage capacity of different building materials is influenced by various parameters like material properties, thickness and heat transfer coefficient. The limitation of storing energy in a traditional concrete element is mainly caused by poor heat transfer at the surface. The penetration depth is not sufficient to utilise the entire material and therefore the study concludes that the dynamic heat storage capacity for massive elements, like concrete, highly depends on the heat transfer coefficients.

To make concrete more receptive to heat storage the heat transfer coefficient or the surface area has to be enlarged. In this project the surface area of the concrete is changed by making an air permeable concrete. By implementing an air flow through the concrete it should be possible to utilise the entire thermal mass. Making of permeable concrete is based on the intentional formation of interconnected air channels in the concrete.

1.4 PCM

The thermal mass of concrete can be further increased by adding phase change materials (PCM). Phase change materials are characterised by being able to accumulate significant amounts of energy when the material changes phase from solid to liquid and releasing it again by the opposite process. These properties actually apply to all materials and substances when the melting point is reached. However, for the building sector only materials with high heat storage ability and, more important, with melting temperature in the range of thermal comfort are of interest. This can dampen the temperature increase due to internal gains by accumulating the excessive energy, as illustrated in figure 1.3. When the temperature drops, the energy is once again released.

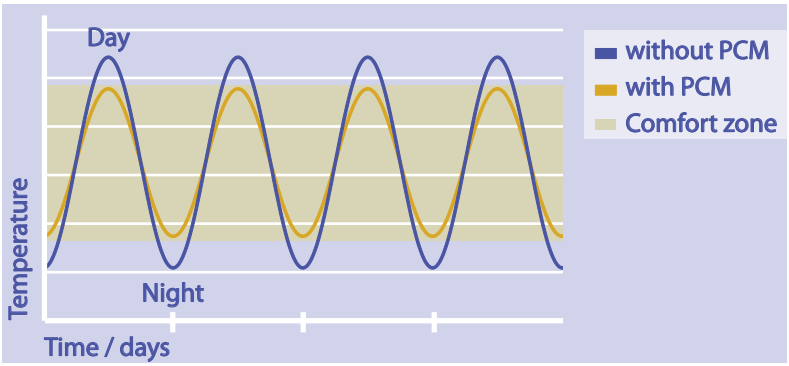

Fig. 1.3. Daily temperature fluctuations kept within comfort range with PCM [8].

The liquid cement paste is well suited to add the microscopic PCM particles, perfectly integrating the PCM in the hardened concrete. However, studies have shown that not all PCM is activated due to the previously mentioned poor penetration depth and heat transfer at the surface. Permeable concrete on the other hand should enable activation of the entire thermal mass and thereby also the PCM. Thus, it constitutes as a promising solution in combination with permeable concrete and night-time ventilation as a method to control the temperature fluctuations.

1.5 State-of-the-art

Permeable Concrete

Imbabi et al. [9] made pre-cast concrete blocks possessing the necessary permeability and strength for the construction of energy efficient, breathing buildings, and tests on more than 50 formulations were completed. The tortuous permeation channels in this new type of material can be optimised to provide adequate structural strength, significantly reduce thermal conductivity, and function as a ventilation source. The results confirm that pre-cast breathable concrete blocks provide an elegant and sustainable building material.

In a patent by Imbabi et al. [1] it is described how a mixture for forming a permeable concrete is produced. It consists of aggregate particles, a paste comprising water, cement or cement substitute and a plasticiser. The purpose is to achieve a high permeability in order to minimise the energy used to ventilate the concrete element. Unfortunately the higher the permeability the less the strength the concrete will obtain, hence it is essential to find a balance. To achieve the highest structural strengths in the concrete the w/c ratio must be as low as possible. The best result presented in [1] regarding the highest structural strength has a w/c ratio of 0.25. The permeability can be adjusted by changing the degree of filling, where low values equals larger permeability. The degree of filling is varied from 0.30 to 0.80 and in the results presented, 0.5 - 0.7 is the chosen range with structural strengths ranging from 11 to 25 MPa and permeability from 0.60 to 0.18 m^2/Pa h.

The main purpose of a study made by Imbabi et al. [10] was to evaluate the thermal

conductivity of air permeable concrete, but a description of the different parameters influencing the properties of the concrete is also included. The air permeable concrete specimens are optimised by carefully controlling the aggregate sizing and securing that a specific volume of cement paste is mixed with the aggregates before being put into a mould. According to [1] the size of the aggregate should preferably have a diameter of 2-3 mm and be as perfectly rounded as possible.

When using small values of w/c ratio, the use of a superplasticiser is necessary to ensure good flow characteristics of the cement paste such that all aggregates are enveloped [1]. The plasticiser is controlling the viscosity of the paste such that the paste is able to form a substantially uniform layer around the grains. The plasticiser recommended is melamine formaldehyde condensate but naphthalene formaldehyde condensate or polycarboxylate ether is usable as well. The proportion preferred is 0.2-0.7 % of the cement weight.

Application

Comprehensive reviews on different possibilities for application of porous concrete are presented in various references. Taylor et al. [11, 12] have investigated the use of porous building materials in a dynamically insulated 'Breathing envelope'. The system allows the movement of air and moisture through the external walls of the building, rather than traditionally stopping them by means of air and vapour barriers. With low-velocity air movement drawn into the building in the opposite direction to the conductive heat flux (contra-flux), the heat losses of the building are minimised. The insulation layer comprises a cellulose insulation material.

Imbabi [13] describes a new generation of modular breathing wall systems, which offer a clean, energy efficient method of delivering fresh, filtered air to the building. The method also involves drawing air into the building (by active and/or passive means) through an air permeable, dynamically insulated envelope. Compared to a traditional wall consisting of an external screen, insulation and an internal surface, this necessitates the use of porous concrete to ensure air movement. The conventional insulation is replaced by breathing wall panels, comprising a fibre-based material in a supporting frame. Combined it enables the wall system to function as a supply source, filter and heat exchanger, due to the incoming air recovering the heat, which would have been lost by conduction. It is shown that the U-value decreases with increasing air flow and is near-zero at normal ventilation rates. Furthermore the filter performance is proved to function for a lifetime.

Khedari et al. [14] have redesigned a traditional Trombe wall. A Trombe wall is a passive design solution where a massive wall is separated from the outdoors by glazing and an air space. The construction can absorb solar radiation during the day and release it towards the interior by means of conduction and convection by night. The latter due to operable openings added to the top and bottom of the air spacing between the glazing and the thermal mass. The redesigned concept consists in replacing the conventional concrete with porous concrete and adding an insulator on the inner surface. A fan and control valves also permits air circulation and combined with the porous concrete, this improves the convective heat transfer and heat storage ability. The most promising discharge configuration with regard to heat comfort is a balanced mixture of discharge air from the wall, recycled air from the interior and fresh air from the exterior.

Permeable concrete has also been used in two American infrastructure pilot projects [15]. The concept consists in paving streets and parking lots with permeable slabs to cope with large rain intensities and stormwater runoff. The concrete is designed with 15 % voids, making it able to absorb huge amounts of water from intensities as high as 2000 mm/h.

The concept of breathing walls is also presented with other materials and configurations. Yoon and Hoyano [16] experimentally investigated the heat recovery capability of a breathing wall for use in a passive solar house. The breathing wall concept was applied as a pitched roof with perforated aluminium sheets as key material. The outcome of the research was the most effective opening area for different pitches. Stone [17] describes a green solution with breathing wall biofilters for offices. Fans draw air into a block of porous, constantly wetted lava-rock, which is covered in mosses and ferns. To ensure a saturated filter, water is circulated to the wall from an aquarium. The water acts as a dissolver of airborne pollutants from the indoor air. Finally the system supports plants and amphibians, which break down the pollutants and removes CO_2 from the air.

Thermal conductivity

A one-dimensional heat flow model for predicting the effective thermal conductivity (λ_e) of air permeable concrete has been presented using as variables the fractions of voids, aggregate and cement paste comprising the material [10]. Measured values of λ_e were 0.7-1.4 W/m K. A theoretical model predicts and further improves the performance and formulation of air permeable concrete. The w/c ratio also influences the λ_e. Increasing w/c ratio increases the volume of capillary pores in the hardened cement paste, adding resistance to heat flow.

The theoretical static model for calculating thermal conductivity is a combination of the average thermal conductivity $\overline{\lambda}$ for the series and parallel approximations [9]. When considering a static model it is not important which part of a subject is pore space and isolated pores, because these will have the same properties. In a dynamic situation convection must be added to the air in the pore spaces.

It is possible to achieve very different thermal conductivities by changing the w/c ratio and the degree of filling [10]. Values from 0.6 to 1.5 W/m K are presented with a w/c ratio varying from 0.25 to 0.35. Other values are presented by [1], where the static thermal conductivities of the breathable concrete are in the range 0.1-1.4 W/m k. In a porous concrete the heat will transfer faster in the aggregates and cement paste than in the air, for which reason the air functions as an insulator [9].

Kook et al. discovered that the highest conductivities are acquired at low temperature conditions like 20 °C [18]. This, however, means more in wet conditions than in dry. Furthermore, the lower the w/c ratio and the higher the aggregate volume ratio, the higher the conductivity. The age of the concrete has little impact on the thermal conductivity, which indicates that hardening of the concrete has a minor impact on the thermal properties.

Heat flow in inhomogeneous materials

Taylor el al. [11] are treating two types of breathing envelopes, diffusive and dynamic.

The essential difference between them is that in "dynamic insulation" envelopes, air is drawn through the insulation material by a pressure difference created by either a fan or stack effect, whereas in "diffusive insulation" it is assumed that the only driving forces are concentration gradients [11]. Mathematical expressions to deal with both temperature and water vapour concentration profiles are presented as part of both conductive and convective heat flux. [11] describes how to handle heat transfer through a three-layer dynamic building element. Imbabi et al. [10], working with air permeable concrete, describe more about one single layer and the properties and dynamic function of this layer. The measured values of λ_e were in the range of 0.7-1.4 W/m K. The effective thermal conductivity of air permeable concrete is an important parameter because, if known, one can predict the dynamic U-value of a wall made of this material under both steady state and transient conditions when air is drawn through the material [11].

Permeability

Ruppersberger [19] made tests, showing that air permeability of concrete blocks can vary by a factor greater than 50 (0.63-35 standard l/min m^2 at 3 Pa). The surface texture of the blocks correlates well with air permeability. Test results showed that smoother, closed-surface-texture blocks were usually less air-permeable. These were tests made on concrete blocks which are not meant to be permeable.

Imbabi et al. [1], [10] made permeable concrete with permeabilities from 0.18 to 0.6 m^2/Pa h, which is about 24 times larger than the normal concrete Rubbersberger [19] tested. The parameter in the concrete mixture influencing the permeability is mostly the degree of filling, which is inversely proportional to the structural strength of the concrete.

Phase change materials

A relatively new strategy for natural cooling of buildings is adding phase change material (PCM) to the building in order to raise the thermal mass of the building. PCM has a high storage capacity density for small temperature range applications or at least a range covering the melting temperature [20]. Studies have proved that adding PCM to a structure can reduce peak indoor temperatures by several degrees [21]. The experiments show that all the PCM utilised solidifies and melts in every cycle and that night-time cooling is an important factor to achieve this full cycle and thereby the full potential. Athienitis et al. [22] made experiments and numerical solutions on a full-scale test room with PCM gypsum boards, containing 25 % by weight of Butyl Stearate (BS), as inside wall lining. It was shown that this utilisation of PCM could reduce the maximum room temperature by about 4 K. PCM incorporated in the building structure can also be used for passive solar heating in the winter and by reducing the peak loads of the indoor temperature, reduce room temperature fluctuation ensuring a higher comfort level [23].

Early studies and work made with PCM used inorganic materials [24]. These materials have both attractive and unwanted properties. The inorganic substances have a high latent heat value, are not flammable, comprise a wide range of characteristics for thermal storage applications, are inexpensive and they are readily available. However, they are corrosive and are, therefore, incompatible with many other materials used in buildings. They need special containers which require support and space, have a tendency to super-cool and the components do not melt congruently so that segregation could be a results.

The organic substances can be incorporated in the building materials, which generate an advantage. Also, their constituents melt congruently, super-cooling is not a significant problem, they are chemically stable, comprise a broad choice of substances and they compatible with and suitable for absorption in various building materials. Unwanted properties are that they are flammable and fume generating, some organics react with the products of hydration in concrete, a few have an odour which may be objectionable and in some, the volume change at transition can be appreciable.

Hawes et al. studied three methods of PCM incorporation [24]. These are direct incorporation, immersion and encapsulation. In addition PCM can be incorporated in the form of a single laminated element or combined with other envelope components [23]. The method of direct incorporation is that liquid or powdered PCM is mixed in with building materials such as gypsum or concrete during production [23]. However this method has some adverse effects on the building material, as these are in direct contact.

The immersion method takes porous building materials, like concrete blocks, and dips them into hot melted PCM, where the PCM then is absorbed into the pores of these materials [25]. After the material is removed from the liquid PCM, the PCM remains in the pores making this method good at converting ordinary materials to PCM materials. Unfortunately leakage may be a problem over a period of years [26].

Encapsulating the PCM removes the disadvantage effects of adding PCM directly in the building material. There are two ways to encapsulate the PCM, macro and micro-encapsulation [27]. Macro-encapsulation packs the PCM in tubes, pouches, spheres, panels or other receptacles and then incorporates it into the building material. This method has a disadvantage of needing protection and has a decreasing heat transfer rate during the solidification process with poor heat transfer coefficients of PCM [26]. Micro-encapsulation is enclosing small PCM particles in a very thin and high molecular weight polymeric film. This method ensures easy application and has a good heat transfer due to the increased heat exchange surface and there is no need for protection [26]. The disadvantage is that the adding of micro-encapsulated PCM to a building material may affect the mechanical strength of the element [27].

Laminated PCM boards contain PCM laminated into a single layer and used as an element in the building envelope. Darkwa et al. [28, 29] made studies on the performance of laminated randomly mixed PCM drywalls and they could conclude a significant better result by using the laminated system.

With the increasing demand for cooling buildings it is possible to utilise PCM and chemical reactions for cooling in active or passive systems. Active systems are defined by an actively supported charging or discharging process, for example by ventilated air or a pumped heat transfer fluid. This concept refers to the building's heating or air conditioning system. Passive storage systems (only PCM) are an integral part of the building. They can even out temperature peaks in the building by raising the thermal mass. [30].

Peippo et al. [31] were among the first to discuss the application of PCM in walls for short term passive solar heat storage. Energy savings of up to 5-20 % were expected. In an experiment made by Feldman et al. [32] a large increase in energy storage capacity was achieved by directly incorporating 21-22 % of commercial BS in the mixing stage of

a conventional gypsum board production. In a study by Heim and Clarke [33] PCM-impregnated gypsum plaster-boards were used as an internal room lining. Numerical simulations for this multi-zone, highly glazed and naturally ventilated building suggested that these PCM-panels could reduce the heating demand by up to 90 % at times in the heating season.

1.6 Project goals and phases

The primary objective of this master thesis study is to improve the dynamic heat storage capacity of concrete by permitting air transport through deliberately engineered interconnected permeation channels.

The idea of air permeable concrete originates from the experimental investigations done by Imbabi et al. at University of Aberdeen in Scotland and later published as a patent [1]. Their research has mainly been focused on basic properties, permeability and thermal conductivity, whereas this study intends to expand with the dynamic energy performance of air permeable concrete.

Assisting the primary objective are a number of appertaining goals. The goals are to:

- achieve knowledge within the field of air permeable concrete.
- define criteria for air permeable concrete.
- be able to make and cast well performing recipes.
- investigate material properties relations.
- include suitable theory to establish a connection between this and measurement data (static and dynamic).
- develop mathematical models to predict concrete performance.
- analyse concrete performance based on experimental findings and be able to estimate performance potential.
- develop new setups to measure permeability and dynamic heat capacity.
- investigate potential of phase change material in air permeable concrete.

The project goals has been fulfilled through different phases. Initially, an overview and knowledge about central problems, methods and terminology within the field of air permeable concrete has been gained through a literature review. Subsequently a three phase experimental study began. This started with a study on material properties and their correlation based on a parameter variation. Selected cases with good properties were subjected to energy performance measurements. The last experimental study has dealt with an evaluation of the phase change material potential in permeable concrete.

After the large experimental period, the results has been evaluated and used to create mathematical models, linking the measurements and theory. Being in possession of mathematical models reflecting reality correctly is very valuable, being able to change parameters and time freely and simply simulate again without having to do corresponding time-consuming measurements. Based on the conclusions of the results and models, design solutions and the implementation potential in office buildings has been considered and evaluated. Finally the work is documented in the present project report.

Part II

Theory, performance criteria and mathematical models

Concrete technology 2

Traditional concrete is an inorganic, composite construction material characterised by being plastic and workable in the process of production and a hard solid in the final hardened phase. It is the most widely used construction material in the world [34]. Concrete consists of aggregates, cement and water. Also, a natural content of air is present as well as different admixtures can be added to manipulate the properties. The terminology and constituents of traditional concrete is graphically shown in figure 2.1.

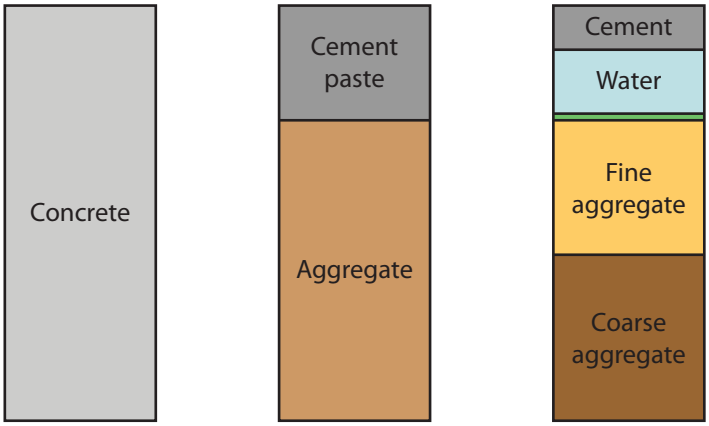

Fig. 2.1. The composition of traditional concrete. The green bar represents natural content of air and optional admixtures.

The aggregates covers both fine aggregate such as sand and coarser aggregates such as gravel or crushed rock. Cement is a complex, fine powder of clinker minerals processed from limestone, clay, sand and other minerals. The rich deposits of these components and aggregates too in the Earth's crust and low production energy consumption, makes concrete a very attractive construction material. The different clinker minerals contribute to the cement properties such as strength development, final strength, heat generation and durability. Cement and water merge in a chemical reaction (hydration) forming a binding material (cement paste), which bonds the aggregate together in a structure creating a robust stone-like material. [35]

Hydration

The initial state of the fresh cement paste can be considered as cement particles suspended in water, but shortly after the cement will react with the water - it is hydrated. By the chemical reaction the clinker minerals are transformed into new complex hydration

products (gel solid). The deposit of hydration products gradually fills the initial space of water and leads to the formation of a stiff network of colloidal particles (called cement gel because of its colloidal nature and large surface area). The development of strength is referred to as curing.

Typical Portland cement consists of a number of oxides combined in clinker minerals. The most commonly occurring oxides are quite naturally a reflection of the main contents of the raw materials, from which cement is produced. In table 2.1 the main oxides are listed with chemical formula, notation symbol and typical percentage-wise distribution [35].

Oxide	Chemical formula	Symbol	Typical distribution
Lime	CaO	C	65 %
Silica	SiO_2	S	22 %
Alumina	Al_2O_3	A	4 %
Iron oxide	Fe_2O_3	F	3 %

Table 2.1. Most commonly occurring oxides in traditional Portland cement and their chemical formula, notation symbol and typical percentage-wise distribution [35].

In the fine cement powder these oxides are found combined in mainly the four clinker minerals C_3S, C_2S, C_3A and C_4AF. To the cement is also added small amounts of gypsum to slow (retard) the C_3A-reaction. The cement binding material ability is linked to the complex hydration products forming as the clinker minerals react with water. The most important is a series of calcium silicate hydrates (approximately denoted $C_3S_2H_3$), which is formed by hydration of C_3S and C_2S. These are correspondingly dominant by volume in the cement gel due to the high fraction of lime and silica. The hydration of C_3S is elaborated in the following reaction:

$$2\ C_3S + 6\ H \rightarrow C_3S_2H_3 + 3\ CH$$

To complete the shown chemical reaction, 0.24 g of water is needed for every g of cement. In a weighted average with the other clinker minerals the total water requirement for complete hydration is approximately 25 % in a Portland Rapid cement. The reaction also forms calcium hydroxide, $Ca(OH)_2$, which makes the environment strongly alkaline. However, the liberated calcium hydroxide will crystallise in the available free space and contribute to the cement gel volume [34]. The distribution in cement paste is approximately 70 % by volume of cement gel and 20 % calcium hydroxide. [35]

As the hydration proceeds, the deposit of hydration products on the surface of the original cement particles complicates the diffusion of water towards still unhydrated cement. Thus, the rate of hydration is slowed over time. [34]

w/c ratio

The robustness, or mechanical strength, of the concrete is primarily determined by the strength of the cement paste matrix due to a significantly stronger aggregate. The strength of the cement paste is known to correlate with the water to cement ratio (w/c ratio), which

is the weight ratio of water and cement. It influences the quality of the cast concrete in the way that a low w/c ratio results in a higher strength and a high w/c ratio in lower strength. The latter due to increased porosity in the hardened concrete, which is elaborated later. Furthermore, too much water content can lead to bleeding and/or segregation of the aggregate components and cement paste. [35]

Bolomey's formula

On the basis of the correlation between the w/c ratio and concrete strength, different studies have over the years lead to a number of empirical laws describing this relation for use in practice. An acknowledged approach is using Bolomey's formula, who discovered a linear correlation when plotting the concrete strength against the reciprocal value of the w/c ratio (valid for $0.45 < \text{w/c} < 1.25$). The corresponding analytical expression is:

$$f_c = K \cdot \left(\frac{1}{w/c} - \alpha \right)$$

K and α are constants depending on cement type, cement content, type of aggregate and finally maturity.

Normally it is assumed that the strength, f_c, refers to the 28-day strength. Measuring the ultimate strength is not very practical requiring a wait of several years, as the hydration process continues over a long period of time. At 28 days of age, a substantial percentage of the hydration has taken place and has been chosen as international reference. The age presupposes curing at 20 °C. Deviations from this in negative direction will cause the process to slow down, while a temperature increase of the environment will accelerate the curing. To take this factor into account, the property development of concrete is often quoted as a function of maturity. [35]

Rheology and SPA

Bolomey's formula suggests a w/c ratio as low as possible if a high strength is required. However, this will reduce the workability of the fresh concrete because the fresh mixture is more dry and viscous. The workability can be measured by a number of methods. A simple and popular method is the concrete slump test. It reveals the impact of gravity on a compacted inverted cone of concrete [34, 36]. This is shown in figure 2.2.

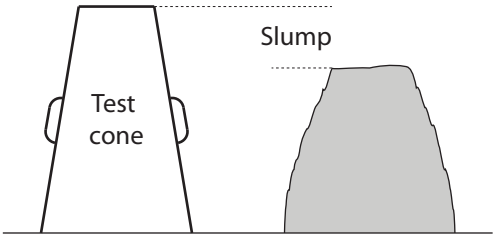

Fig. 2.2. Concrete slump test, which shows the impact of gravity on the inverted cone of concrete.

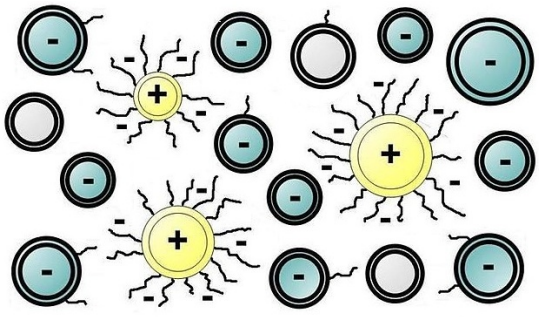

Fig. 2.3. Adsorption of SPA on colloidal particles enabling good particle dispersion and avoiding friction [37].

The flow characteristics of the concrete (rheology) can be improved by adding a plasticising or superplasticising admixture (SPA). They are additives, which increase the plasticity of the concrete. The newest generation of SPA is represented by the chemical polycarboxylate ether. These long negatively charged polymer chains are adsorbed on the positively charged colloidal particles in a suspension, see figure 2.3. The plasticity of the mixture is improved due to a suspension of only negative particles, enabling good particle dispersion and avoiding friction. Besides the electrostatic dispersion forces, also steric forces contribute due to the enlargement of particles. The cement paste is a complex suspension with particles probably varying in both size and charge. However, the effect of SPA is most likely dominated by steric forces. In terms of concrete technology this enables the use of low w/c ratios, maintaining the same workability of the mixture. It also enables the production of self-consolidating concrete. [37, 38]

Pores

Permeable concrete with permitted air transport obviously requires a porous structure. The pores intended for air transport and the making of these are described later. However, it is important to distinguish between these coarse pores and the different fine pores located in all types of concrete. The presence of these has great influence on almost all properties of the hardened concrete. Generally there are following sources to pores in concrete [35]:

- Aggregate porosity
- Pores in the cement paste
- Natural content of air or added air for frost resistance
- Encapsulated air due to insufficient consolidation
- Cracks along aggregate particles or due to damage/overload

Only the aggregate and cement paste pores will be discussed in this section. The natural content of air is throughout the project assessed not to deviate from normal levels (approximately 1.5 % of concrete volume) and deliberately added air for frost resistance is not considered in this project. The last two elements are believed to be a result of poor production and processing, for which reason it is disregarded in this theoretical description of concrete pores.

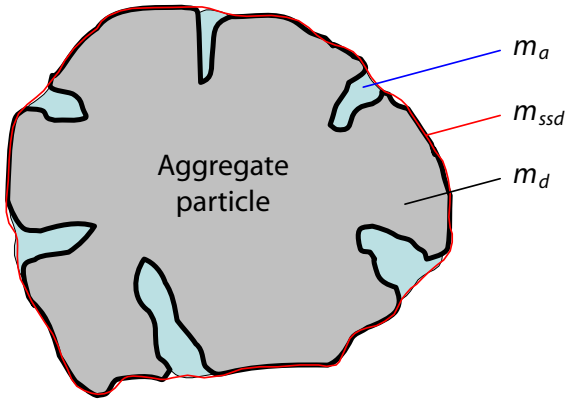

Fig. 2.4. Saturated surface dry (SSD) aggregate particle with absorbed water in the microscopic pores. Absorption (m_a/m_d) of approximately 0.5 %.

Aggregate particles contain several microscopic cracks or pores. They can absorb approximately 0.5 % of water compared to the dry mass. To avoid absorbing the water intended for the hydration, possibly interfering with the w/c ratio and the concrete properties, this additional amount of water can be added as compensation. The aggregate then attains the state of saturated surface dry (SSD). This is illustrated in figure 2.4.

As opposed to the aggregate, the pores in the cement paste are not initially present, but form gradually along with the hydration. In figure 2.5 a hardened cement paste is illustrated, where the components of the system are shown separately (hypothetical division).

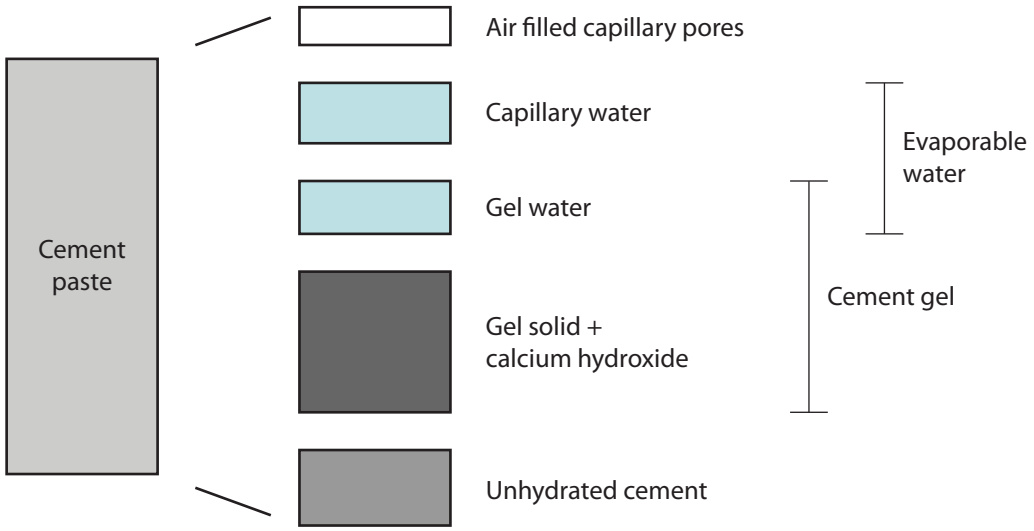

Fig. 2.5. Hypothetical division of the cement paste components.

Air filled capillary pores form as a result of the volume reduction (shrinkage), which takes place when the water chemically binds in the hydration products. The products have a smaller volume than the one of the initial cement and water from which they are formed (approximately 75 % of the initial volume of the chemically bound water). The shrinkage does not noticeably affect the outer volume, which necessarily leaves pores in the cement paste. Capillary pores are 2 nm to 5 µm in diameter. [39]

Capillary water is water in capillary pores. These pores are present in the fresh cement paste because the capillary water at time t=0 in fact corresponds to the added amount of water. During the hydration the amount is gradually reduced, but in case all water is not consumed when the cement is, the hardened concrete will still contain capillary water. Correspondingly it applies that the hydration will stop if the capillary water is consumed before the cement. From the coarse, open pores it is possible to evaporate the capillary water. This enables interchange of moisture with the surroundings. [39]

Due to its colloidal structure the cement gel has a very large internal surface, resulting in the smallest of all concrete pores: Gel pores. They are ranging from 0.5 nm to 2 nm in diameter and their volume is approximately 25 % of the cement gel volume. Immediately after the formation of a gel solid particle, the surface is able to attract and retain a

corresponding amount of water, which is referred to as gel water. This is no longer available for the continuing hydration, as it is adsorbed in a way so it is unable to react with unhydrated cement. It is, however, evaporable like the capillary water. The mass of gel water equals approximately 15 % of the initial cement mass. As a consequence of this, the amount of water needed for complete hydration is not 25 % as previously mentioned but 40 % (25 % for chemically bonded water and 15 % for gel water). This corresponds to a w/c ratio of 0.40. [35, 39]

Responsible for the cement binding ability is the structure of complex hydration products (gel solid). These are mainly $C_3S_2H_3$ and calcium hydroxide. Embedded in here is of course the chemically bonded water, which is non-evaporable. The hydration products and gel water constitutes the cement gel. Finally the cement paste contains unhydrated cement. [39]

The distribution of components in the cement paste can also be illustrated as a function of w/c ratio (full hydration) and as a function of degree of hydration (referred to as Powers' model). The first mentioned is shown in figure 2.6.

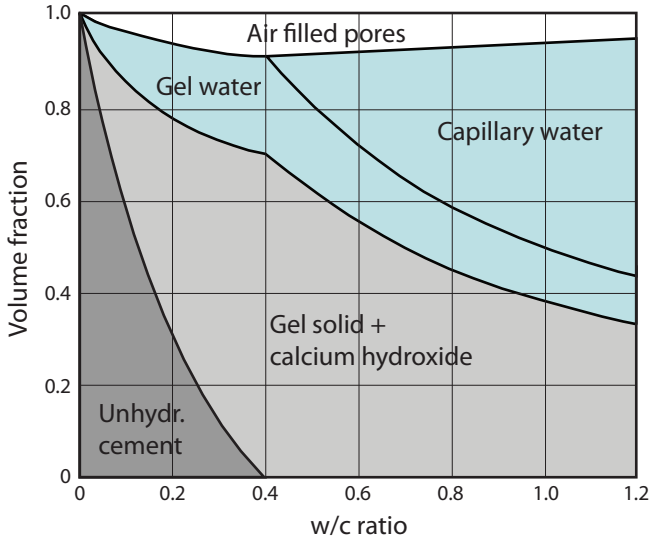

Fig. 2.6. Ratio of volume of cement paste components at full hydration as a function of w/c ratio [35].

Figure 2.6 shows the volume distribution of the phases in hardened cement paste. Full hydration (time-wise) and a sealed environment is a prerequisite. Full hydration describes the state when either all water or all cement is consumed. From the figure it is confirmed that complete hydration (both completely consumed) occurs at w/c ratio of 0.40. Here all the cement is consumed and no capillary water is in excess. Lower w/c ratios leave unhydrated cement and higher leave excess water in the capillary pores.

It is furthermore quite obvious why the mechanical strength of the concrete is decreasing with increased w/c ratio. The total volume of pores is increasing correspondingly, which is known to weaken the strength of any material. Finally the figure also enables to easily distinguish between the different stages of water in the cement paste. The chemically

bound in the hydration products, the physically bonded (adsorbed) in the gel pores and the physically retained in the capillary pores [35].

Powers' model

T. C. Powers was a profiled researcher and writer within the field of structure and properties of Portland cement pastes and concrete. Based on this work, P. Freiesleben Hansen [39] developed a model for the volume distribution of the cement paste components as a function of degree of hydration (α). It is known as Powers' model. The degree of hydration is at a given time defined as the elapsed fraction of the hydration process. This can for instance be reflected by the mass fraction of hydrated cement to initial cement. Figure 2.7 shows two Powers' models for different w/c ratios.

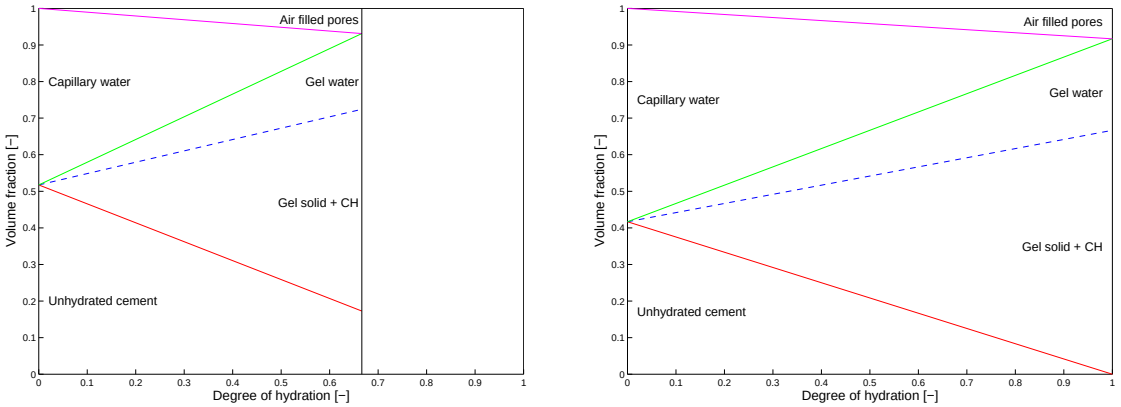

Fig. 2.7. Volume distribution of the cement paste components as a function of degree of hydration, known as Powers' model. Here displayed for w/c ratio 0.30 (left) and w/c ratio 0.40 (right).

The substance transformation of cement into pores and solid is seen to have a linear dependence of the degree of hydration. At w/c ratio 0.30 it is clear that the process has stopped due to an insufficient amount of water (left), while at w/c ratio 0.40 (right) there is a convergence of totally consumed water and cement at finished hydration (α=1 because all cement is consumed). The total porosities of the cement pastes at the maximum degree of hydration are approximately 28 % and 33 %, respectively.

The distributions illustrated at full hydration in the Powers' models correspond to those in figure 2.6. Full hydration must be considered as a theoretical boundary condition, though. In practice the hydration continues for years and still leaves unhydrated cement, even at w/c ratios larger than 0.40 [39].

2.1 Air permeable concrete

Making of permeable concrete involves the intentional formation of air channels in the concrete. The goal is not to make use of the lately described pores in the cement paste. Instead the natural porosity (NP) of the aggregate is utilised. The natural porosity is defined as the void fraction between the non-vibrated aggregate particles compared to

the mould volume. The remaining fraction of solids is referred to as the natural packing density (NPD). In figure 2.8 a picture of the used aggregate (SSD state) is shown, where it is noticeable that the particles are unable to pack completely. In figure 2.9 the principle is graphically illustrated.

Fig. 2.8. Saturated aggregate of 2-3.55 mm filter sand.

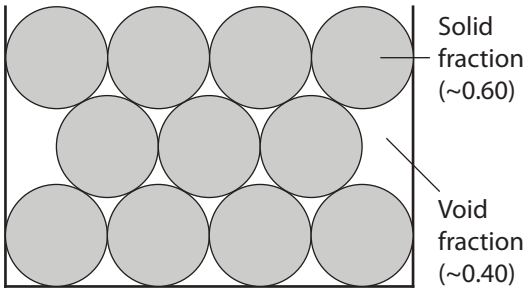

Fig. 2.9. Void and solid fraction of perfectly rounded, packed spheres.

Permeable concrete differs from traditional concrete in two ways. In part because a wide size fraction of aggregates is selected in traditional concrete and partly because the entire void fraction is normally filled with cement paste. On the contrary permeable concrete is formed by manipulating aggregate sizing, cement paste volume and the rheological properties of the fresh mix to obtain the desired permeation [10]. The shape, angularity and size fraction of aggregates affect how much space is available for cement filling, corresponding to the NP. By selecting a narrow size fraction and rounded particles this volume approaches the theoretical maximum (perfectly rounded spheres as displayed in figure 2.9). This is necessary in order to create a good permeable concrete, even though the mechanical strength is weakened. A broader particle size distribution will form an interlocking grid and reduce the porosity, which will increase the strength as previously stated. A particle size distribution curve of the used aggregate is shown in figure 2.10 [40].

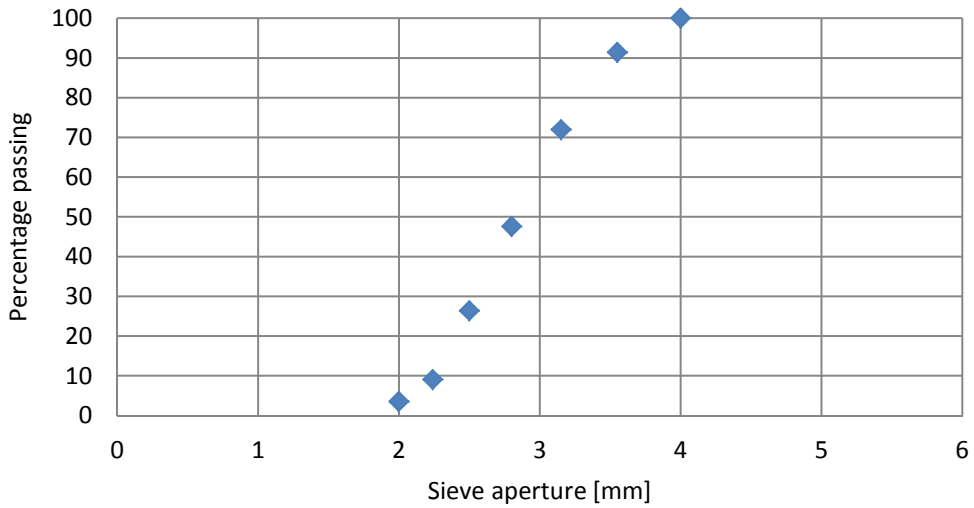

Fig. 2.10. Particle size distribution curve of the used aggregate [40].

In order to make permeable concrete, the mono-size aggregate particles are coated with a precisely specified volume of cement paste. The volume is characterised by being insufficient to fill the void fraction between the aggregates. This relation between the cement paste volume and the natural porosity is defined as the degree of filling (DF). After curing the permeable concrete is highly porous and the voids have formed interconnected channels allowing air transport. An idealisation of the principle is illustrated in figure 2.11, showing the coated aggregates bridged by layers of cement paste [10].

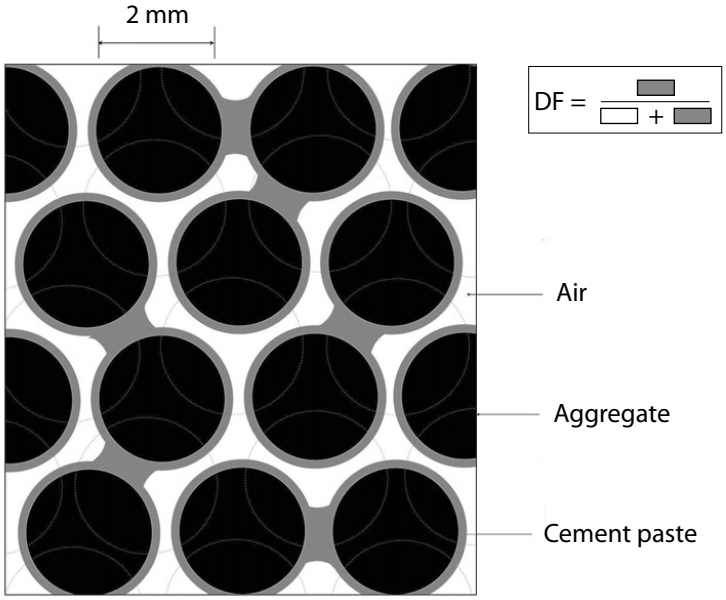

Fig. 2.11. Idealisation of the interconnected channels in permeable concrete [10].

The mechanical strength of permeable concrete cannot be predicted with Bolomey's formula due to its complexity. It is obviously still related to the w/c ratio and also the degree of filling. However, a relation depending on these parameters is not developed elsewhere and will be beyond the scope of this study.

Phase change materials 3

A phase change material (PCM) is a material with a high heat of fusion which, melting and solidifying at a specific temperature, is capable of storing and releasing large amounts of energy, respectively. Heat is absorbed or released when the material changes from solid to liquid and vice versa. PCM or thermal salts are latent energy storage materials and they use chemical bonds to store and release the heat. The material absorbs a large amount of energy (or heat) in the process of melting and this result in thermal stabilisation of the surroundings.

As mentioned in the state-of-the-art, three methods of PCM incorporation exist - direct incorporation, immersion and encapsulation [24]. For permeable concrete only direct incorporation and encapsulation is a possibility because immersion will fill the interconnected channels and pores intended for air transport. For this study it is chosen to use micro-encapsulated paraffin wax from BASF. The coating is an acrylic polymer shell, as shown in figure 3.1 (right).

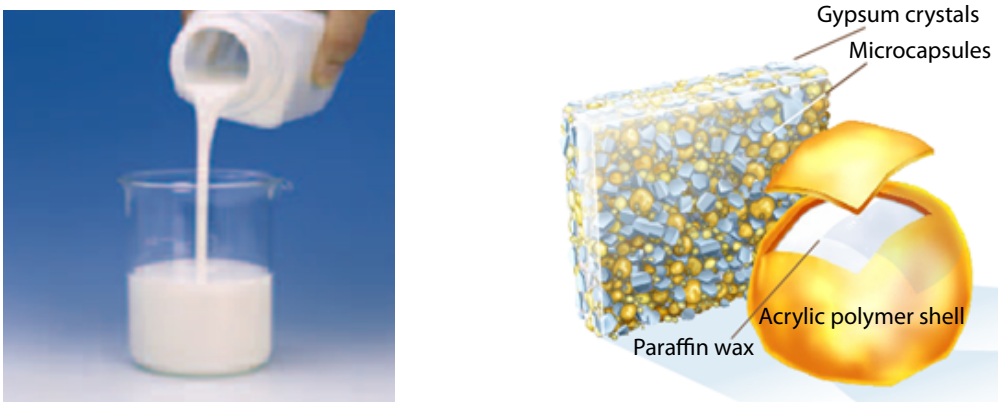

Fig. 3.1. Suspension with PCM solid (left) and close-up illustration of the paraffin wax encapsulated in an acrylic polymer shell (right).

The micro-encapsulated PCM is manufactured in a liquid suspension, where the acrylic polymer is applied to the paraffin wax. For application in the displayed gypsum board (example) the suspension must be dried out. However, when added to a concrete mixture this is unnecessary, so the original liquid like shown in fiugre 3.1 (left) is used. Simultaneously this is beneficial in order to avoid agglomeration of the microscopic PCM particles.

PCM is intended for use in buildings are designed so the phase changes, melting and

solidifying, occur within the range of thermal comfort. This enables storage of excess heat before the temperature rises to a discomfortable level. In figure 3.2 the enthalpy curves for the used PCM are shown.

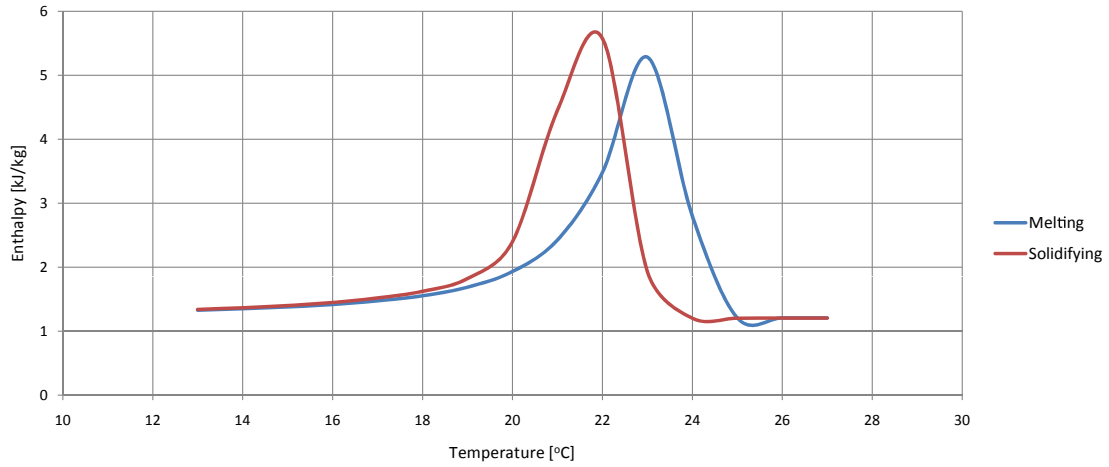

Fig. 3.2. Enthalpy curves for PCM in the temperature range of melting and solidifying.

The figure reveals that the PCM is capable of storing and releasing large amounts of energy around 22-23 °C with a peak enthalpy of almost five times the normal value. Thus, it constitutes as a promising way of increasing the thermal mass dampening temperature fluctuations.

Air permeable concrete criteria 4

Permeable concrete is a fairly new concept in the building sector and various possibilities of application has been highlighted in the state-of-the-art. The mostly described in the literature is implementation as dynamic insulation or breathing walls, functioning as a fresh air supply, filter and heat exchanger. However, this study will only consider the energy performance of the concrete, with regard to the dynamic heat exchanger efficiency. The dynamic mode refers to daily cycles of heat exchange, which is in common with the breathing wall concept. More about the permeable concrete criteria, functional requirements and ideas for implementation in buildings will follow subsequently.

The concept idea is to utilise the thermal mass for storage of excess heat produced in office buildings during working hours and release the energy again during night as a passive cooling solution. The discharged concrete is then ready to absorb energy again in a new daily cycle. The concept of storing heat in heavy building materials is not revolutionary and this already helps to dampen temperature fluctuations in many buildings. The new part is the use of permeable concrete with forced air transport, enabling activation of the entire thermal mass. This brings the element of heat exchange into focus. An illustration of the concept is shown in figure 4.1.

The internal building air is constantly circulated through the permeable concrete. Initially, at the beginning of working hours, the concrete is around 20 °C. During the day the building air temperature is gradually rising due to internal gains. The energy is exchanged with and gradually heating the concrete, resulting in a colder air outlet. The goal is a 12 h charge period ending with an energy saturated concrete and air within range of acceptable thermal comfort temperature of typically 26 °C. At this point the cycle is changed, for the purpose of discharging the heat again. If the building has a heating demand over night the heat can be released here and alternatively natural ventilation can be applied and the excess heat discharged with cold outdoor air. At the beginning of working hours a new cycle can begin.

The system will function at low velocities, which also induce a low pressure drop and a low SFP-value (Specific Fan Power) for the fan driving the circulation. This is important because the permeable concrete concept is suggested as a separate air system, which means energy is already used for the traditional mechanical ventilation system supplying the fresh air. According to the building regulations, only a certain amount of electric energy can be used to drive the air, which is expanded to include two systems with the concept.

The permeable concrete system is thought as a core structure in the center of a typical rectangular office building, possibly containing technical services. However, the goal is load bearing concrete, so it may also be integrated in the additional structure.

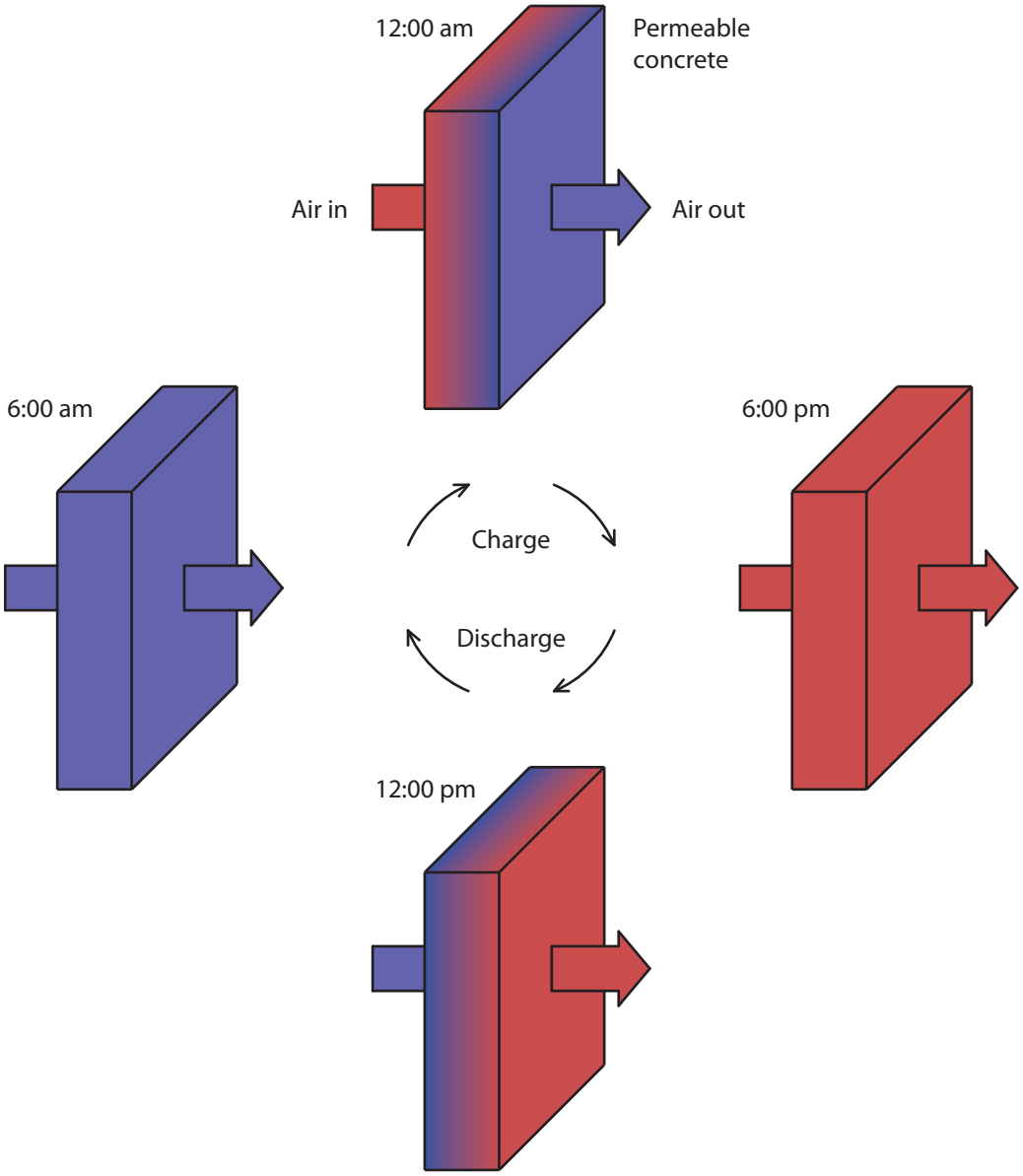

Fig. 4.1. Concept of permeable concrete with air transport as thermal mass in a daily cycle. During office hours the concrete is gradually heated due to storage of excess heat. The opposite occurs when the concrete is discharged with cold night air.

4.1 Initial performance potential evaluation

In order to evaluate the implementation and performance potential of permeable concrete, the heat storage ability will be estimated in the following. The estimate is based on some assumptions on how the concrete is affected by heat transfer and temperature distributions. Finally this performance will be compared with traditional concrete and an estimated COP-value using the energi delivered to the concrete in relation to the electrical power needed for transporting the air will be presented.

To be able to illustrate the effect of using air permeable concrete, a concrete wall with a thickness of 200 mm is used. With this thickness it is not possible, using EN ISO 13786

(Thermal performance of building components) as calculation tool [41], to activate the entire thermal mass in traditional concrete in a 24 h cycle of heating and cooling. The program used for this initial evaluation is performance_ini.m, which can be seen on the [Enclosures-CD, Matlab folder].

The estimate will be calculated as a result of a 12 h period of keeping an environment at a comfortable temperature level. It is the work day scenario of an office building, where extensive internal heat gains are present during the working hours.

4.1.1 Assumptions

As mentioned, this initial performance calculation of air permeable concrete is based on a few assumptions. The first assumption is that the concrete element is treated as just one object for the sake of simplicity. This means that the energy transferred or extracted by the air is transferred or extracted equally to the entire object. The extract scenario is illustrated in figure 4.2.

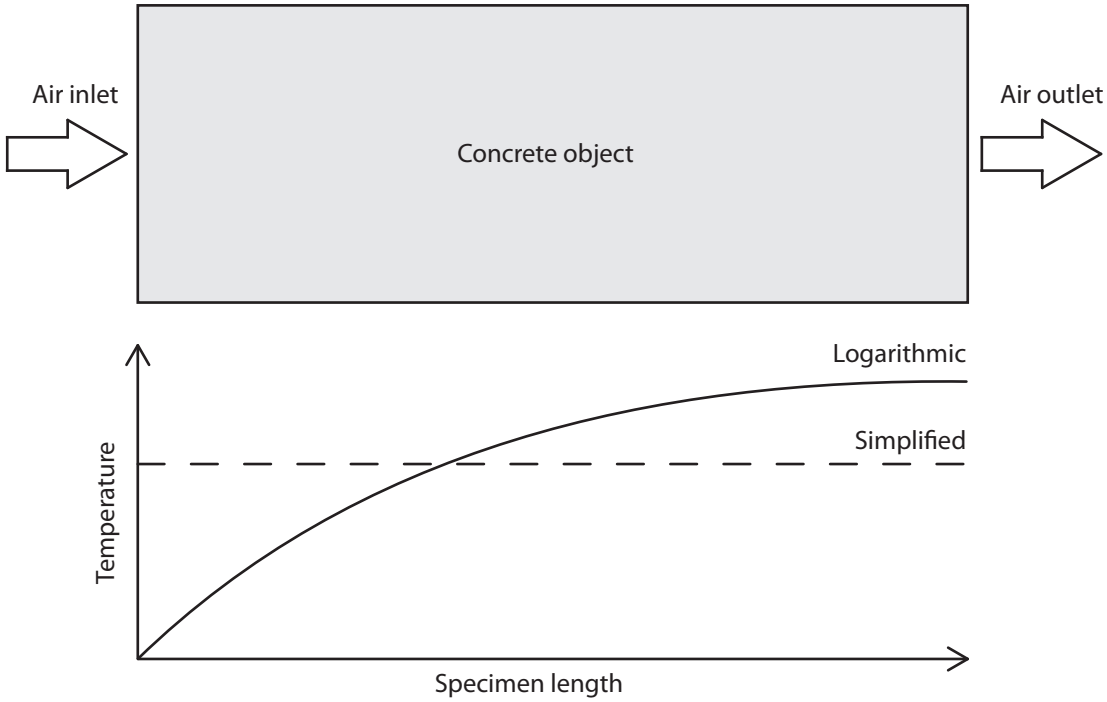

Fig. 4.2. Concrete temperature and energy transfer distribution through an air permeable concrete element.

When the transferred energy is evenly distributed in the entire concrete element, this means that the temperature will change evenly as well, illustrated in figure 4.2 (bottom). In reality it will follow a logarithmic function, because as the air transfers energy to the concrete the temperature difference between the air and the concrete decreases accordingly making the heat transfer decrease.

Another assumption is, that the air temperature is constant during the 12 h period.

4.1.2 Performance calculation

This calculation is a 12 h simulation of the concrete temperature. The concrete element is treated as a heat exchanger with one medium flowing through it. Depending on the efficiency of the heat exchanger (η_e), the air temperature will, when having passed through the concrete, have the same temperature as the concrete (corresponding to $\eta_e = 1.00$). However this might not be possible, for which reason this factor of efficiency is included in the calculation. In equation 4.1 the air temperature after the heat exchanger is calculated based on selected efficiencies.

$$T_{out,n} = T_{air} - \eta_e \cdot (T_{air} - T_{c,n}) \tag{4.1}$$

Where:

$T_{out,n}$	Air temperature after passing through concrete wall in the n'th time step [°C]
T_{air}	Air temperature before entering concrete wall [°C]
η_e	Heat exchanger efficiency [-]
$T_{c,n}$	Temperature of the concrete wall in the n'th time step [°C]

When the temperature difference of the air is known, the energy delivered by the air to the concrete can be calculated. This is done in equation 4.2, where the time step resolution is defined also.

$$E_{air,n} = \rho_{air} \cdot c_{p,air} \cdot q_v \cdot (T_{air} - T_{out,n}) \cdot t \tag{4.2}$$

Where:

$E_{air,n}$	Energy delivered to the wall by the air in the n'th time step [J]
ρ_{air}	Density of air [kg/m^3]
$c_{p,air}$	Specific heat capacity of air [J/kg K]
q_v	Air flow rate [m^3/s]
t	Time step resolution [s]

The energy transferred to the concrete is then transformed to a temperature increase. An illustration of the development from time step to time step is shown in figure 4.3.

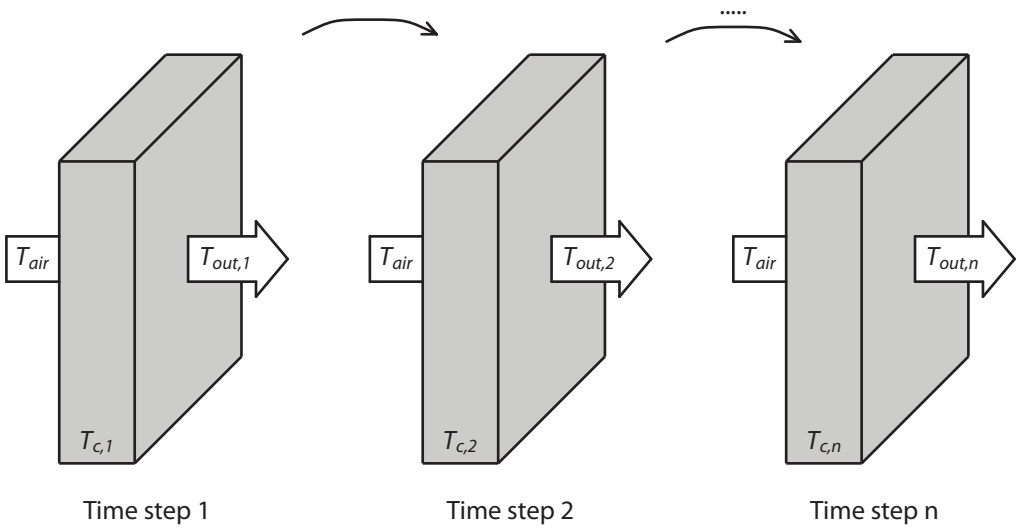

Fig. 4.3. Physical development through the time steps.

Equation 4.3 calculates the new concrete temperature after the present time step.

$$T_{c,n+1} = \frac{E_{air,n}}{c_{p,con} \cdot m_{con}} + T_{c,n} \tag{4.3}$$

Where:

$T_{c,n+1}$	Concrete wall temperature in the n'th+1 time step [°C]
$c_{p,con}$	Calculated mean specific heat capacity of concrete [J/kg K]
m_{con}	Mass of concrete wall [kg]

The total transferred amount of energy to the concrete can be calculated by taking the sum of E_{air} for all time steps. In the following section the results of the calculation will be presented.

4.1.3 Performance results

The calculations have been conducted with a time step resolution of 10 s in a 12 h period. The results will be presented in figures where the air flow and the time will be the variables on the x-axis and the heat storage effectiveness (η_s) will be on the y-axis. The heat storage effectiveness is defined as the fraction of the thermal mass utilised in a cooling or heating period.

The heat transfer coefficient is dependent of the air flow through the concrete, for which reason it is important which air flow is necessary for a given case. In figure 4.4 the influence of the air flow on the heat storage effectiveness is shown.

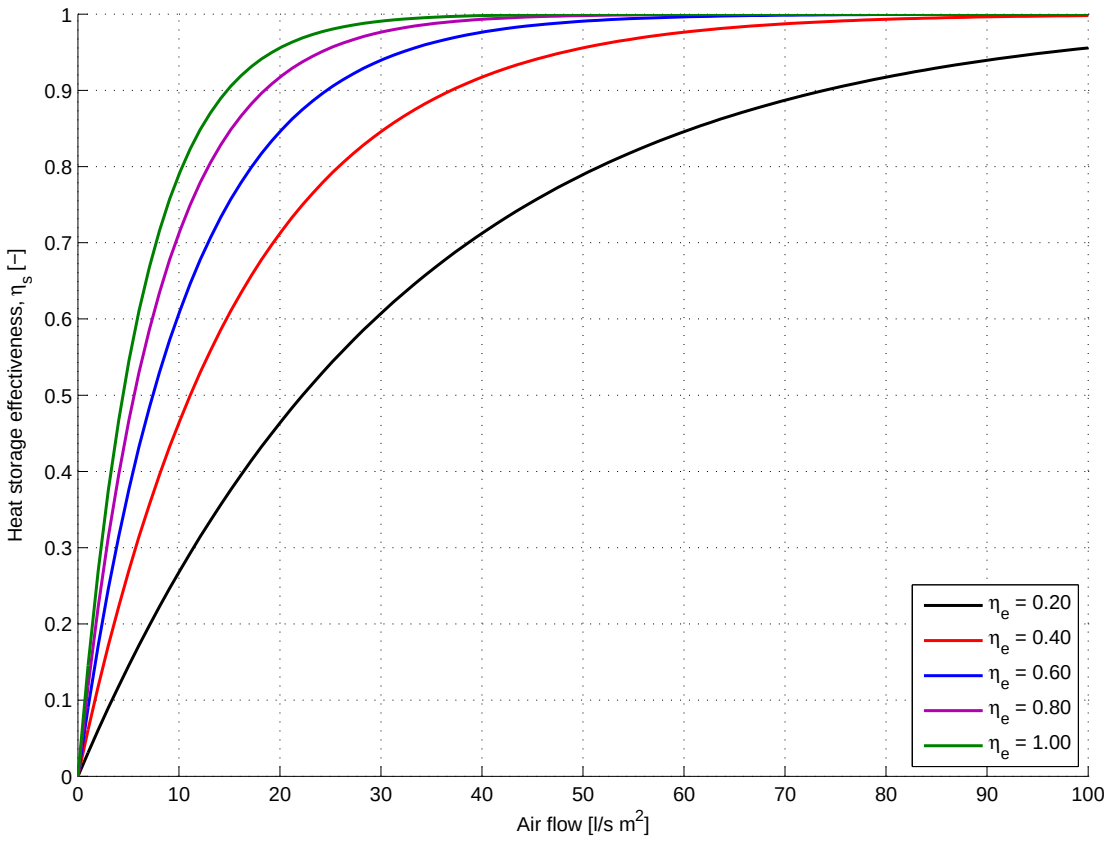

Fig. 4.4. Heat storage effectiveness after 12 h as a function of air flow, where the heat exchanger efficiency is presented by individual values.

It is very clear that the heat exchanger efficiency has a great influence on the effectiveness of the heat storage. To achieve an effectiveness of 0.90 with an η_e of 0.20 an air flow of approximately 75 l/s m^2 is necessary, where only 18 l/s m^2 is enough with an η_e of 0.80. Another finding is, that a minimum air flow of 10 l/s m^2 is necessary to achieve fairly high effectiveness', and with an η_e of ≥ 0.60 air flows above 30 l/s m^2 will not increase η_s much.

For the next scenario the air flow is chosen to be constant at the value of 15 l/s m^2 and time will be the varying parameter. The result is shown in figure 4.5.

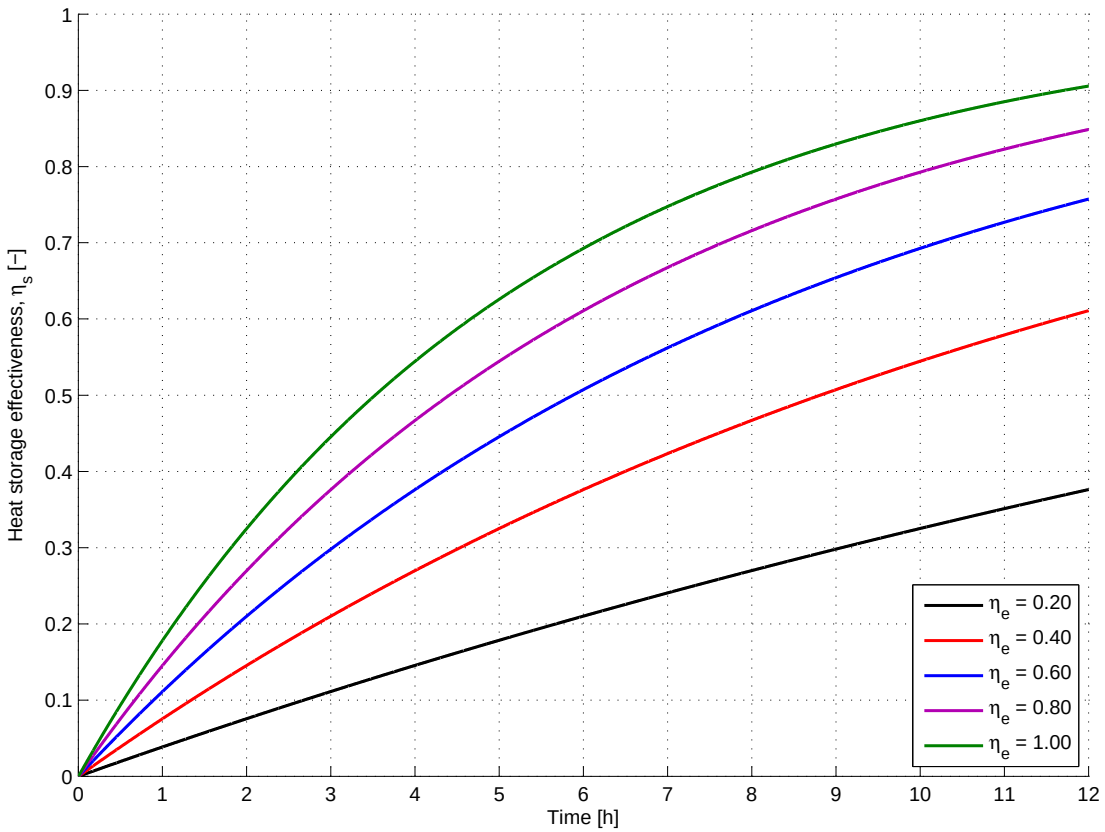

Fig. 4.5. Heat storage effectiveness as a function of time, where the heat exchanger efficiency is presented by individual values. Air flow rate 15 l/s m^2.

As previously mentioned, the time period is chosen to be 12 h because the remaining hours of the day should then be used to discharge the stored energy again. It is clear that it is necessary to have a high temperature efficiency in order to utilise a large part of thermal mass in a 12 h period with the given parameters. If η_e is 0.80 it takes approximately 4.5 h to heat or cool the concrete half of the temperature difference between the air and the concrete.

4.1.4 Comparison with traditional concrete

In a study made by Nikolai Artmann [3] the theoretical dynamic heat capacity of traditional concrete is calculated over a 24 h cycle of heating and cooling. In figure 4.6 this result is shown as a function of the heat transfer coefficient.

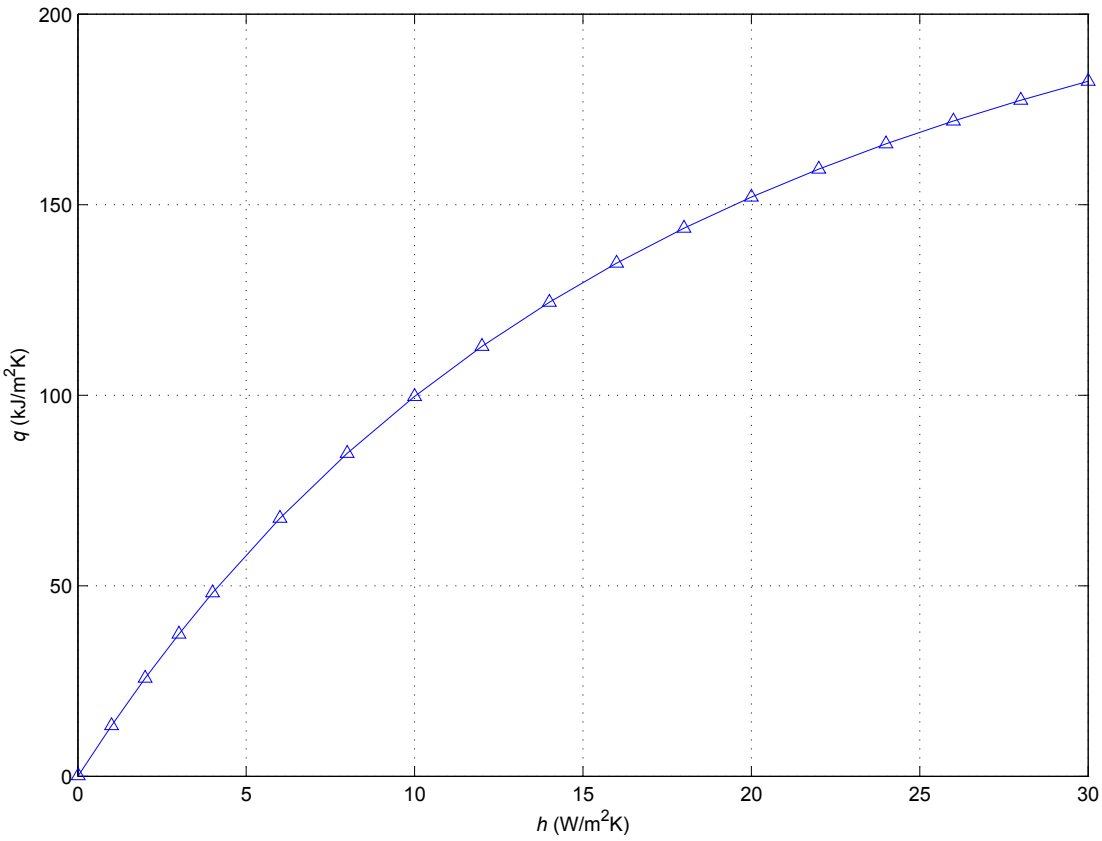

Fig. 4.6. Dynamic heat capacity (q) of traditional 200 mm concrete depending on the heat transfer coefficient (h).

For the comparison with air permeable concrete it is chosen to use a heat transfer coefficient of 10 W/m^2 K, approximately 5 W/m^2 K from radiation and 5 W/m^2 K from convection. This gives a heat capacity of 100 kJ/m^2 K. As this value is based on a 24 h cycle of heating and cooling and the comparison is for only heating, a 12 h period of heating is used calculating the heat capacity for the air permeable concrete.

To calculate the heat capacity of the air permeable concrete an air flow of 15 l/s m^2 and a heat exchanger efficiency of 0.80 is used as reasonable estimates. With these values the total amount of transferred energy, or the dynamic heat capacity, is 281 kJ/m^2 K, which is a factor 2.81 higher than for the traditional concrete.

This value is very dependent of the two chosen parameters for this calculation, so if either of them is decreased the heat capacity will decrease accordingly.

4.1.5 Coefficient of performance

As a part of this potential evaluation of air permeable concrete, it is important to assess whether it could be an energy efficient solution for office buildings. As example the coefficient of performance (COP) for heat pumps is up to 4-5, which is very efficient. For this reason the COP for this type of concrete must be higher in order to compete which

such devices and others.

In section 4.1.4 the dynamic heat capacity of air permeable concrete is found to be 281 kJ/m^2 K with an air flow of 15 l/s m^2 and a heat exchanger efficiency of 0.80. This value will be used to compare with the energy needed to drive the air flow rate.

Imbabi et al. found that values in permeability of 0.18-0.60 m^2/Pa h are obtainable and these values are used as reference for the electrical power needed to drive the wanted air flow rate. The pressure difference needed is calculated with Darcy's law, see equation 4.4.

$$\Delta p = \frac{A}{q_v} \cdot \frac{L}{\kappa} \tag{4.4}$$

Where:

Δp	Pressure difference across object [Pa]
A	Inlet surface area [m^2]
q_v	Air flow rate [m^3/s]
L	Thickness of treated object [m]
κ	Permeability [m^2/Pa h]

The pressure difference is the only variable used in this scenario, so the electrical energy needed to drive the air can be calculated from equation 4.5. The fan efficiency is set to 0.80.

$$E_p = \frac{\Delta p \cdot q_v}{\eta} \cdot t \tag{4.5}$$

Where:

E_p	Electrical power [J]
η_f	Fan efficiency [-]
t	Time [s]

The coefficient of performance can now be calculated from the energy transferred to the concrete in relation to the energy used to drive the air, shown in equation 4.6.

$$COP = \frac{E_{con}}{E_p} \tag{4.6}$$

Where:

COP	Coefficient of performance [-]
E_{con}	Energy transferred to concrete element [J]

With values of 0.18, 0.32 and 0.60 m^2/Pa h in permeability and a 12 h period, COP-values of 5.8, 10.3 and 19.3 are calculated. These values are very satisfactory as they are all higher than the 5.0 for heat pumps. The relation between permeability and COP, when all other parameters are constants, are linear and visualised in figure 4.7. To calculate this COP the program COP.m are used, which can be seen on the [Enclosures-CD, Matlab folder].

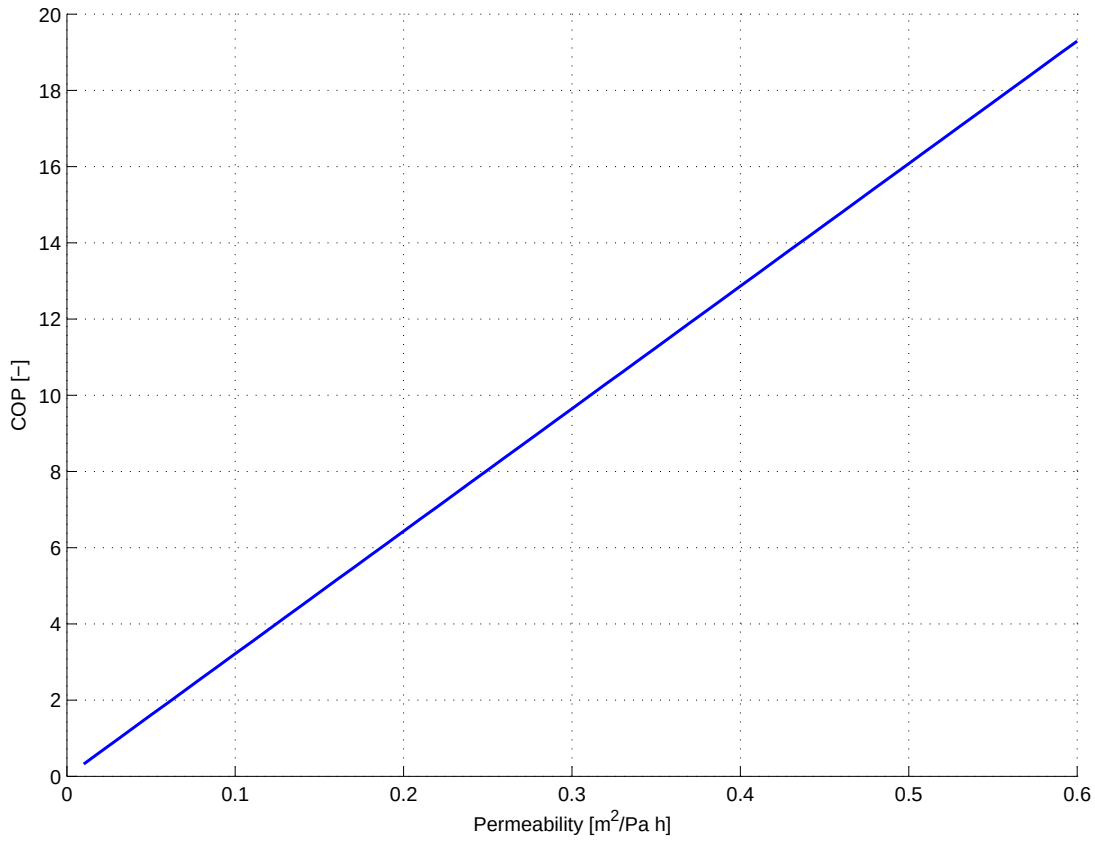

Fig. 4.7. Calculated COP-value as a function of permeability.

It is interesting that a value higher than approximately 0.15 in permeability gives a COP > 5.0. This estimates that relatively small permeabilities (> 0.15) can generate fairly high COP-values.

5 Mathematical models

Combining theory with practice requires a number of mathematical models to predict and estimate experiment outcomes. These models will be described using theory and in later sections missing factors will be added and the models tested, possibly adjusted. The models span from predicting compressive strength and permeability to estimating temperature profiles through a concrete specimen. In several cases certain factors have to be added after measurements are conducted in order to adjust the models to fit with this type of concrete.

5.1 Prediction of compressive strength and air permeability

In this section mathematical models for prediction of the compressive strength and permeability will be developed. For these models to work measurement data has to be included, adjusting factors making the models precise for this type of concrete, though only using ingredients corresponding to this study.

The parameter which will be the variable in these models is the density of the concrete specimens. Basically it will be possible, with reasonable certainty, to calculate a compressive strength and permeability from a calculated density. In section 5.1.1 it is described how the density is calculated based on known parameters. In chapter 12 these models will be reconsidered and adjusted to fit the measured data and compared with the measurements.

5.1.1 Density calculation

The theoretical density is calculated from the ingredients' density and their volume fraction in the concrete. This model includes SPA but does not include PCM, because there are not sufficient data to support a PCM model. Equation 5.1 shows the density calculation of air permeable concrete.

$$\rho_{APC} = \phi_c \cdot \rho_c + \phi_w \cdot \rho_w + \phi_{SPA} \cdot \rho_{SPA} + \phi_a \cdot \rho_a \tag{5.1}$$

Where:

ρ_{APC}	Density of air permeable concrete [kg/m^3]
ϕ_c	Volume fraction of cement [-]
ρ_c	Density of cement [kg/m^3]
ϕ_w	Volume fraction of water [-]
ρ_w	Density of water [kg/m^3]
ϕ_{SPA}	Volume fraction of SPA [-]
ρ_{SPA}	Density of SPA [kg/m^3]
ϕ_a	Volume fraction of aggregate [-]
ρ_a	Density of aggregate [kg/m^3]

In order to calculate ρ_{APC} all the volume fractions must be found. The densities of the ingredients are known beforehand. The volume fraction of aggregate is calculated from the natural porosity of the aggregate, which for this study is 0.402. The natural porosity is the fraction of void in the aggregate. The fraction of aggregate material, or the natural packing density, must be 0.598 accordingly.

The volume fractions of cement and water are calculated in equations 5.2 and 5.3.

$$\phi_c = \frac{NP \cdot DF - \phi_{air} - \phi_{SPA}}{1 + (w/c) \cdot \frac{\rho_c}{\rho_w}} \tag{5.2}$$

$$\phi_w = (NP \cdot DF - \phi_{air} - \phi_{SPA}) \left(1 - \frac{1}{1 + (w/c) \cdot \frac{\rho_c}{\rho_w}}\right) \tag{5.3}$$

Where:

DF	Degree of filling [-]
ϕ_{air}	Volume fraction of air in the cement paste [-]
(w/c)	w/c ratio [-]

The volume fraction of SPA is still unknown and is impossible to calculate without iterations. To solve this issue a data spread sheet with SPA volume fractions are made and the outcome is a plot, shown in figure 5.1 where it is possible to read the volume fraction in question. This reading needs the w/c ratio, degree of filling and the wanted SPA contents in % by weight of the cement contents.

The plot contains calculated data of w/c ratio and degree of filling used in this study and an expanded SPA content to cover the maximum content of 2 % suggested by the manufacturer BASF. With this volume fraction in place a complete model for calculation of a theoretical density is developed.

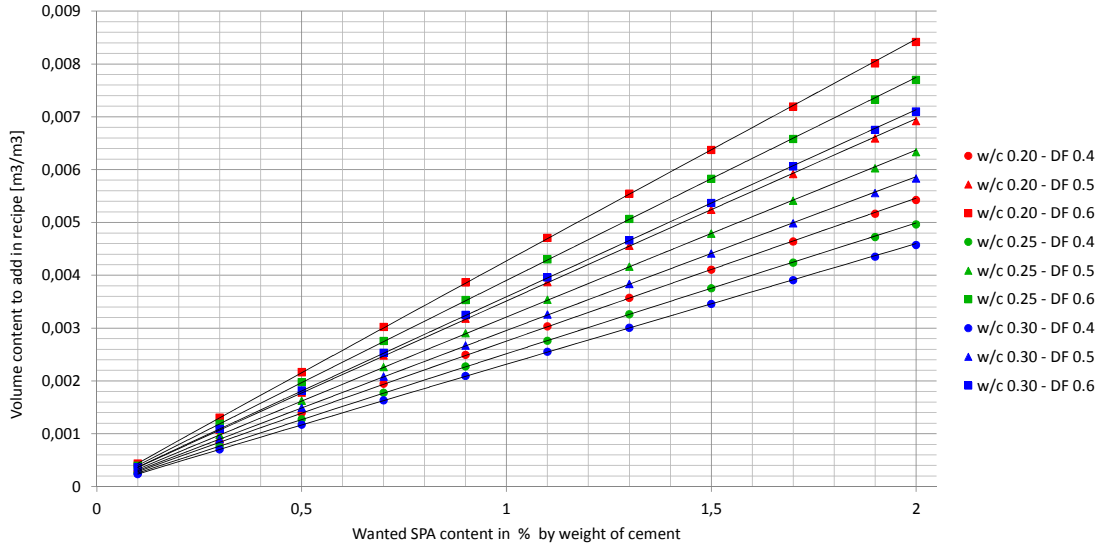

Fig. 5.1. Plot of SPA volume fraction depending on the degree of filling, w/c ratio and the wanted SPA content in % by weight of the cement content.

5.1.2 Compressive strength

The model to predict the compressive strength based on the density is thought to be a 1st order polynomial, because it is believed that the relation between these two parameters is linear. The reason for this is that this type of concrete has a degree of filling (strongly correlated with density) below 1.0, for which reason more or less cement paste must have a direct impact on the compressive strength. It might be necessary to introduce a function for each w/c ratio used, as the effect of this is unclear. An increase of the w/c ratio should weaken the concrete, but whether this effect overlaps with a decrease in degree of filling is considered very uncertain. The suggested equation is shown in equation 5.4.

$$f_{ck} = a \cdot \rho_{APC} + b \tag{5.4}$$

Where:

f_c	Mean compressive strength [MPa]
a	Factor based on measurements [-]
b	Factor based on measurements [-]

To fit the data to a function, in this case a 1st order polynomial, the method of least squares regression is used. In this way there will be an indication of how good the function fits and based on that result, if bad, it might be necessary to change the function.

5.1.3 Permeability

The permeability model is believed to follow a different function than a 1st order polynomial because of the flow characterisation, which is necessary to determine the

permeability from measured data. Calculation of permeability is treated in section 7.3. Air flow and corresponding pressure difference has a relation which follows a power function. If the flow is fully laminar the pressure exponent will be 1.0. Because of this relation it is believed that this model must be a power function as well and in equation 5.5 the model is shown. The model contains two constants, which will be found from a fit using least squares regression.

$$\kappa = k \cdot {\rho_{APC}}^{n} \tag{5.5}$$

Where:

κ	Permeability [m^2/Pa h]
k	Factor based on measurements [-]
n	Factor based on measurements [-]

A lot of factors have an impact on the permeability, like the size of interconnected channels or a bad cross-sectional area where the pressure loss is much higher than in the rest of the specimen. Due to these uncertainties the model described is the best estimate of the outcome of the measurements.

5.2 Prediction of static heat transport

When considering thermal conductivity, this value is related to the volume fraction of a material's components. For air permeable concrete these are aggregate, cement paste and the air which fills the voids. In this section a model to predict the thermal conductivity of air permeable concrete will be presented, starting with general theory and afterwards introducing a model made by Imbabi et al. The model will also be applied in this study. [10]

General heat transfer by conduction is divided into two types of heat transfer parallel and series heat conduction. These are sometimes used individually depending on the objective of the system. A normal outer building wall, where the heat conduction is aimed to be as low as possible, is built with materials in series. If the heat is going from a to b through a series heat transfer the same amount of energy has to go through every material in the construction, whereas with parallel heat transfer this can vary. The two types are illustrated in figure 5.2.

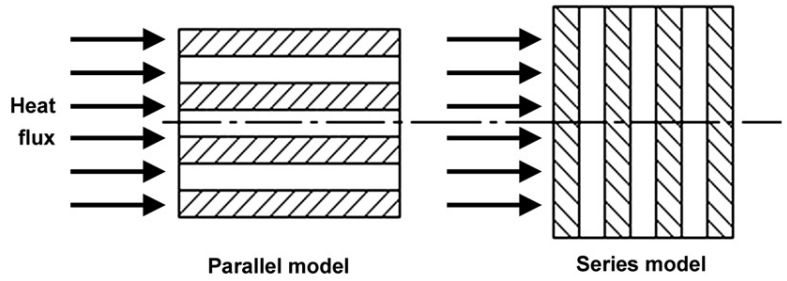

Fig. 5.2. Illustration of the concept of parallel and series heat flow [10].

If an inhomogeneous material is analysed it can contain both types of heat transfer in different fractions. In a general concrete with relatively large aggregates it is hard to tell if parallel or series heat transfer are the dominant type. This can be done be setting up a model for the material, containing equations from both types and adjusting their fraction according to conducted measurements of λ-values on the material. The equations for parallel and series heat conduction are shown in 5.6 and 5.7.

$$\lambda_p = \phi_1\lambda_1 + \phi_2\lambda_2 + \ \ldots \ + \phi_n\lambda_n \tag{5.6}$$

$$\lambda_s = \frac{\lambda_1\lambda_2 \ \ldots \ \lambda_n}{\phi_2\lambda_2\lambda_3 \ \ldots \ \lambda_n + \phi_2\lambda_1\lambda_3 \ \ldots \ \lambda_n + \phi_n\lambda_1\lambda_2 \ \ldots \ \lambda_{n-1}} \tag{5.7}$$

Where:

λ_p	Parallel thermal conductivity [W/mK]
λ_s	Series thermal conductivity [W/mK]
$\phi_{1,2,3..n}$	Fraction of the material [-]
$\lambda_{1,2,3..n}$	Thermal conductivity of the material [W/mK]

Considering air permeable concrete, it is clear that it is an inhomogeneous material containing aggregates, cement paste and voids (air). This means that a model to predict the thermal conductivity needs both equations at some fraction to function. This fraction of parallel and series heat transfer is the unknown factor when attempting to calculate the conductivity and measurements are necessary to verify a model. A general assumption of the heat flow through air permeable concrete is shown in figure 5.3. In this illustration it is assumed that the aggregates have the largest thermal conductivity followed by the cement paste and the least conductive material is the stagnant air.

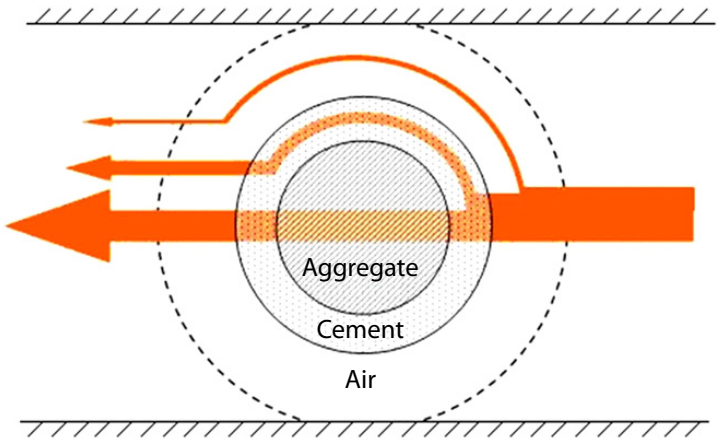

Fig. 5.3. Illustration of heat flow fraction through the materials in air permeable concrete [10].

This is a very simplified assumption, but shows that a model containing both parallel and series heat transfer is necessary. A developed model, based on air permeable concrete, will be presented and verified by measurements.

5.2.1 Thermal conductivity model

Imbabi et al. [10] developed a model for predicting the static thermal conductivity, based on the measurements conducted in their study and it proved very accurate. The model is not experimentally validated for a degree of filling under 0.5, but theoretically it can be used for air permeable concrete with a degree of filling between 0 - 1.0. According to their findings, the main factors which influences the thermal conductivity is the volume fractions of the concrete components, their conductive properties and the w/c ratio of the cement paste. In figure 5.4 an analogy network model is showing how the heat transfer through air permeable concrete is considered.

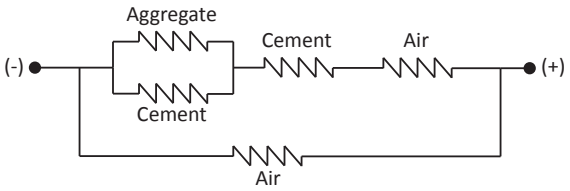

Fig. 5.4. An electrical analogy network model showing the heat flow in air permeable concrete [10].

This model shows the multiple heat flow pathways which are possible. Air to air, air to cement paste and air to cement to aggregate are the possibilities, where the largest part of the heat flow will go through the aggregate, as it has the largest thermal conductivity. The concrete consists of voids and solids, where solids is treated as a composite and an equation for calculating the conductivity using these two fractions are shown in 5.8.

$$\lambda = \varphi_v \lambda_v + \varphi_s \lambda_{composite} \tag{5.8}$$

Where:

λ	Thermal conductivity of air permeable concrete [W/mK]
φ_v	Volume fraction of voids [-]
λ_v	Thermal conductivity of voids [W/mK]
φ_s	Volume fraction of solids [-]
$\lambda_{composite}$	Combined thermal conductivity (makro air pockets, aggregate and cement paste) [W/mK]

When the medium in the porous material is air, and air is a very poor conductor, a large part of the heat will go through the solids. This part is believed to be sufficiently large to ignore the conduction through the air. The volume fraction of the solids, aggregate and cement paste is expressed in equation 5.9.

$$\varphi_s = \varphi_a + \varphi_c \tag{5.9}$$

Where:

φ_a	Volume fraction of aggregates [-]
φ_c	Volume fraction of cement paste [-]

From figure 5.4 and equations 5.6 and 5.7 the thermal conductivity for the solids ($\lambda_{composite}$) can be written as equation 5.10.

$$\lambda_{composite} = (\varphi_a \lambda_a + \varphi_c \lambda_c) + \frac{\lambda_c \lambda_v}{\varphi_v \lambda_c + \varphi_c \lambda_v} \tag{5.10}$$

Where:

λ_a	Thermal conductivity of aggregates [W/m K]
λ_c	Thermal conductivity of cement paste [W/m K]

Gathering these equations in equation 5.8 and assuming that the material is dry, the expression for heat conduction through air permeable concrete yields as shown in equation 5.11.

$$\lambda = (\varphi_a + \varphi_c) \left((\varphi_a \lambda_a + \varphi_c \lambda_c) + \frac{\lambda_c \lambda_v}{\varphi_v \lambda_c + \varphi_c \lambda_v} \right) \tag{5.11}$$

This model have been checked by holding results against measurement data and it has proved to be accurate [10]. Based on the obtained results in their study, this developed model will be used in this study. If it is possible to reproduce their air permeable concrete specimens the model will work, but if not it might be necessary to adjust the model according to the results obtained later in this study.

5.3 Prediction of concrete and air temperature profiles

A numerical model is built to predict the concrete temperature profile and air temperature profile. From the result of running this model the dynamic heat capacity can be calculated. The model is developed for cylinders which correspond with the specimens used to measure heat exchanger efficiency.

It is a one-dimensional explicit model which handles energy changes and contributions inside air permeable concrete for a given amount of time steps. The energy contributions inside the concrete are heat conduction, convection and radiation. Due to the deliberate air flow, convection is forced. According to [42] the effect of natural convection will become significant only if the voids have diameters larger than 1 cm. Radiation between the different materials will only be important when working with temperatures well above ambient. Since void diameters in air permeable concrete lie in the range of 0.5-5 mm and the material operates at or near ambient temperatures, natural convection and radiation is not included in the model [10].

The energy balance for a section of the concrete specimen is shown in equation 5.12.

$$\Delta E_c = E_{conv} + E_{cond} \tag{5.12}$$

Where:

ΔE_c	Energy change in the concrete [J]
E_{conv}	Energy contribution from convection [J]
E_{cond}	Energy contribution from conduction [J]

The energy balance in the concrete depends on the temperature change there might be from one time step to the next. In equation 5.13 this relation is shown.

$$\Delta E_c = c_{p,c} \cdot m \cdot \Delta T \tag{5.13}$$

Where:

$c_{p,c}$	Specific heat capacity of the concrete [J/kg K]
m	Mass of concrete [kg]
ΔT	Temperature change in the concrete between time steps [K]

Energy transferred from thermal conductivity is calculated using equation 5.14, where an energy contribution is calculated on the basis of the length of the time step used, the length between points or sections and a temperature difference.

$$E_{cond} = \lambda \cdot L \cdot \Delta T \cdot t \tag{5.14}$$

Where:

λ	Thermal conductivity [W/m K]
L	Length between points or sections [m]
ΔT	Temperature difference between points or sections [K]
t	Length of time step [s]

The contribution from convection is shown in equation 5.15. In this equation the convective heat transfer coefficient is included in order to calculate an air temperature in each section through the specimen. The size of the heat transfer coefficient is iterated until the temperature of the outlet air is equal to the later measured temperatures. Normally the unit is W/m^2 K, but the inside surface area of the concrete is unknown, so the unit used in the model is changed to W/K.

$$E_{conv} = h \cdot \Delta T_1 \cdot t = q_v \cdot c_{p,air} \cdot \rho_{air} \cdot \Delta T_2 \cdot t \tag{5.15}$$

Where:

h	Convective heat transfer coefficient [W/K]
ΔT_1	Temperature difference between the concrete and the air [K]
ΔT_2	Temperature difference of the air between two points [K]

In the model the specimen will be divided in sections of equally sized pieces, which will not decrease the accuracy of the model as the sample is one inhomogeneous material and only one dimension is used. The listed equations are discretised in time and space to fit the explicit model. The discretisation in space is illustrated in figure 5.5.

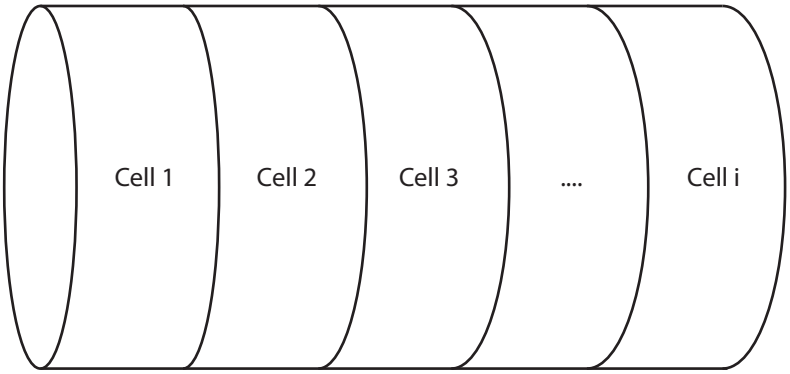

Fig. 5.5. Illustration of the decretisation of space for the explicit model.

This explicit scheme is stable within the range specified in equation 5.16.

$$\Delta t < \frac{\rho \cdot c_p \cdot (\Delta x)^2}{2 \cdot \lambda} \tag{5.16}$$

As this equation depends on the number of sections the specimen is divided into, the necessary time step discretisation will vary during different presentations in the results, section 15.2. Here it will be further explained which temperatures are used in which equations and for what purpose, which time steps are used and so on.

Part III

Air permeable concrete - Experimental, results and discussion

Concrete specimens 6

This part of the study deals with casting of air permeable concrete and the corresponding measurements. From the results the basic material properties can be calculated - density, compressive strength and permeability. Measurement procedures, data treatment, uncertainties and results will be presented as well as an analysis of these parameters and how they interact.

The element of casting is treated in this chapter, where the process of developing a method for casting air permeable concrete will be described, together with experiences, examples of recipes and the effect various parameters have on the cast specimens. Initial experiments and choices will briefly be explained and further descriptions can be found in appendix A.

6.1 Concrete mixing, casting and curing

From the literature it was found which parameters are important when designing air permeable concrete in relation to both performance, permeability and strength [1], [9], [10]. This knowledge formed the basis for casting initial test specimens, from which experience with mixing procedures and curing was gained. A detailed description of the whole process of casting air permeable concrete specimens can be found in appendix A.

The mixing procedure starts by carefully weighing all the needed ingredients. The aggregate is completely dry, for which reason it is necessary to mix with water for 10 min to make it water saturated. The amount of water needed, or the absorption of the aggregate, is set to 0.4 % by weight aggregate. Afterwards the cement is added and the mixture is mixed for another 2 min. Now that all the dry materials are added, water and SPA can be added. Finally the concrete is mixed for another 10 min and it is ready to cast.

Initial test specimens were cast using cylindrical moulds of the size 60 mm in diameter and 120 mm in height. When the study reached the parameter variation phase, large moulds of the size 100 mm × 200 mm were utilised. The process of casting is described in appendix A.4. The concrete is filled in the moulds, which are vibrated twice, the latter with a counterweight on top of the mould to ensure the top layer the same vibration as the bottom, and then closed. The weight of the counterweight is approximately 0.5 kg. If the weight is too heavy the vibration is not very effective because the particles cannot move freely into space. A too light weight is has no effect.

After approximately 24 hours the specimens are demoulded. For the curing stage it is important that this takes place in a water saturated environment, so the water will

not evaporate but react with the cement. Initially this was tested in a water bath, but unfortunately this leads to the deposit of salt (calcium hydroxide) on the surface of the specimens. The deposit is unfortunate as it could interfere with subsequent measurements, where the pores intended for air transport might be blocked. The salt could possibly be removed with acid, however there is no guarantee that everything is removed from inside the specimen and the interconnected channels. The second method tested was curing the specimens in plastic bags, which revealed no down sides and was chosen as curing method in the study.

As a preparation for the various measurements that are to be conducted on the specimens, the top 3-4 cm is cut off. This is done to eliminate an uncertainty factor in the top surface, where the porosity is much less than in the rest of the specimen due to the closing procedure of the moulds. Unfortunately this closing procedure is the only way to make uniform and consistent specimens.

Initial experiences will now be presented and explanations for different choices made during this development process can be found.

6.2 Preliminary experiences with various parameters

During preliminary tests with mixing and curing this very special type of concrete, experiences with various parameters were gained. Some relates to the specific concrete mixture and others regard casting and curing as well as mixing of the concrete. These experiences will be discussed in the following.

Initially an aggregate was used with a diameter of 1-4 mm even though Imbabi et al. [1], in a patent, proposes that a diameter of 2-3 mm would be the optimal. The reason for using the wider range was to determine what effect this would have on the concrete in relation to the patent and later experiments. This wider range of diameter proved to have a large influence on the concrete, as test results were relatively far from the results provided in the patent. Later tests showed that the small diameters improved the compressive strength of the concrete whereas it decreased the permeability. Larger diameters have the opposite effect and on this basis it was chosen to use 2-3 mm like the patent proposes. The experiments were conducted with the same degree of filling and w/c ratio.

The content of SPA used in the mixtures was tested using only cement paste. It is important that the SPA does not substitute water in the concrete mixture so that the w/c ratio is not compromised, but only the rheology is altered. Through several tests it was discovered that when using a small w/c ratio of 0.2 it was necessary with 1 % by weight of the cement to create a suitable rheology. For a w/c ratio of 0.3 the needed amount of SPA was 0.5 %. In between these limits interpolation was used. The results are based on experiences with vibrating the concrete as well as working with different recipes. If too much SPA is added the cement paste will settle in the bottom of the moulds which is unacceptable and if too little is added the concrete becomes very hard to handle and in some cases the concrete was not coherent.

The phase of vibrating each concrete specimen was initially introduced to ensure

consistency, but it was discovered that vibration frequency and time has a large effect on the result. Because of this influence a test was conducted by measuring the density in order to understand the impact of these two parameters and from this establish suitable values, so they will not appear as variables. Several specimens were made of the same recipe and then vibrated the same amount of time, but with different frequencies. After curing for 10 days these specimens were cut into five pieces each. A density measurement was conducted both before and after the specimens were cut and the results can be seen in figure 6.1. A problem with this method is that when cutting the specimens, edges tend to break off due to the relatively small strength. This problem generated some errors.

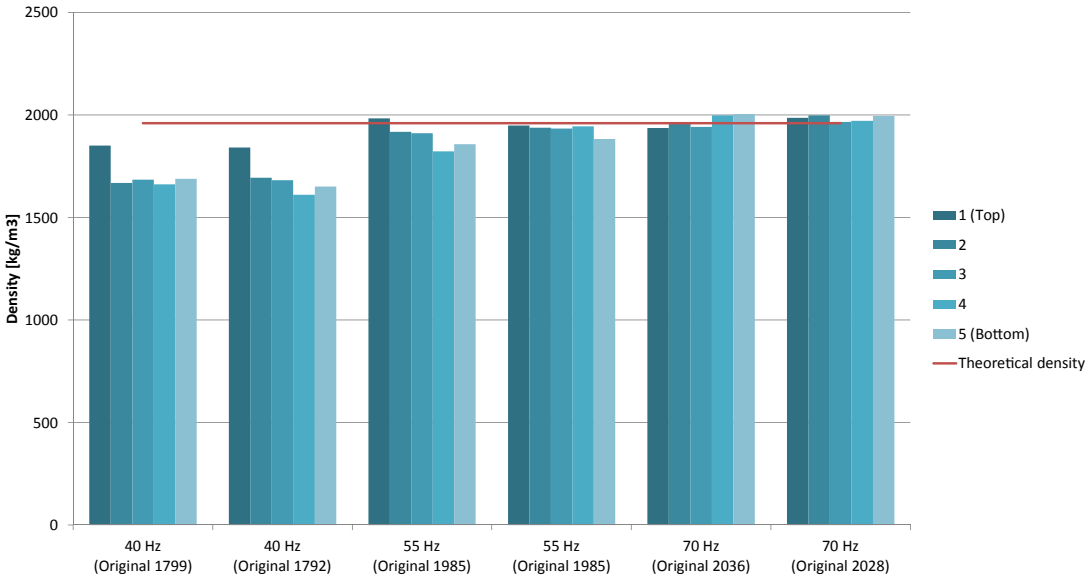

Fig. 6.1. Consistency and vibration test. Piece 1 represents the top of each specimen and piece 5 the bottom. The case ID's represent vibration frequencies from 40 to 70 Hz together with their density before being cut. The theoretical density represents the total mass of ingredients in 1 m^3 concrete according to the recipe.

Shown in the figure are six cases with their theoretical, original and cut into five pieces densities. As expected the most consistent specimens are the ones made with the highest frequency. The figure clearly shows that a frequency of 40 Hz generates a large deviation in density going from bottom to top in the specimen. The problem with the edges breaking off is visible as no pieces, in the 55 and 70 Hz cases, have a larger density than the original. However, as all pieces have been cut they must, more or less, have lost the same amount of concrete and can still be compared with each other. When determining which frequency to use the original densities are included. A frequency of 40 Hz seems to generate a very small density and 55 Hz a little too high. On this basis it was decided to use 50 Hz and then cut off one end to counteract the inconsistencies this might generate.

The vibration time was tested over a series of cases. Experiences showed that vibrating longer and shorter had the same effect as adjusting the vibration frequency. Therefore a routine was developed where the concrete was vibrated two times, each 15 seconds, with a counterweight on top the last time.

These initial specimens and tests were conducted partly to exclude some combinations of w/c ratio and degree of filling. Specimens were cast with low w/c ratio and degree of filling where the cement paste did not form a paste or there was not enough cement paste to connect the aggregate. In the other end of the scale there were no experiments conducted as all were possible to cast. W/c ratios of 0.1 and 0.15 were discarded and degree of fillings of 0.1 and 0.2 were discarded as well.

6.3 Parameter variation

Based on the preliminary experience gained, a parameter variation is made with w/c ratio and degree of filling as the variables. With the different w/c ratios is a corresponding SPA content. The aggregate size and thereby the natural packing density remains the same throughout the parameter variation.

From the later obtained results of the measurements conducted on the specimens from this parameter variation, two cases are chosen (new specimens cast) to measure thermal conductivity, specific heat capacity and heat exchanger efficiency. After these measurements one case is chosen where PCM is added to test for possible improvements and deteriorations on compressive strength, permeability, conduction and energy. Table 6.1 shows all the cases cast in the parameter variation. The aggregate size is 2-3.55 mm with a natural porosity of 0.402.

Recipe	W/c ratio	Degree of filling	SPA
1	0.20	0.4	1.00
2	0.20	0.5	1.00
3	0.20	0.6	1.00
4	0.25	0.4	0.75
5	0.25	0.5	0.75
6	0.25	0.6	0.75
7*	0.30	0.4	0.50
8*	0.30	0.5	0.50
8 PCM	0.30	0.5	0.50
9	0.30	0.6	0.50

Table 6.1. Cases in the parameter variation. Size of the specimens are 100 mm × 200 mm. The SPA-values are in % by weight of the cement. Aggregate size is 2-3.55 mm with natural porosity of 0.402. *Cases chosen for conductivity and energy measurements.

For each case a minimum of five specimens are cast in order to ensure statistical, representative data for the case. The reason that five specimens in each case is chosen is the time factor in this study, which do not allow for a large population. Besides the minimum of five cylindrical specimens, two square specimens are cast in the two chosen cases to measure thermal conductivity and specific heat capacity and the same for the case with PCM.

6.4 Recipe examples

The recipes used for all the cases are calculated from basic concrete technology knowledge. In the following two examples will be shown and explained - one for air permeable concrete with SPA and one where PCM also is included. The PCM is in liquid form, so it is important to adjust the water content in order to maintain the wanted w/c ratio.

Several parameters are predetermined such as the densities of the materials and the natural porosity of the aggregate. The basis of making recipes in this study is a variation in parameters, for which reason w/c ratio, degree of filling and content of SPA are predetermined from case to case as well. The first recipe is shown in table 6.2 and is for air permeable concrete without PCM. Two of the used recipes (case 8 and case 8 with PCM) can be seen on the [Enclosures-CD, Recipe_case 8+P8.xlsm].

Recipe	Content [kg/m^3 concrete]	Density [kg/m^3]	Content [m^3 component/m^3 concrete]
Cement	C	ρ_c	C/ρ_c
Water	W	ρ_w	W/ρ_w
Air	0	0	0.015
SPA	S	ρ_S	S/ρ_S
Cement paste	$C+W+S$	-	$C/\rho_c + W/\rho_w + 0.015 + S/\rho_S$
Aggregate	AG	ρ_{AG}	AG/ρ_{AG}
Total	$\rho_{concrete}$	-	AG/ρ_{AG} + (Cement paste/DF)

Table 6.2. Recipe for air permeable concrete without PCM.

The water and SPA contents in the concrete are both correlated with the cement content (the water via the w/c ratio and SPA percentage-wise). Thus, they can be calculated if the cement content is known. The cement paste volume content in the concrete must be equal to DF $\cdot$ NP in order to meet the requirements of a certain degree of filling. As the water and SPA volumes are both correlated with the cement content and a part of the cement paste, this becomes an iterative process. Basically an initial estimate of the cement content is necessary and afterwards by using iteration the cement paste volume content can be adjusted to be equal to DF $\cdot$ NP.

The second recipe, which includes PCM, is shown in table 6.3

Recipe	Content $[kg/m^3 concrete]$	Density $[kg/m^3]$	Content $[m^3 component/m^3 concrete]$
Cement	C	ρ_c	C/ρ_c
Water	W	ρ_w	$W/\rho_w - P_w/\rho_w$
Air	0	0	0.015
SPA	S	ρ_S	S/ρ_S
PCM water	P_w	ρ_w	P_w/ρ_w
PCM dry	P	ρ_P	P/ρ_P
Cement paste	$C+W+S+P$	-	$C/\rho_c + W/\rho_w + 0.015 + S/\rho_S + P/\rho_P$
Aggregate	AG	ρ_{AG}	AG/ρ_{AG}
Total	$\rho_{concrete}$	-	AG/ρ_{AG} + (Cement paste/DF)

Table 6.3. Recipe for air permeable concrete with PCM.

The same principle with the iterative process is utilised in this recipe, however, the added PCM must be included. In this study the amount of PCM chosen is 2 % by weight of the concrete. Therefore the contents of PCM dry (only solids) will relate to $\rho_{concrete}$ and at the same time have an influence on the cement paste volume content. When PCM is added this reduces the amount of other materials in the cement paste, as the degree of filling must remain the same. Furthermore the PCM is delivered mixed with water, in order to keep the PCM particles from agglomerating, which reduces the amount of mix water needed in the recipe. The amount of mix water will drop as the amount of PCM dry is increased and at some point the PCM water will exceed the amount of water needed in the concrete and this amount of PCM is the maximum possible to mix in the concrete with the given w/c ratio. This means that two iterative calculations are necessary in order to make the recipe contents fit with both degree of filling, w/c ratio, SPA contents and PCM contents.

7 Measurements

This chapter shortly describes the measurements conducted to find the basic material properties of air permeable concrete. It covers the outline of the measurement, setups, procedures and corresponding data treatment. Thorough descriptions can be found in appendix B.

7.1 Density measurements

The density measurements are conducted by measuring weight and dimensions of the specimens. The dimensions are measured with a vernier caliper, three places for diameter and one place for length. The weight is measured right after the specimens have cured in plastic bags. Two densities have been measured as a test if the specimens are consistently dense. Besides the described original density a reduced density is measured after the top is cut off, which is the developed standard procedure in this study. The procedure is elaborated in appendix A.5. The two densities will then be compared to the theoretical density, calculated from the recipes used. The reduced density is used for further treatment. Further description of the measurements can be found in appendix B.1.

The density measurements have been conducted by measuring dimensions and weighing the specimens, for which reason there are no further treatment of these data than a simple calculation.

7.2 Compressive strength

Roughly the specimens are crushed while measuring the force needed for the crush. When the specimens' compressive strength is tested, the top has been cut off and for that reason it is necessary to correct the results using an equation. A corresponding correction needs to be made for the cylinder diameter. In appendix B.2 the compressive strength measurements are described more thoroughly.

Measuring compressive strength of the permeable concrete specimens on the Tonipact 3000 compressive strength testing instrument gives a voltage output, where 1 V roughly equals 300 kN. The loading rate on the specimens has through all tests been 1 kN/s. From this output and the specimen dimensions the strength can be calculated without further data treatment.

7.3 Permeability calculation

Permeability measurements are conducted using a new developed method, described in appendix B.4. In order to calculate the permeability it is necessary to know the measure the air flow through and the pressure difference across the specimen, together with specimen area and length. Every specimen has been tested with four air flows.

7.3.1 Data treatment

The parameters needed for calculating the air permeability of the concrete specimens are shown in equation 7.1.

$$\kappa = \frac{q}{A} \cdot \mu \cdot \frac{L}{\Delta p} \tag{7.1}$$

Where:

κ	Permeability [m^2/Pa h]
q	Air flow [l/min]
A	Specimen area [m^2]
μ	Air dynamic viscosity [Pa s]
L	Specimen length [m]
Δp	Pressure difference [Pa]

This version of Darcy's law assumes the flow of the medium to be laminar, as the pressure exponent is implicit set to 1.0. If the flow is fully turbulent this exponent will be 0.5. The pressure exponent is introduced as n in equation 7.2.

To be able to compare the results of the measurements with the patent made by Imbabi et al. [1], which is the only other results of air permeability measurements made on highly permeable concrete, it is necessary to remove the dynamic viscosity from Darcy's law. Unfortunately it is not mentioned how they calculated the permeability with the results obtained, so it is not possible to determine if they considered the influence of the pressure exponent and if the flow is laminar or turbulent. The equation used in this study to calculate the permeability is shown in equation 7.2.

$$\kappa = \frac{q}{A} \cdot \frac{L}{\Delta p^n} \tag{7.2}$$

The necessity of adding this pressure exponent, n, is illustrated in figure 7.1, where data from an initial test subject is included together with two functions describing the phenomena. It is obvious that the power function (7.2) fits better than the 1st order polynomial.

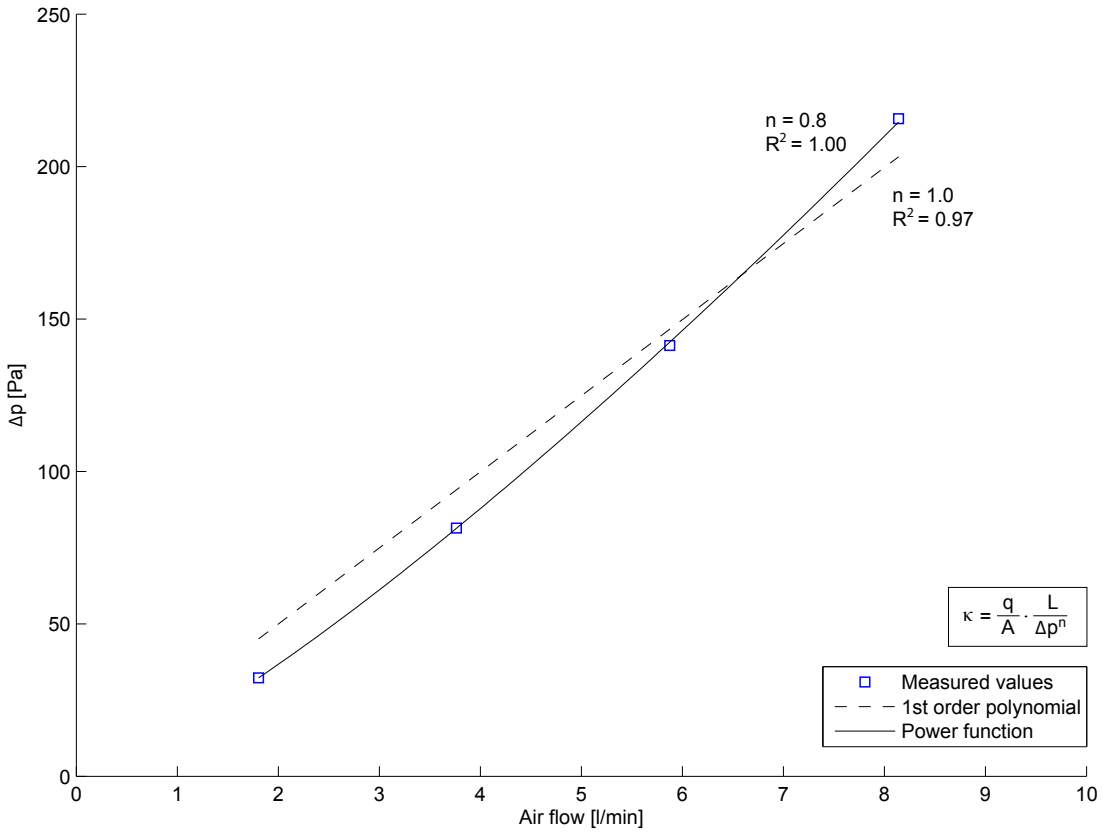

Fig. 7.1. Permeability data fitted with a 1st order polynomial and a power function respectively. The pressure exponent is used in the shown permeability equation.

Every specimen is measured at four air flow rates and these results are used to determine the pressure exponent and calculate the permeability. In order to do this linear regression is used to fit the data to a power function $y = ax^b$. This is applied to equation 7.2, shown in equation 7.3.

$$q(\Delta p) = \frac{\kappa \cdot A}{L} \cdot \Delta p^n \tag{7.3}$$

The two terms representing a and b in the general power function are known when the data is fitted and the permeability can be solved by multiplying by L and dividing by A, which are known parameters of the specimens.

Uncertainty assessment 8

Measurements are the crucial link between theoretical calculations and practice. When seeking applicable results, very often accuracy is the key quality parameter. However, no instrument shows the true exact value. An expensive instrument can have a low measurement uncertainty, but it will never be zero throughout an entire measurement range. An acknowledged and well-proven solution is to use a less expensive but reliable instrument (consistently displaying the same deviation when measuring the same value), which can be calibrated by means of an instrument with higher precision. Whether the instrument is calibrated or not it is subject to uncertainties. For all measurements it is important to quantify the uncertainties.

8.1 Estimation of uncertainties

In the process of quantifying the various uncertainties in the different measurement setups some are known and some are to be estimated. The interest in the uncertainty assessment is quantifying uncertainties of the density, compressive strength and permeability measurements. These uncertainties are affected by a number of different factors altogether.

As relatively few specimens have been cast and correspondingly few measurements conducted it is assessed that random uncertainties cannot be quantified. Therefore it is only systematic uncertainties which will be taken into account and computed in different scenarios. The systematic uncertainties are divided into the contributions from two elements - the uncertainty of instruments and the ones regarding the method/routine. The uncertainty concerning instruments is additionally divided into the two contributions from accuracy and reading, where both have to be included. Accuracy concerns the measurement precision or deviation given by the manufacturer and imprinted on the instruments. Reading is defined as the uncertainty due to user influence, when taking readings from imprinted scales on analogue instruments. The uncertainty of the method is first of all the casting method and the precision with which it is possible to create uniform and identical specimens. The uncertainty is partly due to the routine and equipment and partly due to the operator influence.

The separately calculated or estimated uncertainties, if several exist, must be combined to a total uncertainty of the measurements in order to be able to quantify the precision of the presented results. However, adding the individual percentages together will result in an unrealistic high uncertainty, not taking statistical convergence into account. By instead considering the theory of uncertainty propagation, a more realistic assessment

of the uncertainty is believed to be carried out. Propagation of uncertainty is defined as the effects on a function by a variable's uncertainty and is designed to combine uncertainties from multiple variables, in order to provide an accurate measurement of the total uncertainty of a system. In the following sections the uncertainties for the three individual measurements will be presented.

8.2 Density uncertainty

No specific uncertainties are given when casting air permeable concrete, for which reason it is very hard to quantify the uncertainties of the density measurements. A lot of parameters can have an impact on the final cast density like weighing materials, mixing, procedures of adding materials, filling moulds and vibrating to name a few. To give a realistic estimate of the uncertainty in this study, the casting precision is set to $\pm 4\,\%$, which is largest percentile deviation in specimen density measurements.

8.3 Compressive strength uncertainty

The compressive strength tester in labeled with an uncertainty of up to $\pm 1.2\,\%$. However, applying the calibration from Force Technology yields an uncertainty of approximately $0\,\%$. This is considered negligible. The calibration is described is appendix B.2.1.

8.4 Permeability uncertainty

As permeability is a function of several parameters, it is necessary to treat the uncertainty contributions likewise in order to calculate the total permeability uncertainty. Every parameter in the equation to calculate permeability is a measured value, where all must be taken into account in this calculation of uncertainty. Equation 8.1 shows the general equation used to calculate uncertainty for combined measurements.

$$U = \sqrt{\left(\frac{\delta R}{\delta x} \cdot \overline{U}_{R_x}\right)^2 + \left(\frac{\delta R}{\delta y} \cdot \overline{U}_{R_y}\right)^2 + \left(\frac{\delta R}{\delta z} \cdot \overline{U}_{R_z}\right)^2} \tag{8.1}$$

$\delta R/\delta x$, $\delta R/\delta y$ and $\delta R/\delta z$ are the individual parameters' relative influence on the calculated result and $\overline{U}_{R_x}$, $\overline{U}_{R_y}$ and $\overline{U}_{R_z}$ is the resulting uncertainty of each separate parameter. To calculate the resulting uncertainty of a direct measurement, equation 8.2 is used.

$$U_R = \sqrt{{U_T}^2 + {U_S}^2} \tag{8.2}$$

Where:

$$U_S = \sqrt{\sum_{i=1}^{n} {U_i}^2} \tag{8.3}$$

As it is assumed that no random uncertainties are present ($U_T = 0$), the uncertainty for the combined measurement of permeability can be calculated. To create an overview of all the contributions to the uncertainty and the categorisation of these, an illustration of how these are connected is shown in Fig. 8.1.

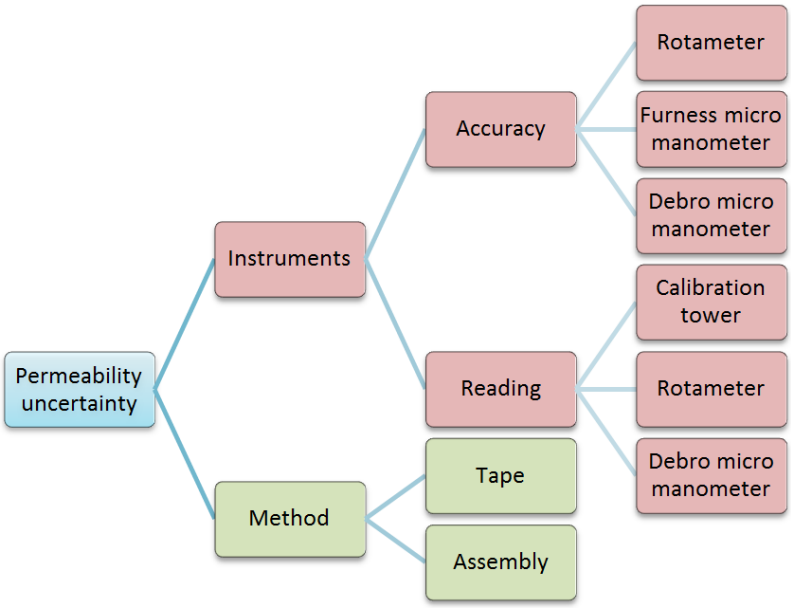

Fig. 8.1. Overview of the different factors affecting the permeability uncertainty.

All the instruments used are placed under the Instruments/Accuracy category, but only instruments which are not digital are placed under Instruments/Reading because a digital instrument gives very low risk of a reading error, which is not considered in the calculation. Additionally it is assessed that the procedure of sealing the specimen in tape and assembling the components in the pressure-box for permeability measurements contribute. The latter is an optimised procedure and done thoroughly, however, small leakages or suchlike may occur. All the parameters and their contributions are listed below.

- Rotameter accuracy ±4 % (with reference to the instrument data sheet)
- Furness micro manometer accuracy ±0.1 % (with reference to the instrument data sheet)
- Debro micro manometer accuracy ±1 % (estimate)
- Calibration tower reading ±2 % (largest percentile deviation during calibration)
- Rotameter reading ±1 % (estimate)
- Debro micro manometer reading ±10 % (estimate - good reading ability, but the system may not be in total equilibrium due to slow reaction)
- Tape ±1 % (estimate)
- Assembly ±2 % (estimate)

As a part of the calculation of the combined measurement uncertainty, these parameters have to be assigned to a measured value in the permeability calculation. But all the relative influences are set to a factor of 1.0. The only measured value which could present with

another value is the pressure difference with the corresponding pressure exponent. The pressure exponent is however, in this calculation, set to 1.0 (laminar flow) as this is close to the later measured result of 0.94. With this assumption and a combination of equations 8.1 and 8.3 the total uncertainty of this combined measurement can be calculated as the square root of the quadrature sum of the single uncertainties.

$$\delta_\kappa = \sqrt{4^2 + 0.1^2 + 1^2 + 2^2 + 1^2 + 10^2 + 1^2 + 2^2} = \pm 11.3\,\%$$

Results 9

This chapter treats the results obtained during the experimental work with air permeable concrete concerning density, compressive strength and permeability. In every case (1-9) five specimens are cast where each specimen has been measured for all three parameters treated in this part. A standard deviation for each case is shown together with the results to give an indication of how consistent the specimens are. Results from the case with PCM will be presented and compared too. All results are calculated from measured values with the program properties_ini.m, which can be seen on the [Enclosures-CD, Matlab folder].

9.1 Density measurements

The mean results obtained during the measurements of the density, shown in table 9.1. It is noticeable that, for some cases, the deviation between the original density and the reduced density are relatively large compared to others. This indicates that some specimens are more consistent in density through the entire length of the specimen than others.

Case	w/c [-]	DF [-]	Org. density [kg/m^3]	σ org. [kg/m^3]	Red. density [kg/m^3]	σ red. [kg/m^3]	Dev. org./red. [%]
1	0.20	0.4	1679	11	1664	14	0.93
2	0.20	0.5	1642	22	1616	20	1.61
3	0.20	0.6	1652	5	1620	11	1.92
4	0.25	0.4	1698	21	1677	21	1.21
5	0.25	0.5	1728	18	1707	21	1.17
6	0.25	0.6	1809	12	1794	11	0.83
7	0.30	0.4	1820	13	1820	17	0.78
8	0.30	0.5	1896	3	1897	6	0.91
9	0.30	0.6	1982	8	1982	10	0.58
P8*	0.30	0.5	1886	17	1869	27	0.91

Table 9.1. Mean density measurements results including the standard deviation, σ. *P for PCM case. Uncertainty: $\pm 4.0\,\%$.

The first three cases, which have the same w/c ratio, should increase in density going from case 1 to 3 as the degree of filling increases. This is not the case, for which reason the casting of these specimens are considered improper. Case P8 has a large standard deviation compared to case 8, which is the same recipe without PCM. This indicates that

the compression of the specimens in case P8 or the rheology have been different. As visualisation these data are shown in figure 9.1 together with the theoretical density for comparison. The figure does not include the case with PCM.

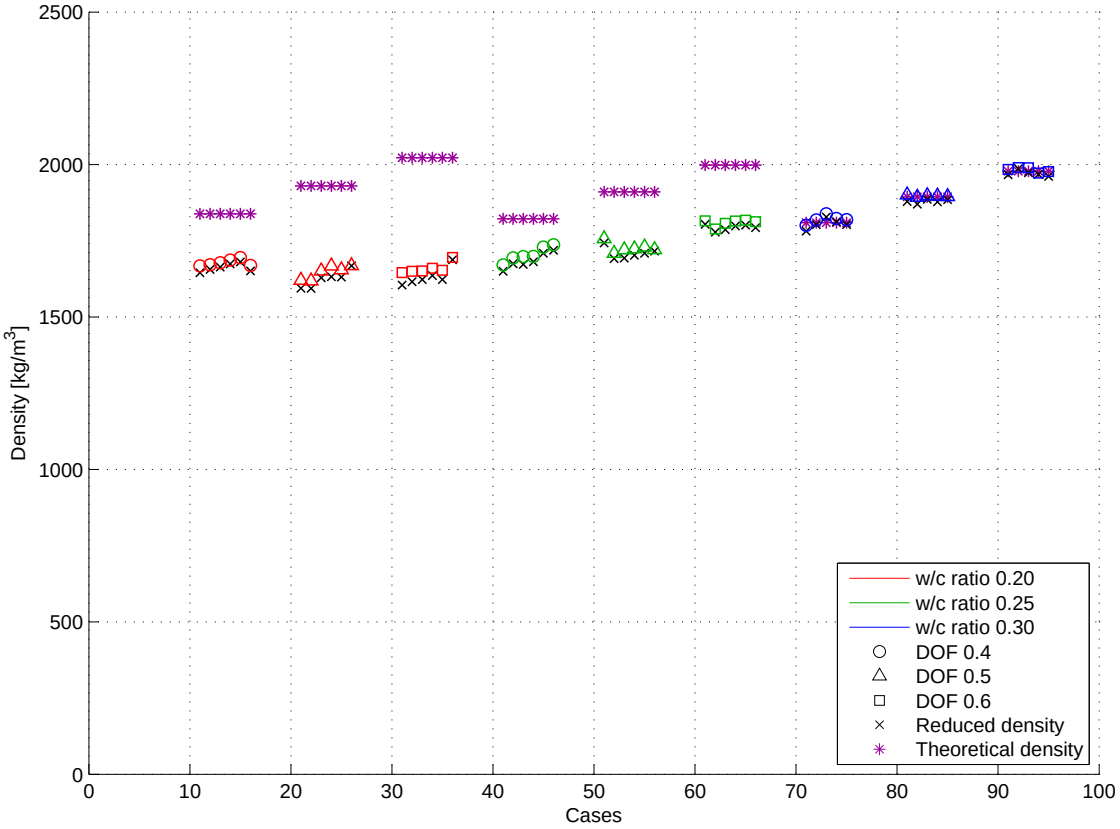

Fig. 9.1. Plot showing the measured density, reduced density and theoretical density of all samples in cases 1-9. The x-axis represents the specimen ID's, where case 1-1 is labeled 11 in the plot, case 2-4 is labeled 24 and so on.

Studying the plot clearly shows that the first six cases are cast improperly. The theoretical density is higher in all six cases. Thus, it must be concluded that the aggregate is not packed sufficiently to match the measured natural packing density used to calculate the recipes, resulting in a lower density. The reason for these circumstances could be that not enough SPA is added to the mixture, making the cement paste less workable. This rheology of the cement paste has not been satisfactory and more tests of the needed amount of SPA are necessary, but given a time factor in this study this has not been possible to conduct. These results, among others, form the basis of a later selection of two cases, which will be subjected to energy performance measurements.

9.2 Compressive strength measurements

Before conducting measurements of compressive strength on the specimens, expectations were discussed on which cases would perform best, also considering the density of the

specimens. Higher degree of filling should generate higher strength and lower w/c ratio should likewise result in a higher compressive strength. The case with PCM should have a lower strength than the corresponding case without PCM, because an amount of cement is substituted in the recipe. The results from the specimens are shown in table 9.2. Results obtained in another study by Imbabi et al. are included in the table.

Case	w/c [-]	DF [-]	Compressive strength [MPa]	σ [MPa]	Imbabi results [MPa]
1	0.20	0.4	4.3	1.02	-
2	0.20	0.5	2.6	0.56	-
3	0.20	0.6	2.8	1.41	-
4	0.25	0.4	6.5	0.61	-
5	0.25	0.5	8.4	1.01	10.8
6	0.25	0.6	12.2	0.68	18.2
7	0.30	0.4	13.3	1.14	-
8	0.30	0.5	17.6	1.58	10.7
9	0.30	0.6	22.5	2.50	15.3
P8*	0.30	0.5	15.3	0.94	-

Table 9.2. Mean compressive strength measurements results including the standard deviation, σ, and results obtained in a study made by Imbabi et al. [1]. (-) means that no results are available matching casting parameters. *P for PCM case.

These results do not meet the expectations discussed beforehand, as can be seen in the table. Looking at cases 1-3 shows no correlation between increasing strength with increasing degree of filling. This is valid within cases 4-6 and 7-9, though. Bolomey's formula suggests increasing strength with lower w/c ratio. However, observing series with matching degree of filling reveals the exact opposite of this. Case 1 is weaker than case 4 weaker than case 7 and the same is seen with w/c ratios 0.25 and 0.30. Combining the expectations yields case 3 as the supposed strongest and case 7 as the weakest. Case P8's mean compressive strength is a little lower than case 8, which was expected.

Compared to the results obtained by Imbabi et al. the results in this study are, for cases 5-6 lower and for cases 8-9 higher. In section 9.1 regarding measured density results it is concluded that, among other, cases 5-6 are cast in an improper way generating a too low density which will make the compressive strength lower as well. In cases 8-9 the values are higher in this study and the amplitude of these results suggests that this type of concrete should be suitable as a load bearing construction.

If theory is held against the measured results, it suggests that there is something wrong with the casting process for cases 1-6, which is the same conclusion made in section 9.1 regarding density measurements results. In the remaining cases there seems to be connection between high and low strength and density and this indicates that the compressive strength and the density might have some form of correlation, which is treated more in chapter 10.

9.3 Permeability measurements

From the permeability measurements the results shown in table 9.3 are obtained. These are listed with both the calculated permeability and the corresponding pressure exponent and their standard deviation. Expectations about the permeability level of the different specimens are that higher degree of filling should generate lower permeability. The w/c ratio should not have much effect on this parameter.

Case	w/c [-]	DF [-]	Permeability (κ) [m^2/Pa h]	σ κ [m^2/Pa h]	p exp. (n) [-]	σ n [-]	Imbabi results [m^2/Pa h]
1	0.20	0.4	0.593	0.035	0.97	0.016	-
2	0.20	0.5	0.624	0.035	0.95	0.020	-
3	0.20	0.6	0.437	0.045	0.95	0.021	-
4	0.25	0.4	0.565	0.019	0.92	0.022	-
5	0.25	0.5	0.443	0.038	0.97	0.014	0.60
6	0.25	0.6	0.297	0.004	0.95	0.012	0.32
7	0.30	0.4	0.313	0.018	0.95	0.038	-
8	0.30	0.5	0.232	0.008	0.94	0.009	0.60
9	0.30	0.6	0.180	0.015	0.88	0.020	0.32
P8*	0.30	0.5	0.290	0.034	0.88	0.014	-

Table 9.3. Mean permeability measurement results including the pressure exponents, standard deviations, σ, and results obtained in another study made by Imbabi et al. [1]. *P for PCM case. Uncertainty: $\pm 11.3\,\%$.

For most of the cases studied the expectations are proven right. In cases 1-3 the permeability is not increasing as the degree of filling is lowered, but this result can be explained by the conclusion drawn about the casting process being improper in section 9.1. The standard deviations for the permeability measurements are low, which is a good sign when aiming for uniform performance. Unfortunately the permeability for case P8 is higher than for case 8, which states that there is either something wrong in the casting process or the PCM particles have an influence on the parameter. If the latter is the explanation, the PCM should have changed the roughness in the interconnected channels.

Comparing the results from Imbabi et al. to the values obtained in this study, shows that Imbabi achieved fairly high permeabilities. By their results, the permeability will be the same when using the same degree of filling, which is also the case from a theoretical perspective. In this study such values has not been possible to achieve.

The calculated pressure exponents are all near 1.00. This points towards the air flow through the specimens being near laminar. No conclusions can be made of the changes in values from case to case, but the standard deviation confirms that the shown mean values are very representative for the five samples in each case. The mean value for the pressure exponent considering the whole population of specimens is 0.94 and the standard deviation is 0.033. This proves that with the small air flows used to measure the permeability the flow should be characterised as laminar with a degree of filling lower than 0.6.

Material properties correlations

10

In this chaper results from the conducted measurements will be studied and analysed. Conclusions made are only valid for air permeable concrete cast with the same ingredients as for this study. Case P8 (case 8 with PCM) is not included as the recipe is different from the others and can therefore not be used in the mathematical models.

From the obtained data, it is noticeable that the compressive strength and permeability are inversely correlated, which is to be expected. Furthermore it is visible that an increase in density generates higher compressive strengths. This is believed to be due to the, also inverse, correlation between the coarse porosity and the strength, which is elaborated in chapter 2. The relation between compressive strength and density is shown in figure 10.1.

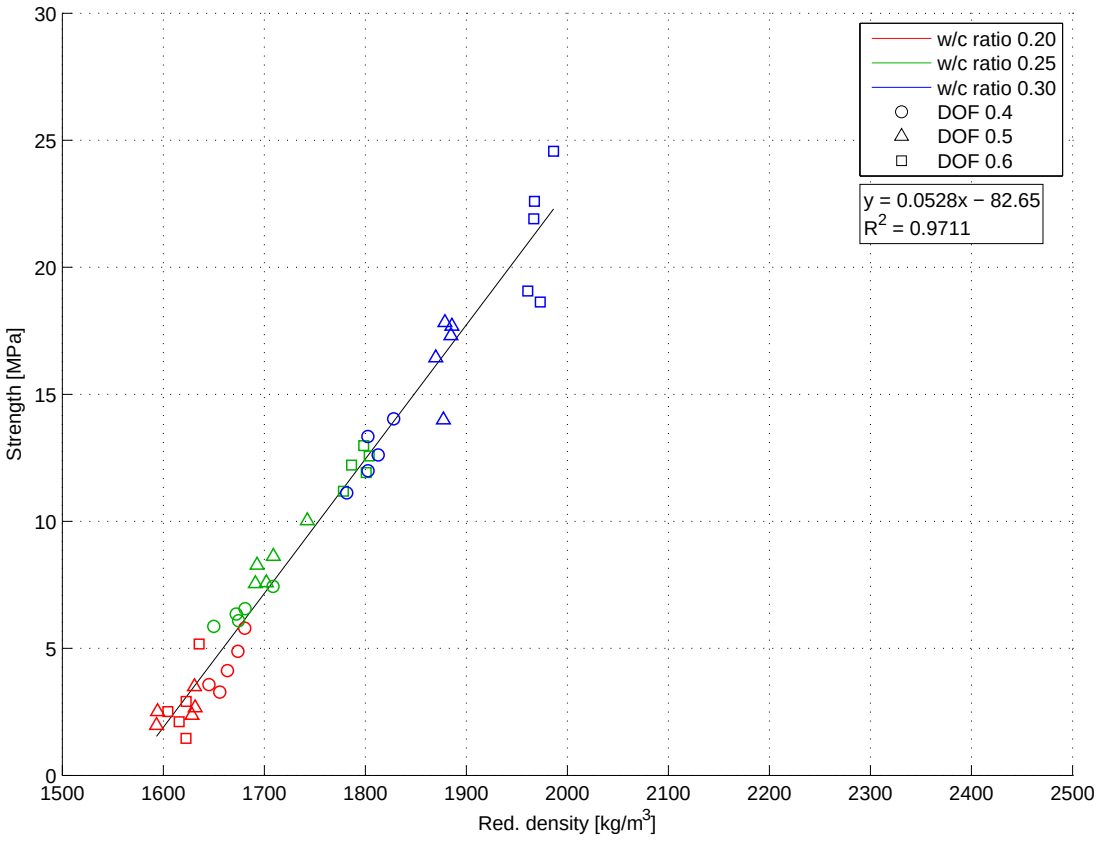

Fig. 10.1. Relation between compressive strength and density. Density uncertainty ±4.0 %.

It is very clear that there is a correlation between density and strength. Achieving

compressive strengths of higher than 10 MPa for the whole series of specimens with a w/c ratio of 0.3 is satisfactory. When approaching 15-20 MPa, this type of concrete should be applicable as load bearing building components. Even though it is concluded in chapter 9 that some problems with casting have occurred during an analysis of the measurement data, density and compressive strength have a good correlation which proves that this connection is valid. The derived function $f_c = 0.0528 \cdot \rho - 82.65$ will be used for a mathematical model to predict the compressive strength from the concrete recipe.

The porosity has not been measured during the main parameter variation, for which reason the density is used instead. To validate this method the correlation between a calculated porosity and the measured density is shown in figure 10.2. Normally the porosity can be calculated using the aggregate natural porosity and the degree of filling, but this approach has proven not to be very accurate when the concrete is cast improperly. Instead another method is used where the porosity is corrected according to the theoretical and real weight of the specimens. As a validation this have been tested on a series of specimens where the porosity have been measured as described in appendix B.3 and the result proved that the method is very accurate.

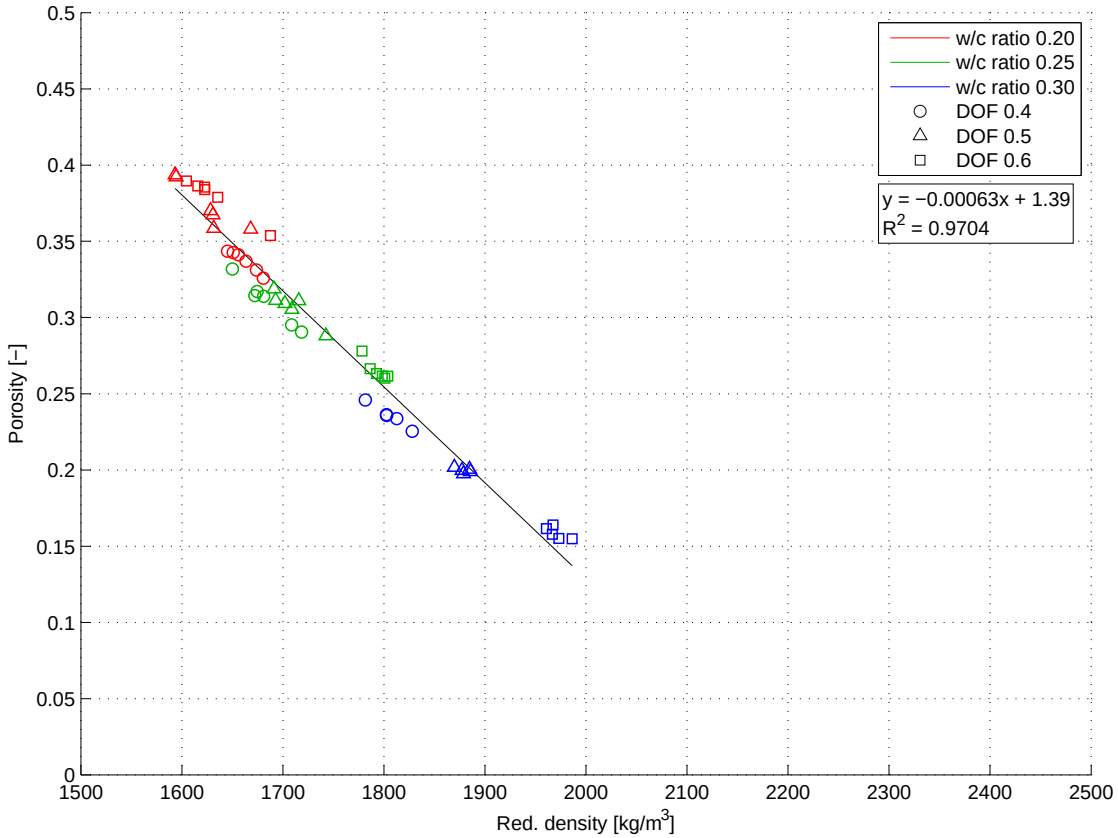

Fig. 10.2. Relation between density and calculated porosity. Uncertainty for density: ±4.0 %.

The plot shows a good linear correlation between these two material properties, for which reason it is assessed to be acceptable to use the density as the variable for finding the permeability in this study.

The good relation between density and compressive strength is passed on into figure 10.3 where the permeability is shown as a function of the density. The pressure exponent proves the air flow to be mostly laminar and implementing theory including friction factors gives the same result, shown in chaper 11.

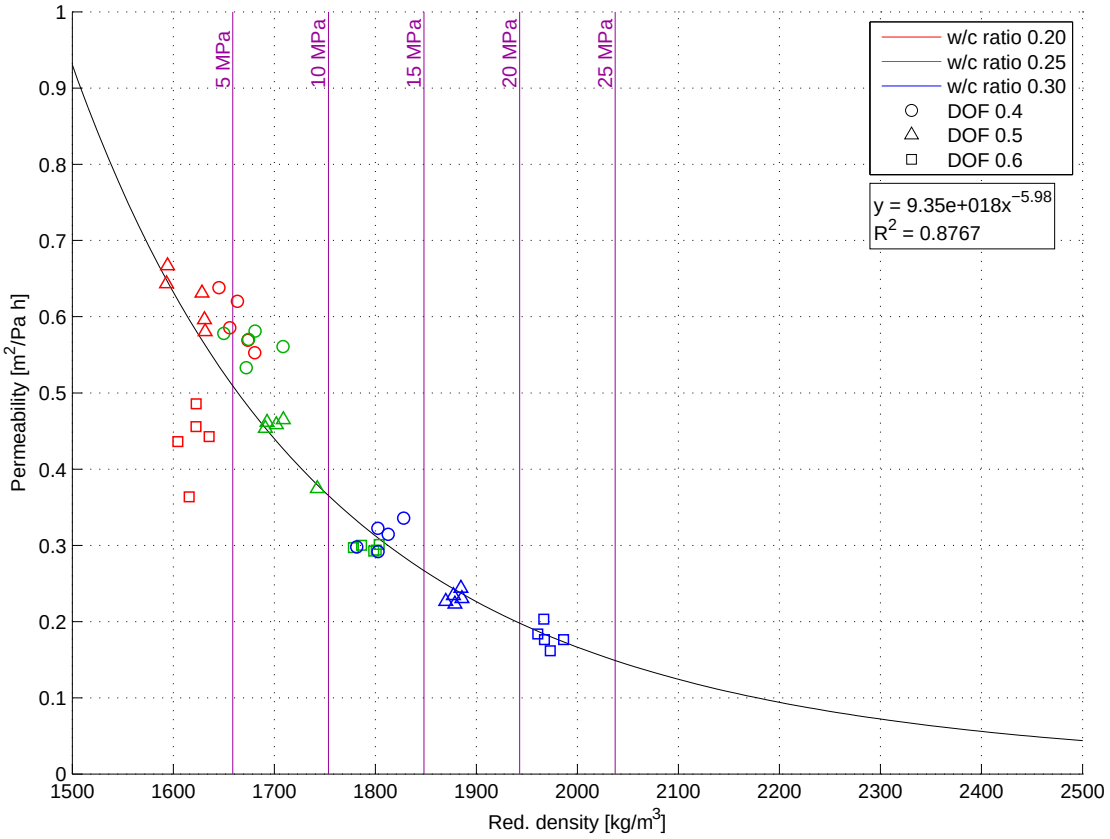

Fig. 10.3. Relation between permeability and density. Uncertainties respectively: $\pm 11.3\,\%$ and $\pm 4.0\,\%$.

Looking at the specimens with a w/c ratio of 0.3 on the plot suggest that it is possible to cast a consistent air permeable concrete, with good correlation between permeability and density. When including all specimens in the function the correlation becomes $R^2 = 0.88$ which is not particularly good. A group of specimens are placed away from the function, of course affecting the function and the correlation, and these are a part of the specimens which are cast improperly. Even though the correlation is not too good, there is a tendency which is believed to be a good finding. Due to this tendency the derived function will be utilised in a mathematical model to give an estimate of the permeability. The function is derived as $\kappa = 9.35 \cdot 10^{18} \cdot \rho^{-5.98}$.

The plotted function, representing the correlation, can, however, only be used on this specific recipe of concrete. If other aggregate, cement or SPA are used, new relations must be computed in order to create a function.

In figure 10.4 the relation between permeability and strength is shown and results from Imbabi et al. [10] are included to compare the obtained data from both studies.

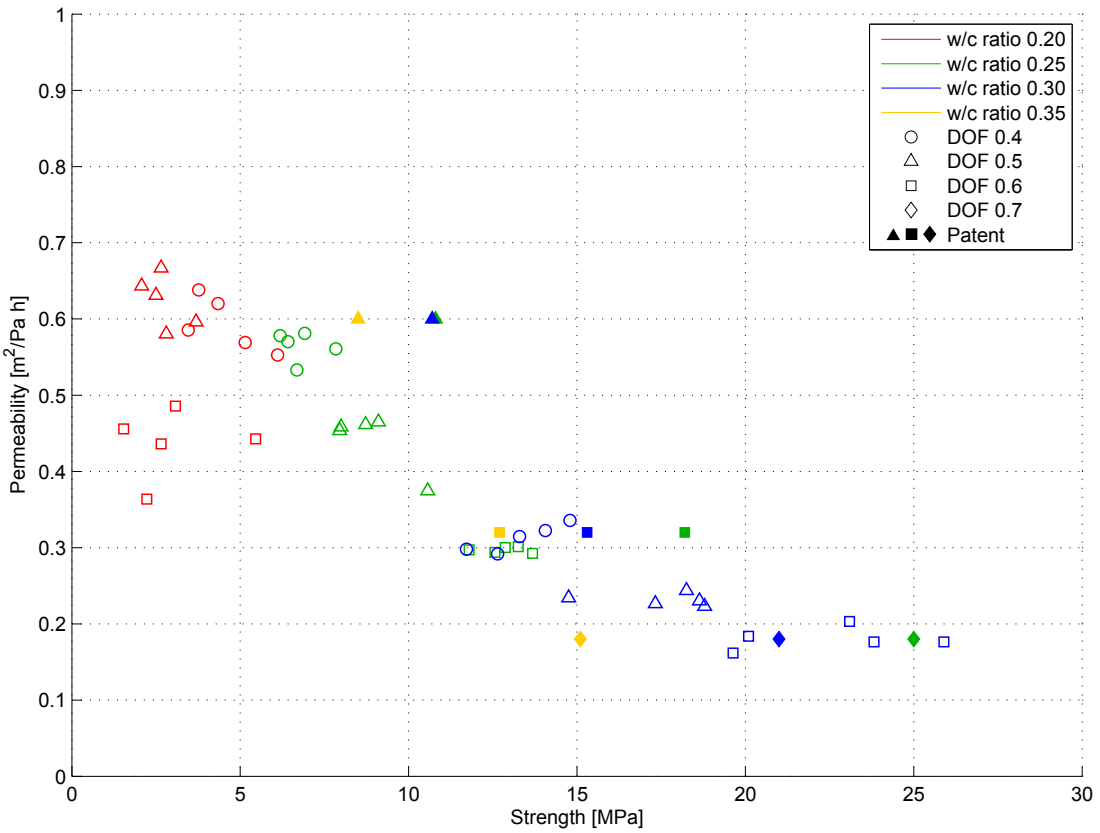

Fig. 10.4. Relation between permeability and compressive strength. Furthermore results from a study made by Imbabi et al. [10] are plotted for comparison.

Comparing the observed data clearly shows that the same material properties have been achieved in the two studies. Although these properties have not been achieved with the same recipes, it is considered acceptable because of the uncertainty of casting processes and methods. With a degree of filling of 0.7 in the Imbabi et al. study, the same properties are obtained with a degree of filling of 0.6 in this study. For some cases it has not been possible to achieve the same results, for example considering samples with a w/c ratio of 0.25 and a degree of filling of 0.5 the same compressive strength is observed but the permeability is approximately 0.2 lower in this study. Furthermore it is very noticeable that very low compressive strengths have been obtained in this study for the low w/c ratios, whereas this is the opposite for the study from Imbabi et al.

Interphase transport in isothermal systems

11

In this chapter an attempt of connecting transport theory with measurements of the air permeable concrete specimens will be made. The factors which are the key parameters when working with air flows through a porous material are the friction factors.

Imbabi et al. [9] discovered a decrease in permeability when higher pressures were used (higher air flow) and they determined it was due to the increase in shear resistance between air and permeation channel boundaries as the flow velocity increased.

To describe this phenomena, theory from Transport Phenomena is used [43]. In section 6.4 of this book (Friction factors for packed columns) the air flow's behaviour in cylindrical tubes packed with spheres is described. This theory will be related to and used on measurements and observations from this study.

Basically three equations are used to describe the nature of a flow through a porous material. These three equations represent fully laminar, turbulent and the area in between, shown in equations 11.1, 11.2 and 11.3.

Blake-Kozeny (for laminar flows)

$$\frac{P_0 - P_L}{L} = 150 \left(\frac{\mu \cdot v_0}{{D_p}^2} \right) \frac{(1-\epsilon)^2}{\epsilon^3} \tag{11.1}$$

This equation is generally good for $(D_p G_0/\mu(1-\epsilon)) < 10$ and for void fractions $\epsilon < 0.5$.

Ergun (for the transition region flows)

$$\left(\frac{(P_0 - P_L) \cdot \rho}{{G_0}^2} \right) \left(\frac{D_p}{L} \right) \left(\frac{\epsilon^3}{1-\epsilon} \right) = 150 \left(\frac{1-\epsilon}{D_p \cdot G_0/\mu} \right) + \frac{7}{4} \tag{11.2}$$

Burke-Plummer (for highly turbulent flows)

$$\frac{P_0 - P_L}{L} = \frac{7}{4} \left(\frac{\rho \cdot {v_0}^2}{D_p} \right) \frac{1-\epsilon}{\epsilon^3} \tag{11.3}$$

This equation is valid for $(D_p \cdot G_0/\mu \cdot (1-\epsilon)) > 1000$.

Where:

$P_0 - P_L$	Pressure difference [Pa]
L	Specimen length [m]
μ	Dynamic viscosity [Pa s]
v_0	Air velocity [m/s]
D_p	Mean particle diameter [m]
ϵ	Void fraction [-]
G_0	Mass flux [kg/m^2 s]
ρ	Density [kg/m^3]

Not all of these parameters are given from measurements of the specimens. The mass flux G_0 through the system must be calculated from other parameters, shown in equation 11.4.

$$G_0 = \rho \cdot v_0 \tag{11.4}$$

Another parameter which is calculated is the mean particle diameter D_p. This diameter is calculated from equation 11.5.

$$D_p = \frac{6 \cdot (\epsilon - 1)}{a} \tag{11.5}$$

Where:

a	$\frac{\text{wetted surface}}{\text{volume of specimen}}$ [m^{-1}]

The volume of the specimens is known from the measurements conducted, but the wetted surface area is not known. In the theory where the cylindrical tube is filled with spheres it is possible to calculate how many spheres the tube can contain and thereby know the wetted surface area. In this study this phenomena is different, even if it is assumed that all aggregates are spheres, due to the cement paste filling a part of the voids, coating and bridging the aggregates. Because of this, the parameter cannot be calculated.

In order to get past this problem, it is necessary to estimate or adjust the wetted surface area until the data fits. This is done be visually adjusting the value until the data seems to fit and is used for all results obtained. The adjusted value of the mean particle diameter will be discussed later.

In the following a series of selected data from measurements will be presented in a plot containing the three equations 11.1, 11.2 and 11.3. During the measurement development process some specimen series have been measured for porosity and other later cast specimens have not, due to a decision of using density as a replacement in a mathematical model for predicting the permeability. Because of this development it is not possible to use a measured void fraction for all cases. In the cases where the porosity has been calculated, this value will be used.

As previously mentioned, selected data from the measurements have been implemented into several plots. The plots contain the Ergun equation for flow in packed beds and the two related asymptotes, the Blake-Kozeny and the Burke-Plummer equation. In figure 11.1 measurements from the specimens of the preliminary test case 7 S are shown. This series has been measured for porosity.

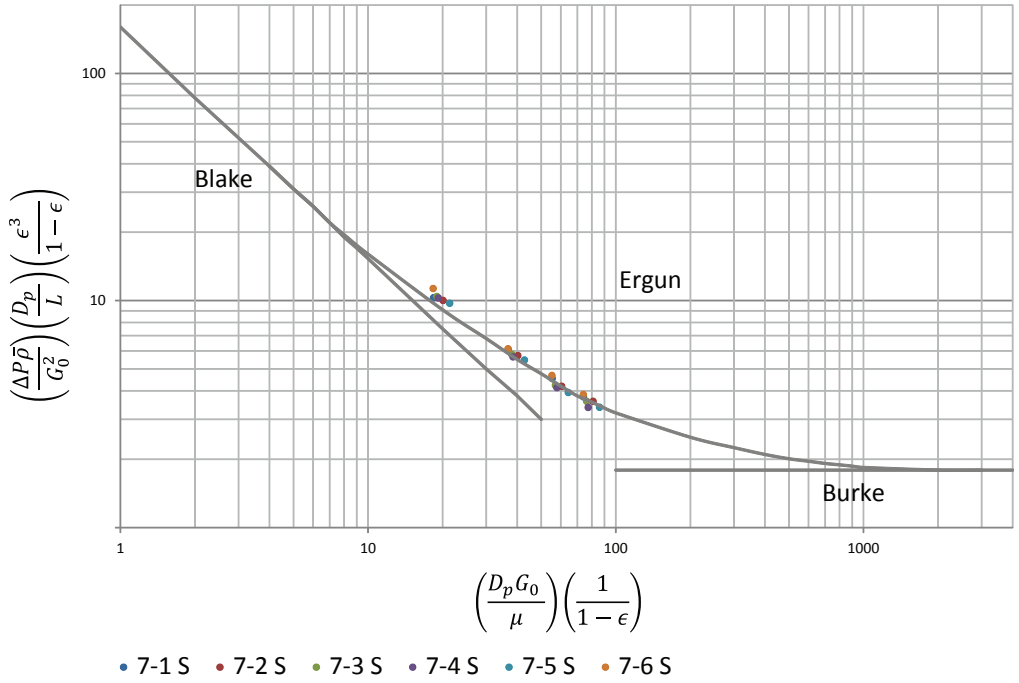

Fig. 11.1. Results from preliminary specimens where the porosity have been measured, case 7 S, which is an initial test case.

It is visible, that when the wetted surface area is adjusted, the data fits very well with the given equations. From calculations it is determined that it should be the Ergun equation, which should fit with the data and this is also clear in the plot. A close-up of the data is shown in figure 11.2.

This close-up clearly shows that the data fits very well. It seems that the data series has a slightly steeper curve than the Ergun equation, indicating a slightly more laminar flow than the theory suggest. The calculated mean particle diameter is roughly 5 mm for all six data series. In case 7 S an aggregate with the size 2-3 mm has been used and considering the added amount of cement paste (degree of filling of 0.5) filling the voids, this value seems reasonable.

In figure 11.3 nine data series from the parameter study, varying w/c ratio and degree of filling, are shown. The selected data is one from each of the nine series, where the one with the highest measured permeability have been chosen. The porosity of these specimens has, as previously mentioned, not been measured and therefore the calculated value have been used as a substitute. If theory and practice can generate the same porosity, this should not be a problem.

Studying the results on the plot shows that some of the data series have steeper curves than the preliminary case 7 S. It is assumed that there is nothing wrong with the permeability measurements, as they have been conducted in the same way. Only one thing has been changed. The porosity is calculated from the natural porosity of the aggregates and the degree of filling instead of measured. This must indicate that the calculated porosity

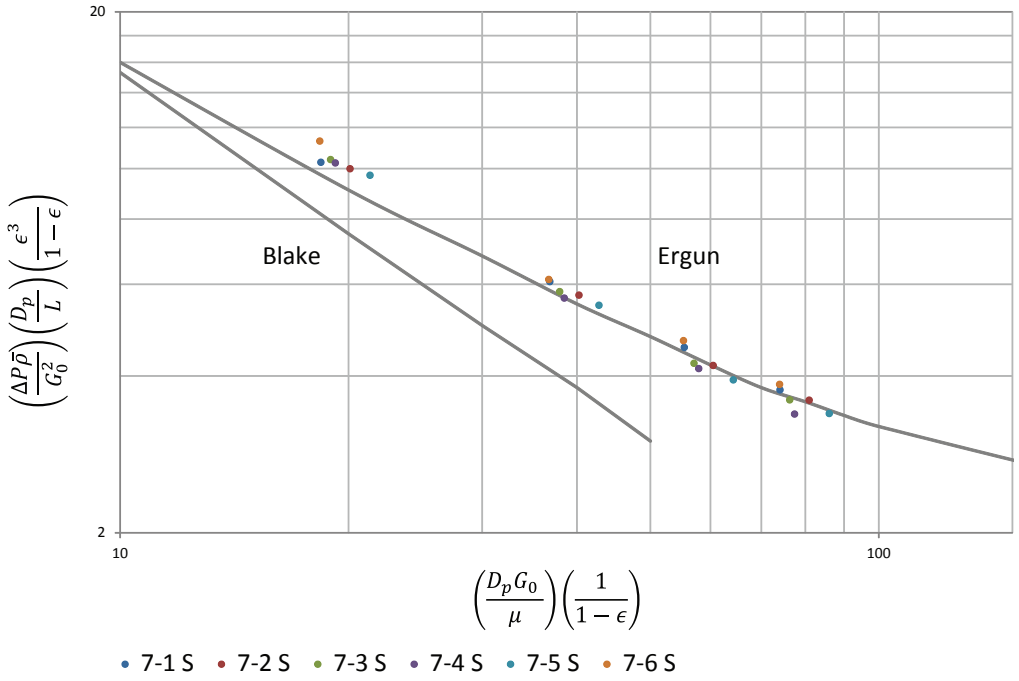

Fig. 11.2. A close-up of the data from case 7 S, which is an initial test case.

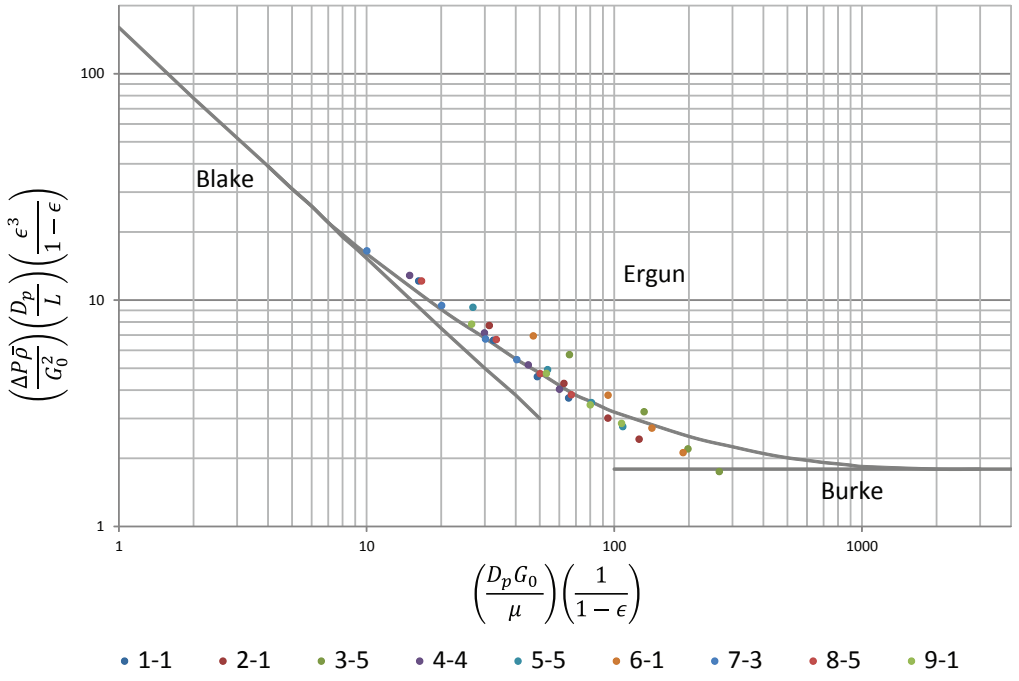

Fig. 11.3. Selected results from the w/c ratio and degree of filling study where the porosity is calculated, showing cases from 1 to 9.

cannot be trusted. The adjustment of the wetted surface area resulted in a large variation in the mean particle diameter. The values span from 7-32 mm, which is much more than for case 7 S and very far from the actual particle diameters.

A good example of the effect the incorrect porosity has on the results is shown in figure 11.4. Two selected data series, one from case 6 and one from case 7, are compared and analysed.

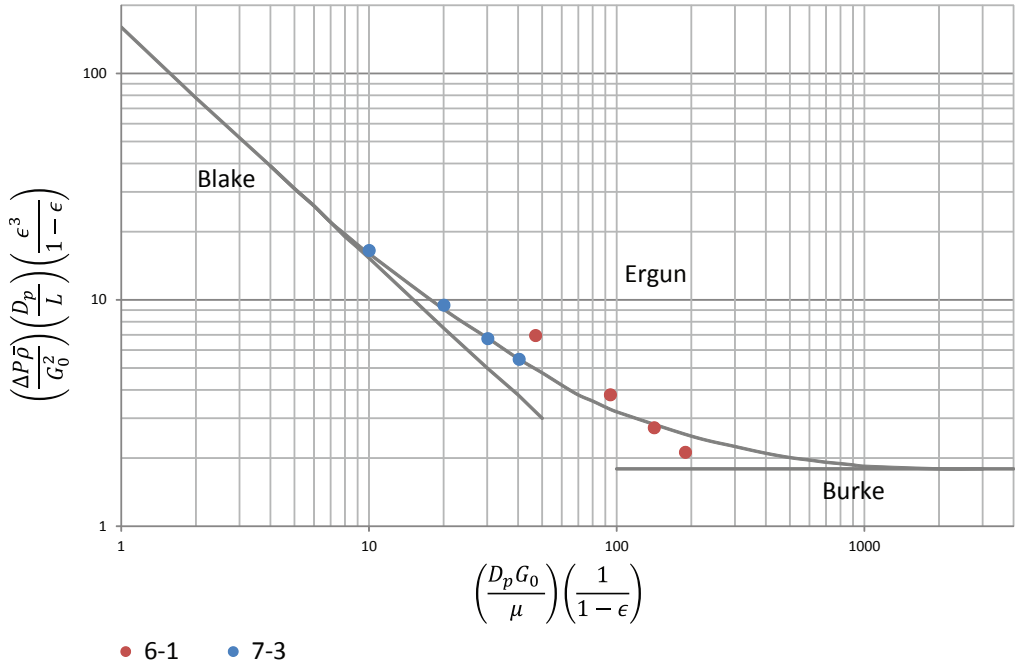

Fig. 11.4. Selected results from cases 6 and 7.

It is very clear that the calculated porosity for case 7 fits better than for case 6. When looking at the calculated values for the mean particle diameter, the same conclusion can be drawn. The mean particle diameter for case 6 is 23 mm and for case 7 it is only 6 mm, which is very close to the result obtained using the preliminary case 7 S. The reason for the mean particle diameter for case 6 is very large is that the porosity used in the calculations not is the correct porosity. The porosity used in all cases is the theoretical value, which for cases 1-6 does not fit with the actual value. If the porosity is calculated based on the density of the specimens, the results will be like the ones for cases 7-9 - case 7 shown in figure 11.4.

When the wetted surface area must be adjusted for each case it could be interesting to investigate if there is a connection between this value and the degree of filling, which directly controls the porosity of the specimens. For this investigation only cases 7-9 are used and the result are shown in figure 11.5.

It is visible that there is some correlation between the porosity and the wetted surface area, but this might be different for different values of w/c ratio. The fitted function is a power function with $R^2 = 0.999$.

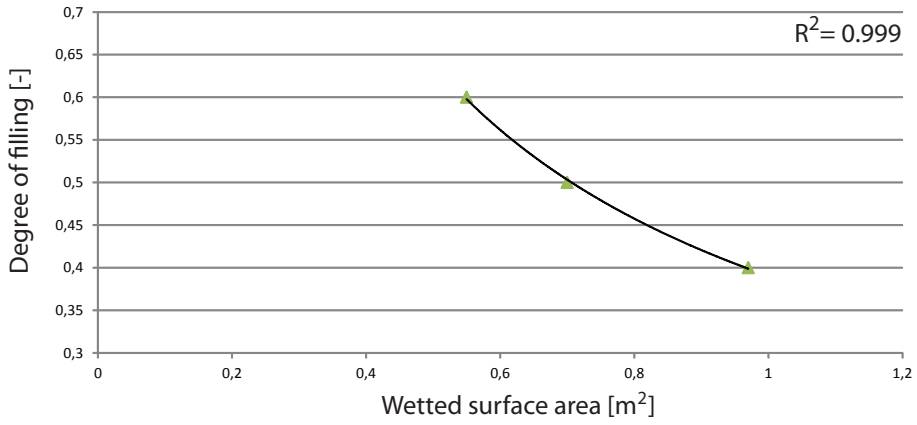

Fig. 11.5. Relation between the adjusted wetted area and the degree of filling of the specimens. Shown for w/c ratio of 0.30.

The conclusion of using the theory from Transport Phenomena [43] is that if the porosity is measured and the wetted surface area is fitted to match the individual data series, the theory fits well. When discussing friction factors and air flow through complex systems the wetted surface area is a very powerful factor. If this value could be obtained through measurements it would be the optimum solution.

Another conclusion which can be made is that according to the theory the air flows in the different series are very close to laminar because the incline of the data series is almost the same as for the Blake-Kozeny equation. The same conclusion is made from the permeability calculation conducted on every specimen, where the pressure exponent for all specimens is found to be between 0.853 and 0.995. This parameter claims a value between 0.5 and 1.0 where 0.5 is highly turbulent and 1.0 is laminar flow. This means a laminar flow as well, so the same result can be obtained from both methods.

Mathematical models 12

The mathematical models described in chapter 5 will be tested and, if needed, adjusted to fit the obtained data better. In chapter 10 it is shown that the derived functions seem to describe the parameter correlations fairly good.

The equations listed in section 5.1.1 is used to calculate the density of a chosen test case with a w/c ratio of 0.3 and a degree of filling of 0.5 (case 8 in the parameter variation). The value obtained is 1893.5 $\mathrm{kg/m^3}$ which is the same as the value calculated in the recipe, proving the density model to be very accurate. The same amount of SPA as used in the casting in this study, is used for every calculated density. The program using these models is matmodels.m, which can be seen on the [Enclosures-CD, Matlab folder].

12.1 Compressive strength

Figure 10.1 shows the relation between density and compressive strength and gives the function $f_c = 0.0528 \cdot \rho - 82.65$ which is used to calculate the strength. In figure 12.1 the compressive strength is plotted with the corresponding degree of fillings. Both calculated values (plotted as lines) and mean compressive strengths from the study cases 1-9 (plotted as circles) are included in the plot.

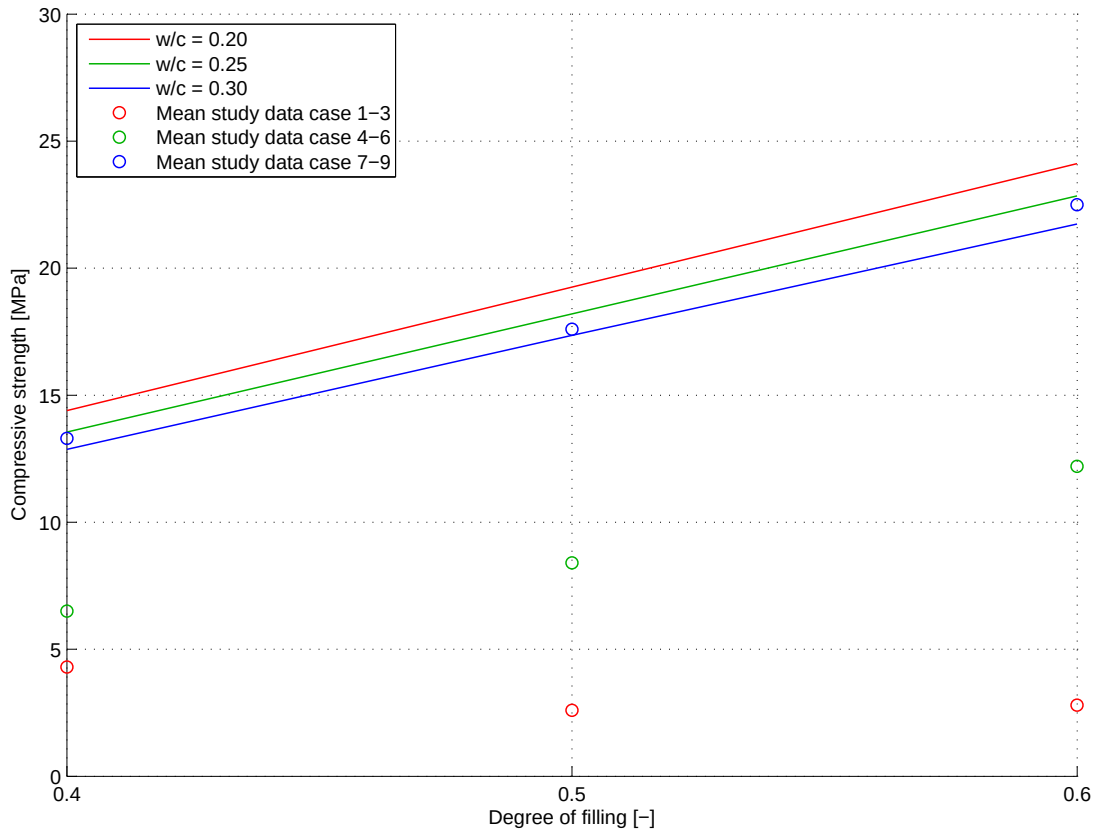

Fig. 12.1. Calculated compressive strength and mean compressive strength from measurements in this study.

The plot clearly states that with a w/c ratio of 0.3 the measured data fits very good with the calculated values, which is obvious due to the theoretical density matching the measured for these cases. However, for the lower values of w/c ratio, the data does not fit to the calculated compressive strength. It is important to emphasise the conclusion made in section 9.1, that the first six case (w/c ratio < 0.3) are cast improper resulting in smaller densities than intended. With the developed mathematical model to calculate the compressive strength the result will then be higher than the measured data. Normally a lower w/c ratio will generate higher strength, but as this is not the case in this study the model should only be used for cases with a w/c ratio of 0.3 when the relation between density and compressive strength probably is incorrect in the other cases. If all cases were cast properly it might have been necessary with a model for each value of w/c ratio.

The variation in the calculated compressive strength from w/c ratio to w/c ratio is very small, which is believed not to be realistic. Going from a w/c ratio of 0.3 to 0.25 gives a small increase in calculated density and thereby an increase in compressive strength. Density alone should not be sufficient to calculate compressive strength for several values of w/c ratio, there should be several functions (one for each w/c ratio).

12.2 Permeability

From the permeability model derived in section 5.1.3 the computed function, based on measurement data, $\kappa = 9.35 \cdot 10^{18} \cdot \rho^{-5.98}$ is shown in figure 10.3 in chapter 10. Using this function on the calculated densities corresponding to the densities in this study's parameter variation, gives the result shown in figure 12.2 (lines) which is plotted together with the mean values of the measured data from each case 1-9 (circles).

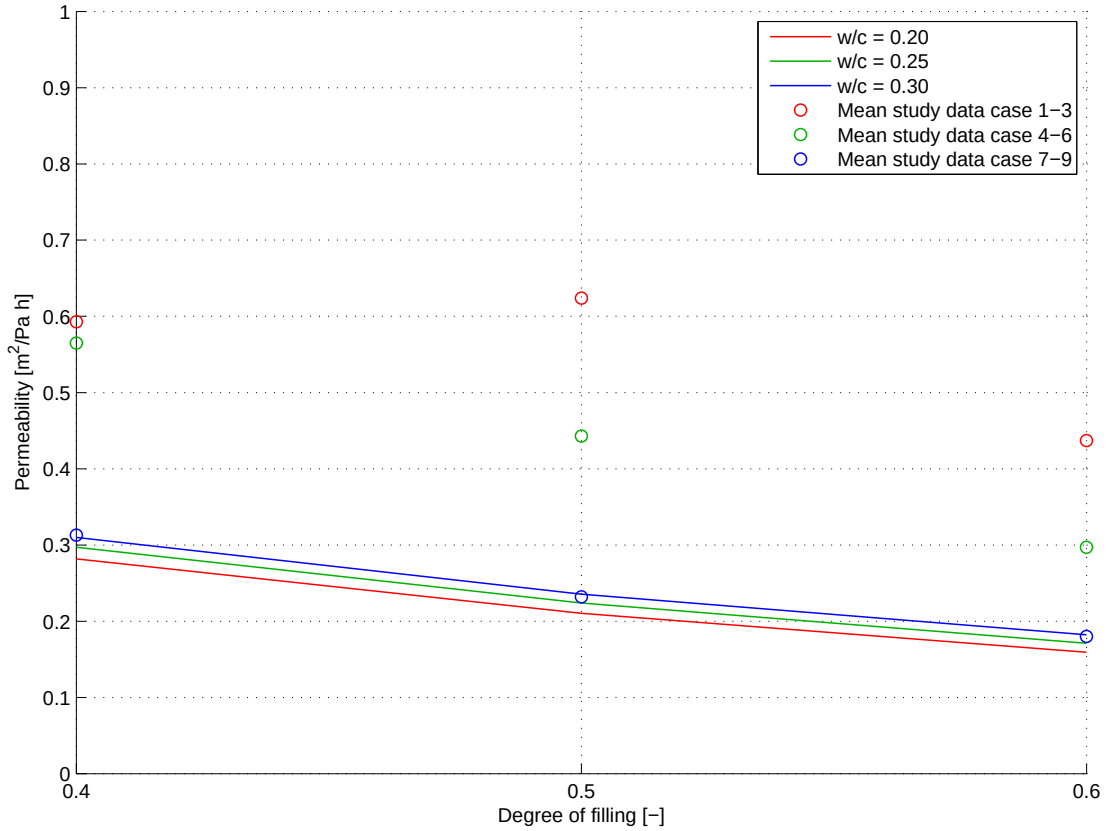

Fig. 12.2. Calculated permeability and mean permeability from measurements in this study.

The mean pressure exponent for the permeability measurements is 0.94, which is near laminar. It is clear that the model and data from cases with a w/c ratio of 0.3 fits well. The same conclusions as in section 12.1 can be made for this scenario, where the six cases with a lower w/c ratio than 0.3 are cast improper, for which reason they do not fit. As for the compressive strength model, it might be necessary to derive functions for each w/c ratio wanted.

Part IV

Energy performance - Experimental, results and discussion

Measurements 13

Part II of this study deals with more advanced experimental investigations of the energy performance of a few selected specimens with good properties, corresponding results and analysis and comparison with dynamical mathematical and numerical models. The measurements of part II covers thermal conductivity, specific heat capacity and heat exchanger efficiency. Detailed descriptions of the measurement setups and processes can be found in appendix B.

The specimens chosen to analyse for heat transfer and energy properties are cases 7 and 8, because these cases are proper cast according to the recipe and are the most air permeable cases with a w/c ratio of 0.3. Furthermore case 8 is chosen for PCM experiments, as this case is proven to be the most consistent.

13.1 Thermal conductivity

To measure the thermal conductivity square samples of the dimensions $15 \times 15 \times 8\,\mathrm{cm}^3$ are measured using a guarded hot plate apparatus λ-meter EP500. With this a series of temperature differences are applied to the upper and lower surfaces of the concrete blocks. The necessary effect to maintain the temperature difference is measured and from this the thermal conductivity is calculated. The criteria for when a stationary case is obtained (where λ can be calculated) is having a deviation of the calculated λ-value of no more than 1 % for 150 minutes. Further description of the setup can be found in appendix B.5.

For the thermal conductivity measurements no data treatment is necessary, as the software controlling the guarded hot plate apparatus λ-meter EP500 gives the result from the measurements.

13.2 Specific heat capacity

For this experiment the square samples ($15 \times 15 \times 8\,\mathrm{cm}^3$) are also used. The measurements are conducted with air permeable concrete and demineralised water in a good insulated environment. A warmer concrete element is put into cold water where these will exchange energy. After a while a state of equilibrium will occur, both materials will have the same temperature and from this equilibrium the specific heat capacity can be calculated by calorimetric principles. The temperature of the water is monitored over time in order to determine when equilibrium is achieved and to quantify the heat exchange with the

surroundings, although fairly small, through the insulating polystyrene box. A thorough description of the measurements can be found in appendix B.6.

13.2.1 Data treatment

From a reference measurement of the setup only with water the heat transfer through the polystyrene box is calculated. The measured temperature increase of the water corresponds to absorption of energy. This effect decreases concurrently with the difference in ambient and water temperatures. The gradient is determined to $\gamma = 0.056\,\mathrm{W/K}$.

Figure 13.1 shows an example of a conducted experiment with a concrete element. After a short period of approximate equalisation between the water and container, the concrete element is added and the measurement started.

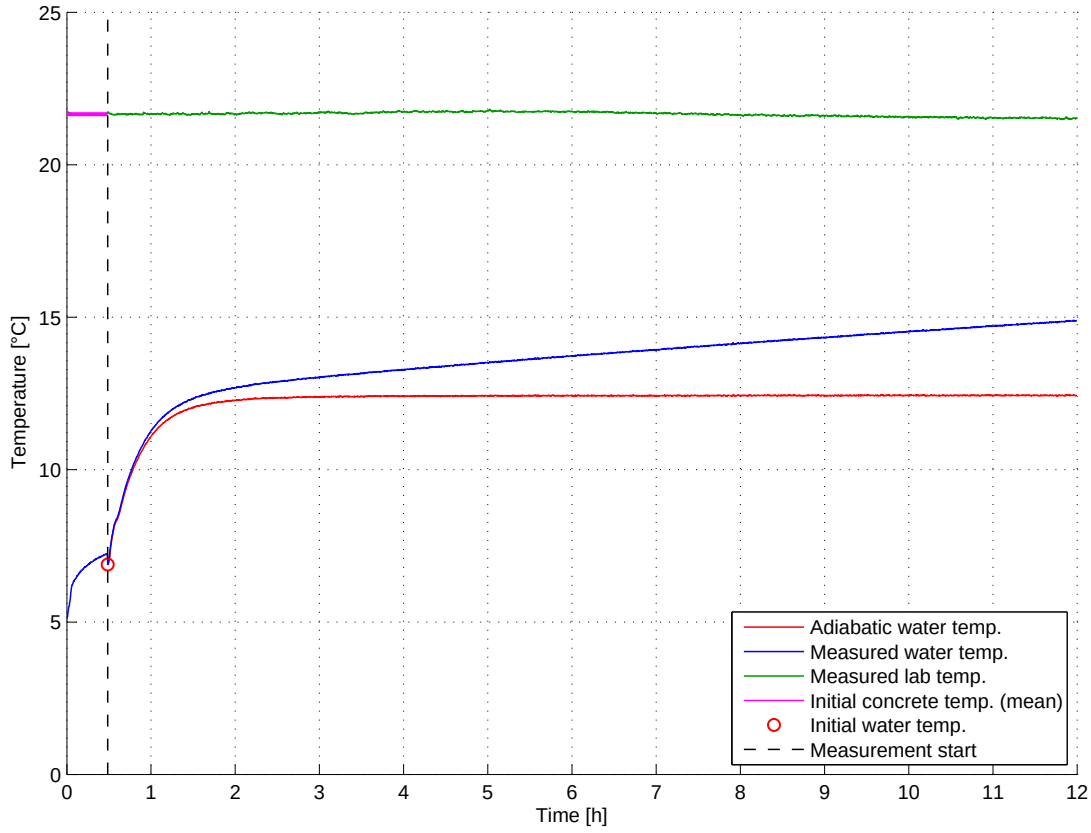

Fig. 13.1. Example of conducted specific heat capacity measurement.

The water temperature is increasing rapidly during the period of heat exchange with the concrete. After approximately 2 h of measurement, only the contribution from the surroundings is heating the setup. When this contribution from γ is subtracted in each time step, the result is the red curve of adiabatic water temperature. This clearly reveals the state of equilibrium and thus, the mutual temperature of water and concrete.

From the initial temperatures of the water and concrete and the achieved mutual temperature after exchange of heat, the specific heat capacity of the concrete can be

calculated. This is illustrated in equation 13.1.

$$cp_c = \frac{m_w \cdot cp_w \cdot (T_{mut} - T_{w,ini})}{m_c \cdot (T_{c,ini} - T_{mut})} \tag{13.1}$$

Where:

cp_c	Specific heat capacity of concrete [J/kg K]
m_w	Mass of water [kg]
cp_w	Specific heat capacity of water (4200 J/kg K)
T_{mut}	Mutual temperature [°C]
$T_{w,ini}$	Initial water temperature [°C]
$T_{c,ini}$	Initial concrete temperature [°C]

This method of data treatment and calculation of the cp-value has been used for all measurements. The program used is cp_static.m, which can be seen on the [Enclosures-CD, Matlab folder].

13.3 Heat exchanger efficiency

An important perspective of evaluating the potential for air permeable concrete is to know the effectiveness (η_s) of the concrete as heat storage at different air flows. For these measurements cylindrical specimens (100 mm × 200 mm) are used. A short presentation of the measurement setup and procedure will follow now and a detailed description can be found in appendix B.7.

13.3.1 Setup of experiment

To measure the heat exchanger efficiency an advanced setup is used. The objective is to send cold air through a warm specimen in a warm, stable environment and measure the cooling of the specimen over a period of time. The setup is illustrated in figure 13.2.

The environment for the specimen is a small box placed in a larger box, which functions as a controllable heating environment. Likewise the permeability setup, tape and the fittings are used to enclose the specimen ends and distribute the air flow. Both boxes are pressurised corresponding to the pressure in chamber 1 in order to avoid leakage to the environment.

The essential outputs from the measurements are temperature profiles, so the temperatures of the air before and after the specimen are logged as well as the temperatures around the specimen and in the environment. Unfortunately it is not possible to measure the temperature of the concrete sample, however it is possible with a few assumptions to calculate the effectiveness from the known air and environment temperatures.

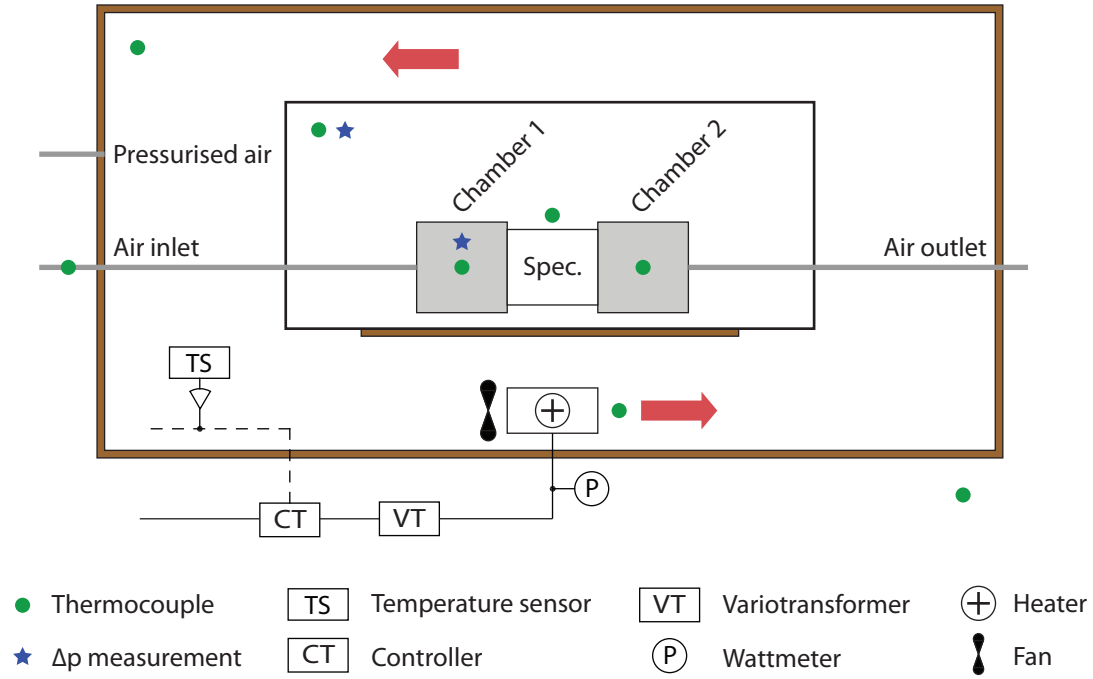

Fig. 13.2. Setup to measure η_e, dynamic heat capacity and COP.

13.3.2 Procedure for measurement

A preheated specimen is inserted in the likewise preheated small box. The system is then given 4-6 hours to achieve the state of equilibrium after which the cold air inlet will be opened and the measurements can begin. They continue for 12 hours, corresponding to the planned discharge period.

The three cases subjected to energy performance measurements are each tested at air flows of 4 and 6 l/min. This gives a total of six planned measurements.

13.3.3 Collection of data

The temperatures from the 12 h measurement period are collected with calibrated thermocouples connected to a data logger and continuously saved to a log file. For all data treatment and calculations, the computational software Matlab is used.

Matlab has been an essential tool of the project in order to process the large amounts of data gathered during the experiments. Several programs (m-files) have been composed to execute the different steps in converting data to results - among these data interpretation, calibration, calculations and plotting. All the m-files can be found on the [Enclosures-CD, Matlab folder].

13.3.4 Data evaluation

The following section serves as an initial evaluation and validation of the obtained data in order to assess whether they are suitable to process and convert to results. An example of a raw, calibrated log file is shown in figure 13.3. The program used for all data evaluation for this experiment is dataevaluation.m, which can be seen on the [Enclosures-CD, Matlab folder].

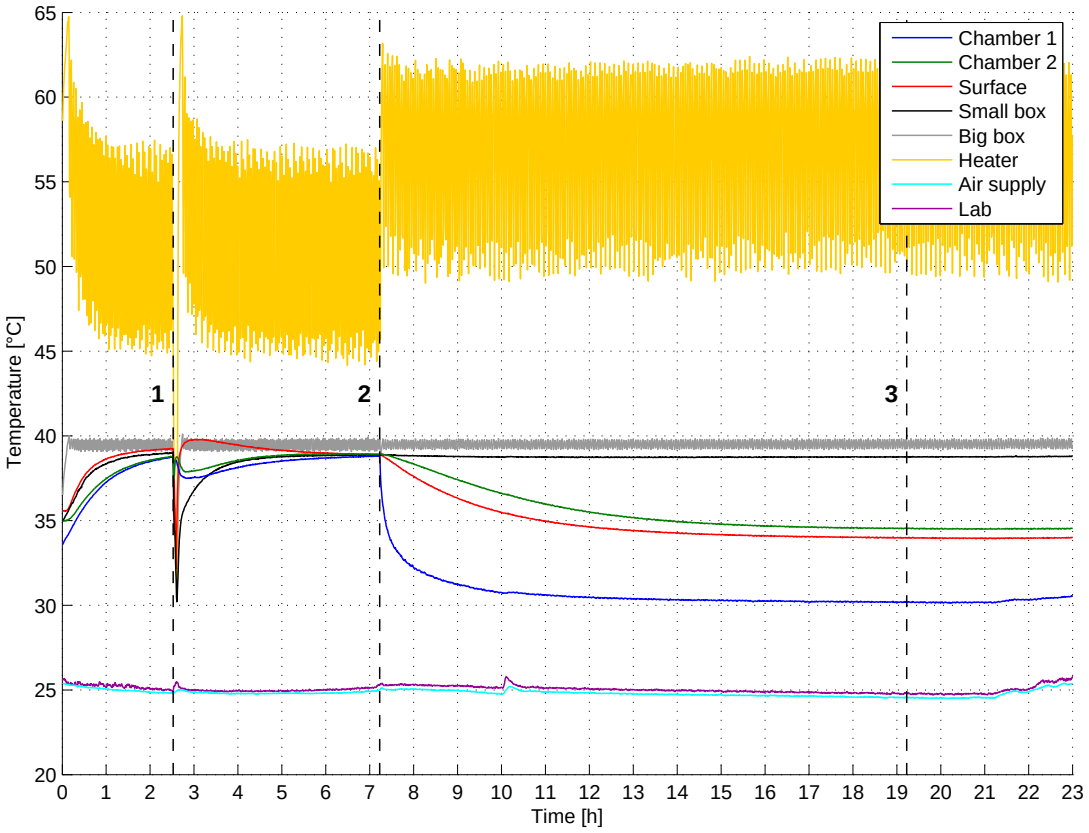

Fig. 13.3. Temperature profiles from the eight measurement points of the setup. Dotted lines represent time steps of interest. 1) The specimen is inserted. 2) Measurement begins. 3) 12 h measurement period ends.

Each temperature profile represents a thermocouple from the locations displayed as green circles in figure 13.2. The on/off control of the heater is seen to induce large fluctuations in temperature nearby. However, the energy is spread in the well-mixed big box resulting in small fluctuations. The point of interest, the small box, is seen to be stable.

The figure is marked with three dotted lines numbered from 1-3 representing elements for discussion and evaluation. The disturbance at mark 1 is a result of the, until then, heated boxes being opened to insert the preheated specimen. Almost 5 hours later the system was considered stable, which is confirmed at mark 2. At this time the cold inlet air is opened and for the energy balance it is important that the four temperatures of the two chambers, the specimen surface and the small box are the same. This is also satisfactory. The temperature at the heater increses to compensate for the energy drawn out of the system

by the air flow. The used temperature profiles for calculation of results are taken from the 12 h measurement period ending at mark 3, where a state of equilibrium is achieved. Later the inlet temperature is disturbed by temperature fluctuations in the laboratory (from hour 21) due to sun radiation in the morning. For this reason measurements run at night.

The temperature in chamber 2 is seen not to correspond to the one of chamber 1. In an idealised setup these will be identical when the concrete element is completely discharged of stored heat. However, this is not the case, due to heat contributions from the surroundings drawn through the specimen and chamber 2 by conduction. These contributions will be eliminated by data treatment.

13.3.5 Data treatment

Eliminating the heat contribution from the surroundings is based on the same principle as described for specific heat capacity calculation. The objective is to find a heat transfer coefficient, α, describing the contribution as a function of the temperature difference between the concrete and the small box (equivalent to the surrounding temperature). The internal surface area is not known, so the heat transfer coefficient is given in W/K. The concrete temperature cannot be measured and is therefore approximated by the surface temperature. The coefficient is calculated from the last time step, shown in equation 13.2.

$$\alpha = \frac{q_v \cdot cp_a \cdot \rho_a \cdot (T_{ch2} - T_{ch1})}{(T_{box} - T_{surf})} \tag{13.2}$$

Where:

α	Heat transfer coefficient [W/K]
q_v	Air flow [m^3/s]
cp_a	Specific heat capacity of air [J/kg K]
ρ_a	Air density [kg/m^3]
T_{ch2}	Temperature chamber 2 [°C]
T_{ch1}	Temperature chamber 1 [°C]
T_{box}	Temperature small box [°C]
T_{surf}	Temperature concrete surface [°C]

For each time step the energy balance is calculated as the air energy subtracted the contribution, yielding the ideal outlet energy in equation 13.3.

$$E_{out,i} = q_v \cdot cp_a \cdot \rho_a \cdot (T_{ch2,i} - T_{ch1,i}) - \alpha \cdot (T_{box,i} - T_{surf,i}) \tag{13.3}$$

From this ideal outlet energy the ideal temperature of chamber 2 can be calculated in each time step as shown in equation 13.4.

$$T_{ch2ideal,i} = \frac{E_{out,i}}{q_v \cdot cp_a \cdot \rho_a} + T_{ch1,i} \tag{13.4}$$

The ideal temperature of chamber 2 is shown in figure 13.4 along with the four other temperatures of interest from the 12 h measurement period.

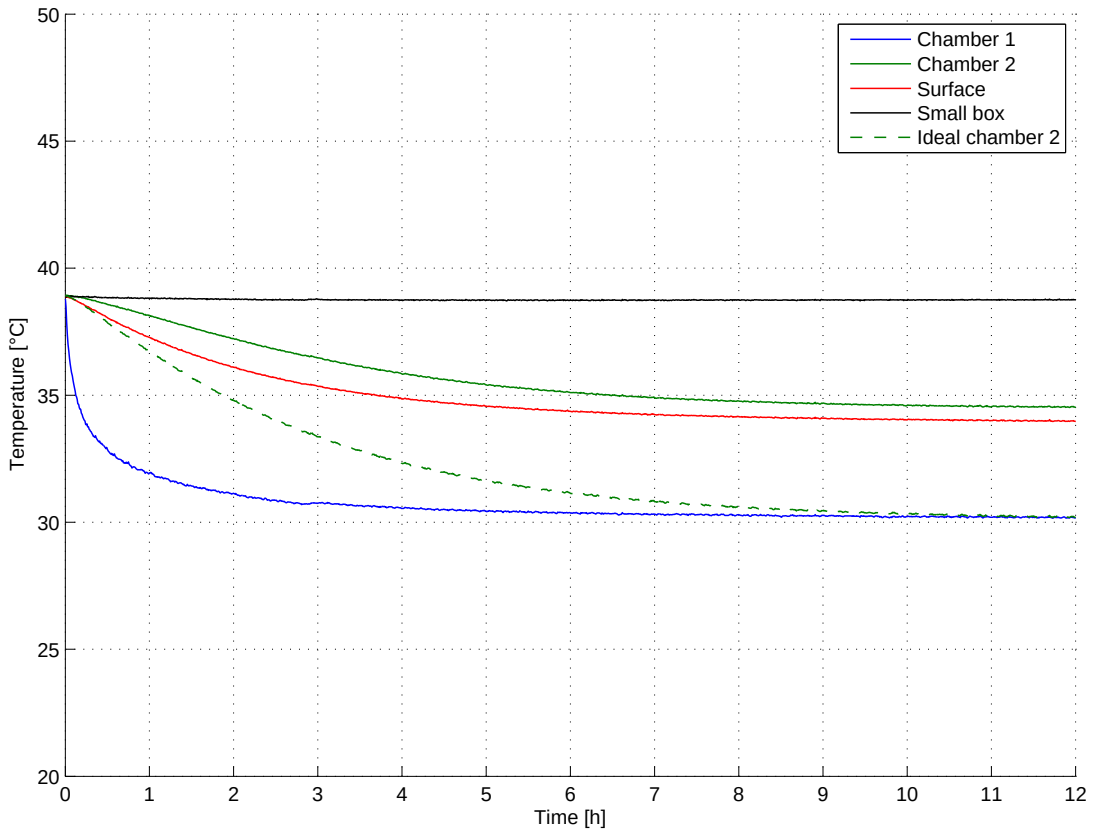

Fig. 13.4. Temperature profiles of the two chambers, the specimen surface, the small box and the idealised chamber 2 from the 12 h measurement period.

It is clear that the temperatures in the two chambers are identical as expected. The ideal temperature of chamber 2 will be used as a substitute for chamber 2 throughout the calculation of results.

13.3.6 Uncertainty assessment

Assessment of uncertainty of the heat exchanger efficiency measurement is likewise the uncertainty of permeability based on combined measurement uncertainty due to the impact of several parameters. The majority of these are the same as for permeability, but also the pressurised air and the thermocouple setup play an important role. The available air pressure fluctuates a little, which influences the 12 h of measurements.

The thermocouple setup and uncertainties of this is obviously also important to consider when measuring temperatures. The accuracy of a single thermocouple is ± 1.5 K, however, much higher accuracy can be achieved by calibration. Details about thermocouples, calibration and the setup can be found in appendix B.7.2. After calibration the absolute uncertainty of thermocouples is 0.083 K [44]. The uncertainty of the system is estimated relative to measured temperatures, though. All the parameters and their contributions are listed below.

- Deviations in available air pressure ±7.5 % (largest observed deviation)
- Thermocouples ±2 % (estimate)
- Furness micro manometer accuracy ±0.1 % (with reference to the instrument data sheet)
- Rotameter accuracy ±4 % (with reference to the instrument data sheet)
- Rotameter reading ±1 % (estimate)
- Tape ±1 % (estimate)
- Assembly ±2 % (estimate)

There is linearity between the parameters, so their relative influence on the total uncertainty is set to a factor of 1.0. The total uncertainty can then found as the square root of the quadrature sum of the single uncertainties.

$$\delta_{\eta s} = \sqrt{7.5^2 + 2^2 + 0.1^2 + 4^2 + 1^2 + 1^2 + 2^2} = \pm 9.1\,\%$$

14 Results

The results of the measurements concerning energy and thermal conductivity will in this chapter be presented and analysed. Three cases, 7, 8 and 8 with PCM (2 % by weight of the concrete), are used in this part of the study. Case 8 and 8 with PCM have the same w/c ratio and degree of filling.

14.1 Thermal conductivity measurements

The thermal conductivity is measured around three different temperatures (10, 20 and 40 °C) with a temperature difference of 15 K. This means that measuring λ around 10 °C yields the cold side at 2.5 °C and the warm side at 17.5 °C. The setup is described in appendix B.5.

Expectation about the thermal conductivity is, that it should be lower than for ordinary concrete which has a thermal conductivity of 1.5-1.8 W/m K. This is due to the stagnant air in the voids and the fact that it works as an insulator. A lower degree of filling creates more or larger voids, for which reason the thermal conductivity must be lower as well. Furthermore the case with PCM should obtain a lower value than the corresponding case without PCM, as PCM has a lower thermal conductivity than cement paste. In table 14.1 the measurement results are shown.

Case ID	λ around 10 °C [mW/m K]	λ around 20 °C [mW/m K]	λ around 40 °C [mW/m K]
7	1200.4	1205.7	1227.4
8	1235.5	1242.6	1264.3
P8	1350.5	1376.8	1374.9

Table 14.1. Thermal conductivity measurement results. Square samples are used in this experiment.

The expectation of a lower degree of filling generating a lower thermal conductivity seems to hold when looking at the results from case 7 and 8. It is observed that an increase in the degree of filling of 0.1 gives an increase in thermal conductivity of approximately 3 %, which could be a singular instance for the measurements conducted in this study due to the small population.

Case P8 shows an increase in the thermal conductivity in relation with case 8. Further

there is a decrease going from λ around 20 °C to λ around 40 °C. These results are not coherent with any literature or other measurements for which reason they are not further treated.

14.2 Specific heat capacity measurements

Traditional concrete has specific heat capacity of approximately 0.8-1.0 kJ/kg K given various literature, which for air permeable concrete is expected to be in that range. This is due to the fact that this parameter is related to weight and not volume. It is furthermore expected that a change in degree of filling will change the specific heat capacity slightly, as the relation between aggregate and cement paste is changed and these do not have the same specific heat capacity. For the case with PCM the specific heat capacity is expected to increase, as this experiment is conducted in a fashion which ensures that the PCM has been activated. The result of the measurement will then be a mean value for that specific temperature range which is used. The specific heat capacity is measured using the setup described in appendix B.6 and the results of the measurements are shown in table 14.2.

Case ID	Specific heat capacity [J/kg K]
7	987.4
8	1019.1
P8	1020.5

Table 14.2. Specific heat capacity measurement results. Square samples have been used in the experiment.

It can be seen that the specific heat capacity increases along with the degree of filling. An increase of 3.2 % is observed. The experiment for the sample with PCM was conducted in a fashion which made sure that all PCM was activated, cooling it from 29 °C to 17.5 °C. The calculated value represents a mean value in this interval, where all PCM is activated and thereby this value can only be used when this criteria is met. Compared to the expectations the specific heat capacity did not increase much by adding PCM to the concrete. The expectations was that it would increase to approximately 1045 J/kg K, which is based on the result from case 8 and an added weighted mean contribution from the PCM.

14.3 Concrete heat exchanger efficiency measurements

In this section the results from the measurements described in appendix B.7 will be presented. Measurements are conducted on three different samples with 4 and 6 l/min. The samples are those chosen from part III and the sample with PCM.

The results will be presented as a heat exchanger efficiency and a corresponding coefficient of performance (COP), calculated based on the measured temperatures in each time step of 30 s. In equation 14.1 the heat exchanger efficiency calculation is shown.

$$\eta_e(i) = \frac{T_{Ch2}(i) - T_{Ch1}(i)}{T_{sur}(i) - T_{Ch1}(i)} \tag{14.1}$$

Where:

$\eta_e(i)$	Heat exchanger efficiency [-]
$T_{Ch2}(i)$	Air temperature in chamber 2 in time step i [°C]
$T_{Ch1}(i)$	Air temperature in chamber 1 in time step i [°C]
$T_{sur}(i)$	Reference surface temperature in time step i [°C]

The reference surface temperature is measured in the middle of the specimen (length-wise) and is used as a reference temperature for the concrete specimen. The measured surface temperature is not a good representative for the mean concrete temperature, but in the absence of an obvious way to measure the concrete temperature it works as a reference point.

Calculation of the COP is shown in equation 14.2.

$$COP(i) = \frac{E_{con}(i)}{E_p} \tag{14.2}$$

Where:

$COP(i)$	Coefficient of performance in time step i [-]
$E_{con}(i)$	Energy transferred to concrete element by driven air in time step i [J]
E_p	Energy needed to drive the air [J]

The energy transferred to the concrete by the air can be calculated using equation 14.3, where the adjusted temperature for chamber 2, described in section 13.3.4, is used.

$$E_{con} = q_v \cdot \rho_{air} \cdot c_{p,air} \cdot (T_{Ch2,i} - T_{Ch1,i}) \tag{14.3}$$

Where:

$T_{Ch2,i}$	Air temperature in chamber 2 in time step i [°C]
$T_{Ch1,i}$	Air temperature in chamber 1 in time step i [°C]

The electrical power needed to drive the air is calculated by using equation 14.4. For this calculation it is necessary to estimate a value of the fan efficiency (η_f), as this is not known. This value is set to 0.8, the same as used in the initial evaluation of performance potential.

$$E_p = \frac{\Delta p \cdot q_v}{\eta_f} \cdot t \tag{14.4}$$

Where:

η_f	Fan efficiency [-]
t	Length of time step [s]

These equations are used to calculate values of heat exchanger efficiency and COP for all time steps. The program used for these calculations are eta_e.m, which can be seen on the [Enclosures-CD, Matlab folder]. The results of these calculations are presented in the following section.

14.3.1 Measurement results

As described in appendix B.7 the procedure when conducting these measurements, is that all temperatures of interest must have the same initial temperature before starting the air flow. In a few cases this has not been possible, for which reason some η_e values do not start with a value of 1.0. This does, however, not affect the shape or development of the rest of the plot. The first measurement to be presented is for case 7, which is shown in figure 14.1.

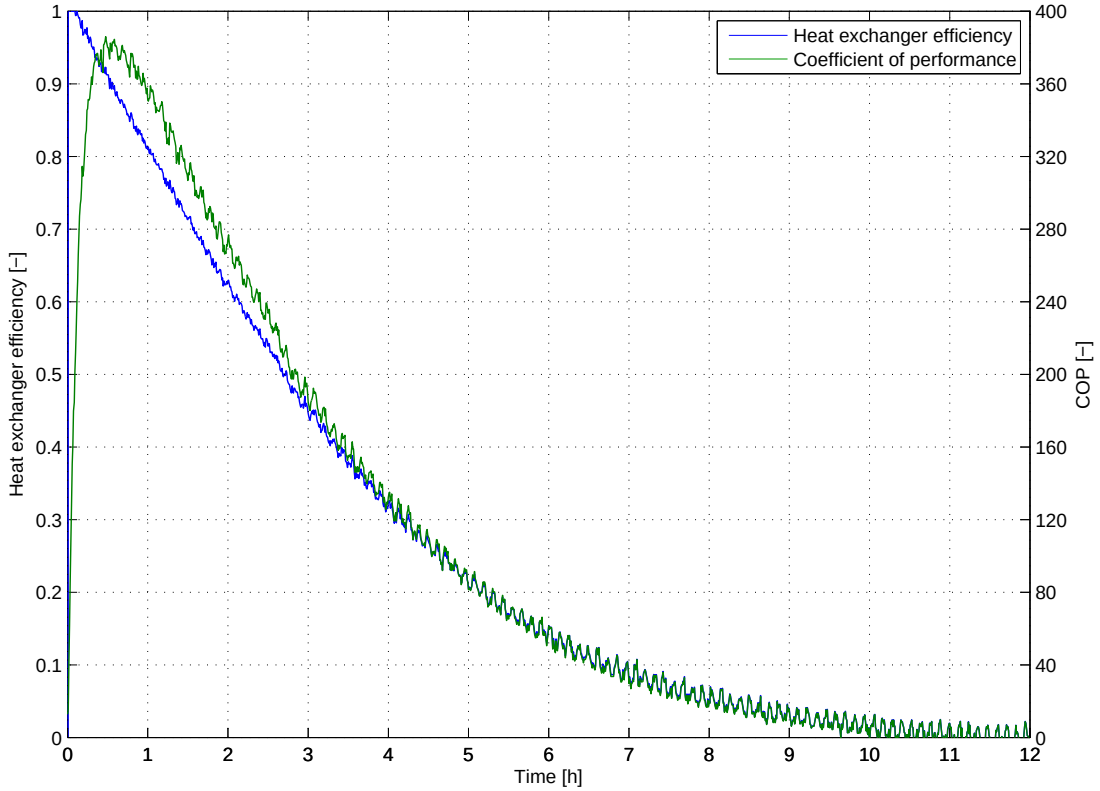

Fig. 14.1. η_e and COP values for cooling case 7 with 4 l/min.

It is clear that the η_e value starts at approximately 1.0 and drops to a value of approximately 0 over the time period. It takes approximately 5 h to discharge the concrete enough for the heat exchanger efficiency to drop to 0.2 (comparison reference value). The highest COP value reach approximately 380, which is extremely high in relation to a

general heat pump COP of approximately 5.0. If the criteria for when to stop air transport through the sample is a COP of 5.0, approximately 10 h of discharge is possible using this concrete recipe. After 12 h both values are visually set to 0.

The same sample with a larger air flow of 6 l/min is shown in figure 14.2.

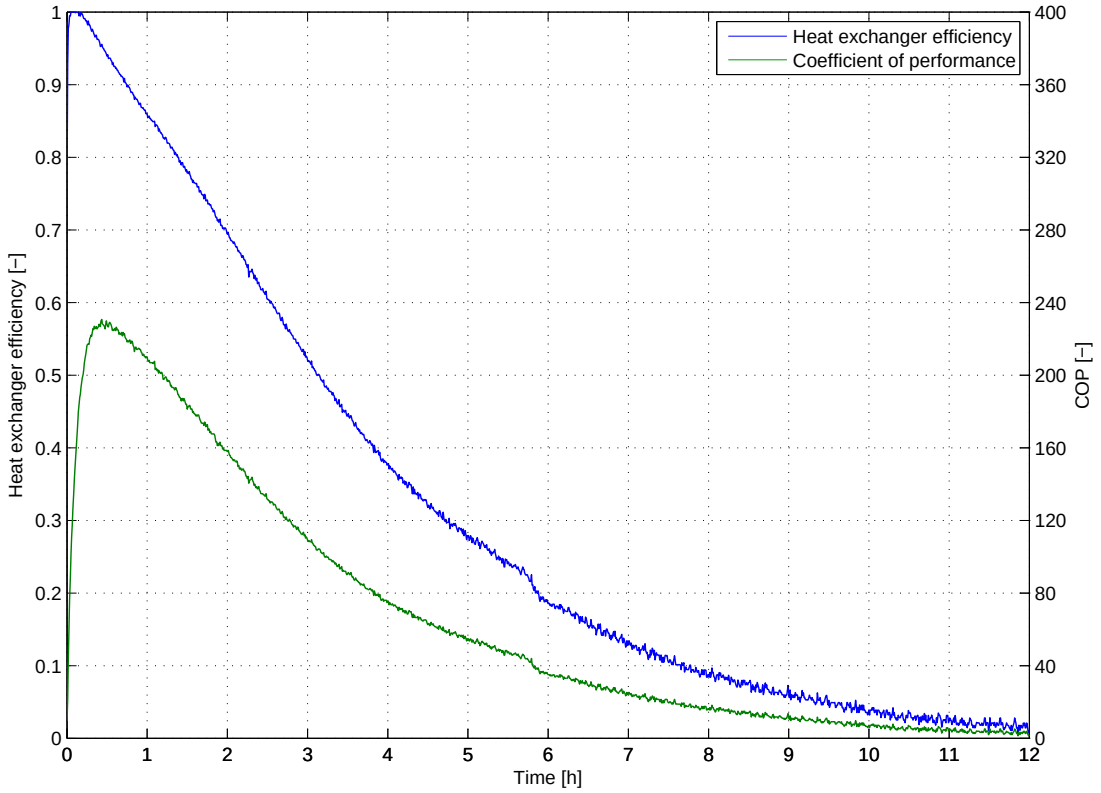

Fig. 14.2. η_e and COP values for cooling case 7 with 6 l/min.

f In this measurement the η_e value forms the same curve from 1.0 to 0 and it takes almost 6 h to drop to a value of 0.2. The COP now has a maximum value of around 230, a reduction of 40 %. The criterion of a COP of 5.0 is still met until approximately 11 h and both curves have almost reached 0 after 12 h.

To check what the difference in the two cases are in relation to the COP calculation, the temperature difference between chamber 1 and 2 are plotted in figure 14.3.

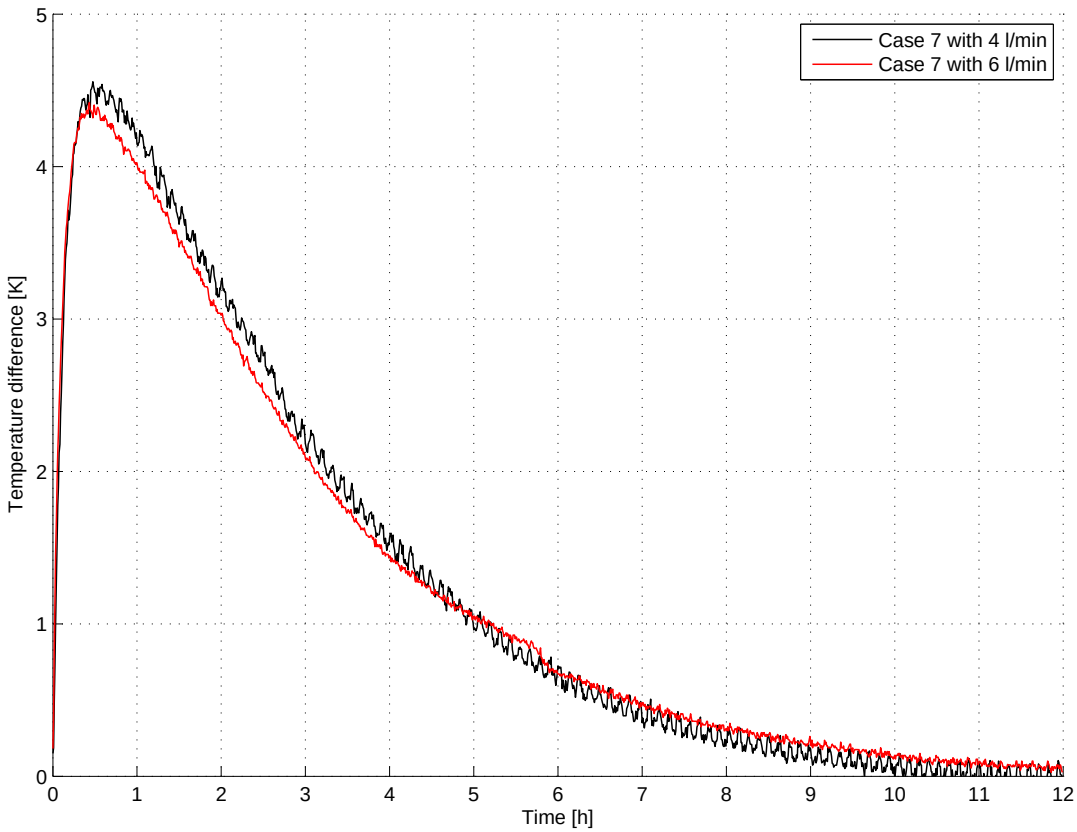

Fig. 14.3. Temperature difference between chamber 1 and chamber 2 with case 7, 4 and 6 l/min of air flow respectively.

As these two temperature differences are almost identical, it cannot be these values which generate the large difference in COP. The permeability or the pressure difference needed to drive the air could be the reason, as this value varies in these two cases. The pressure difference needed to drive 4 l/min is 11.4 Pa and 18.5 Pa for 6 l/min, which also gives a reduction of approximately 40 %. This means that the difference in COP is only due to the reduced electrical power needed to drive the air. It can be concluded from the figure that the energy transferred to air from the surroundings (on its way from chamber 1, through the specimen and to chamber 2) increases when the air flow is increased from 4 l/min to 6 l/min.

The next result is for another concrete sample, case 8, which has a higher degree of filling. A higher degree of filling means a larger thermal mass which should result in a larger area under the η_e curve than for case 7 with corresponding air flows. Furthermore the COP should be decreased as a result of a less permeable specimen, even though there is an increase in thermal mass. In figure 14.4 the result for 4 l/min is shown.

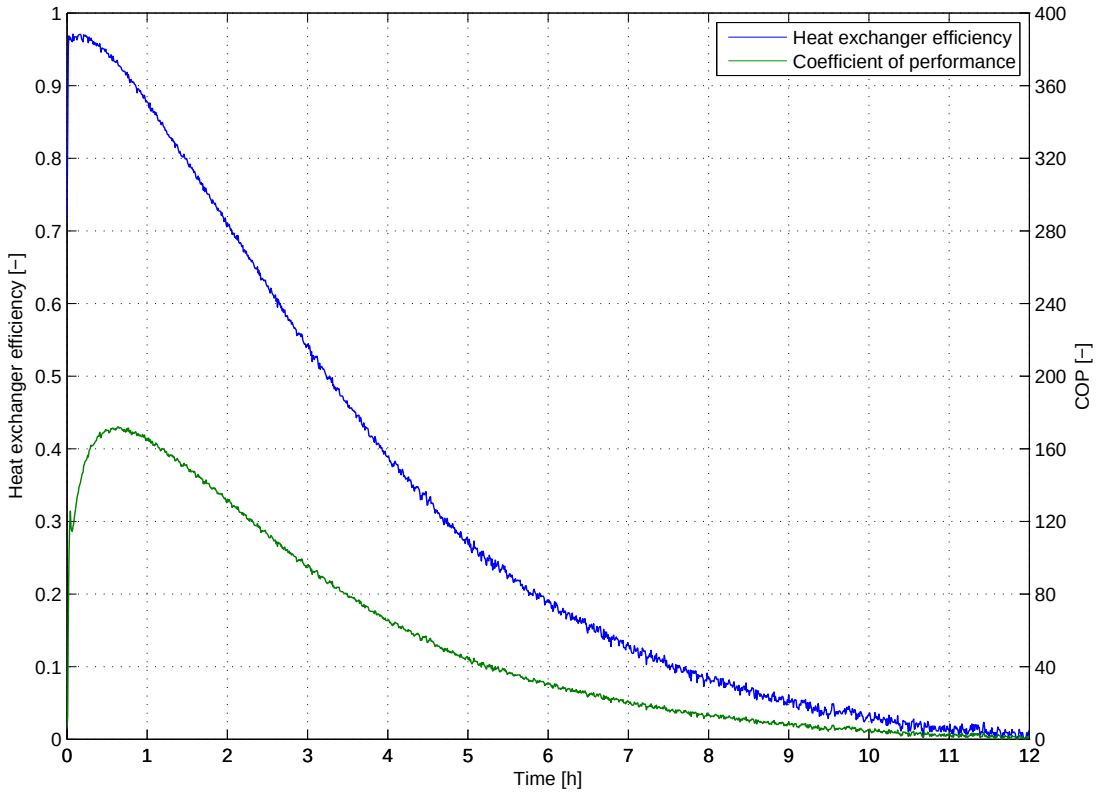

Fig. 14.4. η_e and COP values for cooling case 8 with 4 l/min.

The first observation of the η_e curve is, that is does not start in 1.0, which is due to the starting temperatures not being equal as previously described. It takes almost 6 h for the η_e value to drop to 0.2 and it is near 0 when 12 h have passed. The COP maximum value is approximately 170, which is significantly lower than for case 7. It takes 10 h for the COP to decrease to approximately 5.0 and it is near 0 after 12 h.

The investigation of why the COP dropped with a higher air flow showed that it was due to the increased pressure difference needed. This means that the next result presented, which is for case 8 with 6 l/min, should have a smaller COP in relation. The result of the measurement can be seen in figure 14.5.

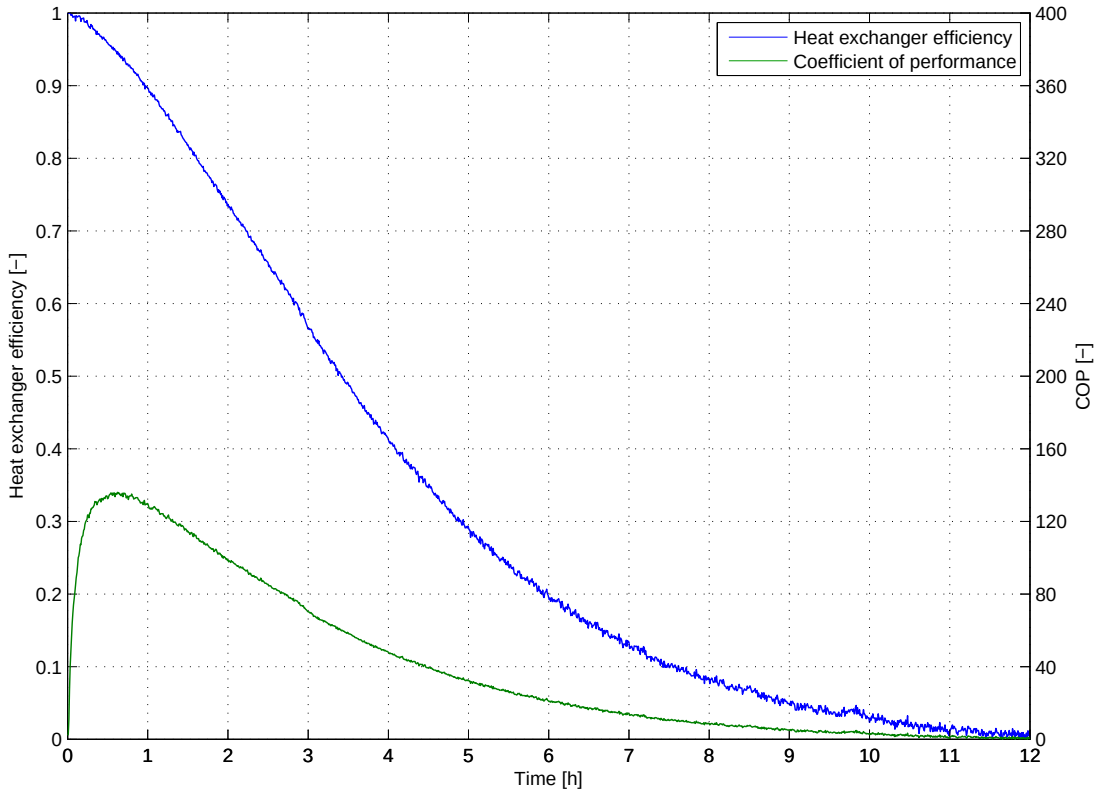

Fig. 14.5. η and COP values for cooling case 8 with 6 l/min.

As can be seen, the COP has a lower peak value of about 135 and is 5.0 after 9 h. In relation to an air flow of 4 l/min it takes 1 h less to reach a COP of 5.0. The η_e curve is down to 0.2 after 6 h and visually 0 after the 12 h period, which is nearly the same.

Conducting this experiment with samples including PCM sets new conditions for starting and ending temperatures in order to activate the PCM. As an attempt of meeting these requirements, the starting temperature was decreased to 30 °C. It was, however, not possible to maintain this temperature in the entire environment, for which reason the starting temperature for the inlet, chamber 2, sample surface and local environment all were different. Furthermore it was not possible to cool the concrete enough to activate the entire amount of PCM using the air flows from the other experiments. For this reason a higher air flow of 20 l/min was tested as a way of minimising the effect of the contributions to the inlet air temperature. With this high air flow the pressure around the specimen could not be maintained, for which reason leakages may be present, generating errors in the experiment. Due to a temperature gradient through the specimen it is believed that some of the PCM have been activated during the measurement, but this amount is unknown. The η_e curve cannot be calculated due to the varying thermal mass of the PCM in the concrete sample. To show the result for case P8 the temperatures of interest are shown in figure 14.6.

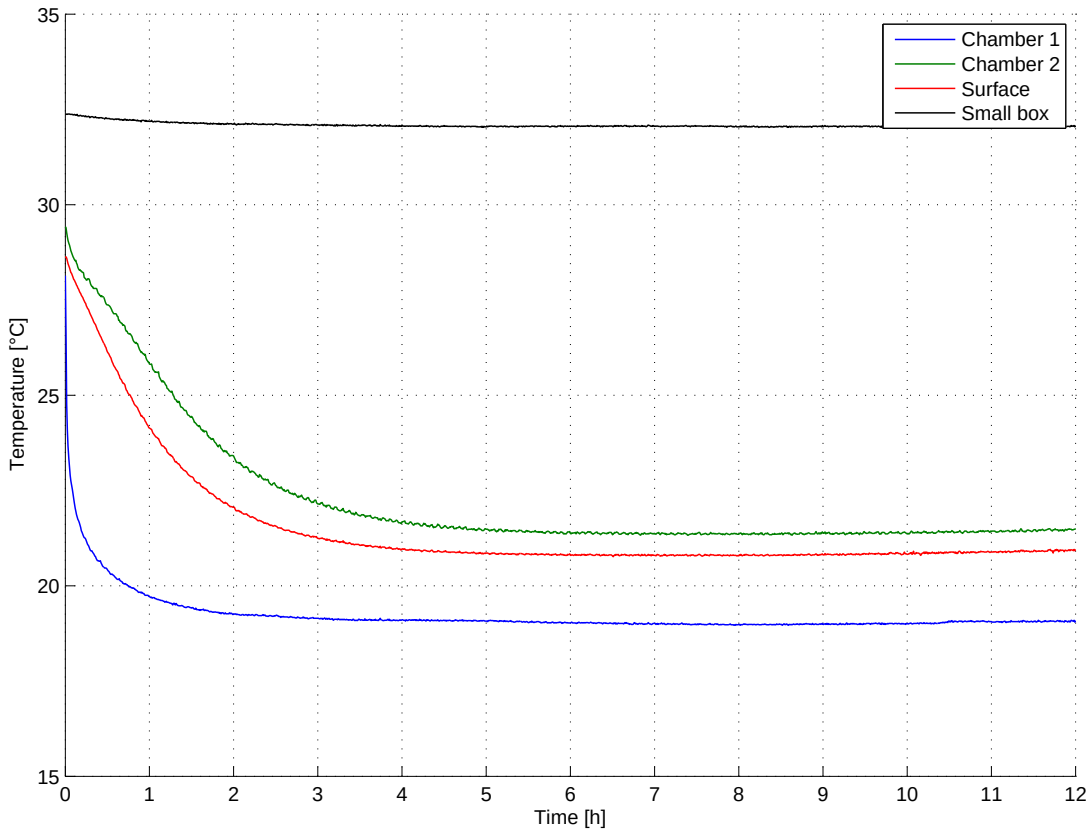

Fig. 14.6. Temperatures through a 12 h period for case P8 with 20 l/min.

From the figure it can be concluded that the specimen is cooled more than in the other experiments, which was expected due to the significantly increased air flow. Furthermore it is visible that the temperature profiles for the specimen surface and chamber 2 are stabilised after only approximately 6 h, showing that the discharge time is decreased significantly in relation to the results of case 8.

For initial performance calculations, described in section 4.1, η_e is used as a constant value, which is clearly proven not to be the case according to the measurements.

14.3.2 Comparison of measurements

In order to get a better indication of how the different measurements performed in relation to each other, plots with η_e values from the cases will be presented in this section. In figure 14.7 case 7 is shown with both air flows tested. If the same starting and end temperatures are achieved in both experiments, the area under the curves should be the same as the same thermal mass is discharged. The higher air flow would discharge the concrete faster, but also maintain a higher η_e value longer time.

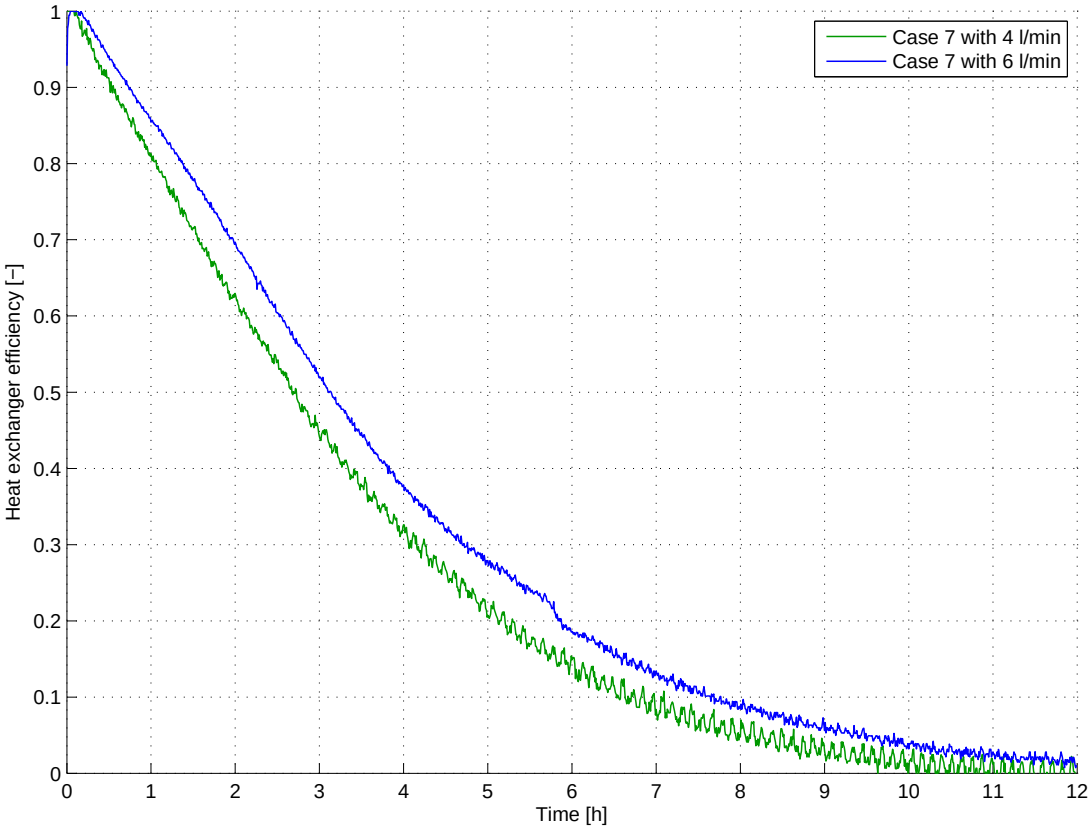

Fig. 14.7. η_e curves for case 7 with 4 and 6 l/min respectively.

It is clear that the area under η_e for 6 l/min is larger than under 4 l/min, which indicates that a larger amount of energy is transferred, meaning in this scenario that the concrete is cooled to a lower temperature. η_e for 6 l/min is larger the whole period and this is due of the contributions to the inlet air from the surroundings and the increased difference between the outlet and concrete reference temperature. The area under the curves are 385 for 4 l/min and 453 for 6 l/min, which is a difference of 18 %.

The next comparison is for case 8 where the same air flows are used. In figure 14.8 the result is shown.

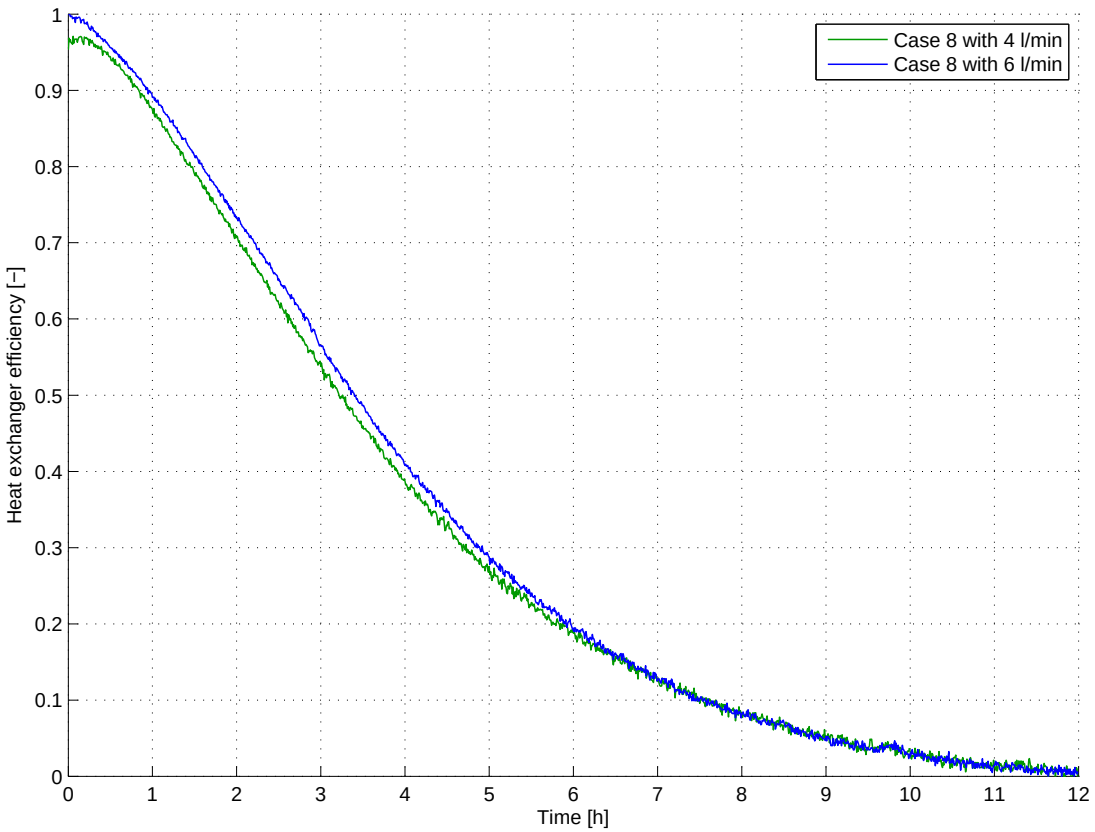

Fig. 14.8. η_e curves for case 8 with 4 and 6 l/min respectively.

As the previous comparison, the areas under the curves are not the same. For this sample the difference is only 4 %, with areas of 453 for 4 l/min and 469 for 4 l/min, which is much lower than for case 7. Again it is the η_e with the highest air flow which has the largest area under the curve.

These comparisons may indicate that the influence from the local environment to the inlet air decreases as the air flow increases. Unfortunately is has not been possible to conduct experiments with higher air flows with the current setup.

To compare with the initial calculated performance, where a value of 281 kJ/m^2 K and traditional concrete with a comparison value of 100 kJ/m^2 K was found, the heat dynamic capacity of each sample in the given period of time with different air flows have been calculated. This calculation can be seen in equation 14.5.

$$c_{dyn} = \frac{\sum(q_v \cdot c_{p,air} \cdot \rho_{air} \left(T_{Ch2,i} - T_{Ch1,i}\right)) \cdot \Delta t}{A_{con} \cdot \left(T_{Ch2,1} - T_{Ch2,12h}\right)} \tag{14.5}$$

The results of this calculation for each case are shown in table 14.3. All values are directly comparable as they all have been calculated from a 12 h period of discharge.

Case	Air flow [l/min]	Dynamic heat capacity [kJ/m^2 K]
7	4	71.9
7	6	108.5
8	4	81.3
8	6	115.3
P8	20	181.5

Table 14.3. Calculated dynamic heat capacities over a period of 12 h.

A previous conclusion in this section states, that the same dynamic heat capacity should be achieved for each sample with different air flows, if the sample is completely discharge in the 12 h period. The contributions from the surroundings to the inlet air changes this assumption, given approximately the same temperature difference of the individual samples through the experiment. This makes the air flow the changing factor in the calculation going from 4 l/min to 6 l/min, generating a 50 % increase from the small to the high air flow. The results show about the same pattern.

The experiment with case P8 shows that more thermal mass has been utilised, as a higher dynamic heat capacity has been calculated. It is known that the method used to calculate the value is not correct for this sample, but it is believed that the result is the best possibility to compare this sample with the others used. The value is a 57 % increase compared to case 8 with 6 l/min. This increase cannot be trusted, however, there is a clear indication that the added PCM contributes to the thermal mass of the specimen.

Mathematical models 15

The mathematical models from chapter 5 will be used and results compared with measured values. The built models do not include PCM in the concrete, so only cases without PCM will be treated.

15.1 Thermal conductivity

The model for thermal conductivity developed by Imbabi et al. [10] will in this section be tested. Heat transfer properties of the individual materials used to cast the concrete are used in the equation. Unfortunately the thermal conductivity of the aggregate used is unknown and due to this problem this value has to be adjusted in order to make the model fit with the measured values. The criteria for if the model fits is then, if the value of thermal conductivity for the aggregate is reasonable. According to various literature this value should be within 1.7-4.0 W/m K. The other materials and parameters needed are listed below:

- Degree of filling [-]
- w/c ratio [-]
- Aggregate natural porosity [-]
- Cement paste thermal conductivity [W/m K]
- Stagnant air thermal conductivity [W/m K]

The thermal conductivity for the cement paste is measured by Michal Pomianowski and is 564 mW/m K . All though this value is not for the same w/c ratio it is valued as the best estimate for this study.

As the thermal conductivity varies with temperature it is chosen to use the measured values for 20 °C. These values are listed in table 15.1 together with the corresponding calculated values.

Case	Measured thermal cond. [mW/m K]	Calculated thermal cond. [mW/m K]
7	1205.7	1185.8
8	1242.6	1266.5

Table 15.1. Measured and calculated value of thermal conductivity for case 7 and 8 (w/c ratio of 0.3 and degrees of fillings of 0.4 and 0.5).

The thermal conductivity for the aggregate is based on the measurements set to 2.36 W/m K, which is within the range given from the literature. A small deviation is observed between the calculated values and the measured, but with the very small statistical population of the experiment the model is seen as valid for this type of concrete.

15.2 Numerical model

This section will treat the built numerical model, which will be tested and evaluated in relation to the conducted measurements. Results from one case will be presented, where results from the remaining cases, together with this one, can been seen as videos located on the [Enclosures-CD, Numerical model videos folder]. The experiment presented here is case 8 with an air flow of 6 l/min.

To be able to compare the calculated values with the measured it is necessary to create a function which can describe the air temperature through the specimen based only on the measured boundary values of temperature in chamber 1 and 2. From theory it is known that this temperature takes a logarithmic form because of the energy exchange based on temperature differences [45]. The logarithmic function used is shown in equation 15.1, where all values on the left side are known.

$$\frac{T_{out} - T_c}{T_{in} - T_c} = exp\left(-\frac{h \cdot A}{q_v \cdot \rho_{air} \cdot c_{p,air}}\right) \tag{15.1}$$

Where:

T_{out}	Outlet temperature [°C]
T_c	Concrete reference temperature [°C]
T_{in}	Inlet temperature [°C]
h	Convective heat transfer coefficient [W/m^2 K]
A	Internal surface area [m^2]

The calculated value from this equation describes the energy flow through the specimen and with the function defined, fractions of this value will represent temperatures in the given fractions. Equation 15.2 describes how this is calculated.

$$\frac{T_s - T_c}{T_{in} - T_c} = exp\left(-\frac{h \cdot C_x}{q_v \cdot \rho_{air} \cdot c_{p,air}}\right) \tag{15.2}$$

Where:

T_n	Temperature i section n [°C]
C_x	Internal surface area from length L_0 to L_x [°C]

With this temperature profile for the air temperature, the results of the numerical model can be compared to the conducted measurements.

Initial conditions for the model are that both the concrete and the air have the same starting temperature, taken from the measurements. After an iterative process the

estiamte of the convective heat transfer coefficient yielded 1.5 W/K to fit the measurement data after a period of 12 h. The time steps used is chosen according to equation 5.16 in section 5.3. The boundary condition for the inlet temperature changes after the first time step to a temperature of the stable inlet temperature from the measurement, which is the inlet temperature after 12 h in the experiment. As boundary condition for the rest of the outer surface area of the specimen, this is chosen to be adiabatic, although this is not the case in the measurement. The program containing this numerical model is numerical_model.m, which can be seen on the [Enclosures-CD, Matlab folder].

Plots from different time steps will be shown starting with the result after 2 h in the numerical model, see figure 15.1. Subsequently results are compared and differences discussed.

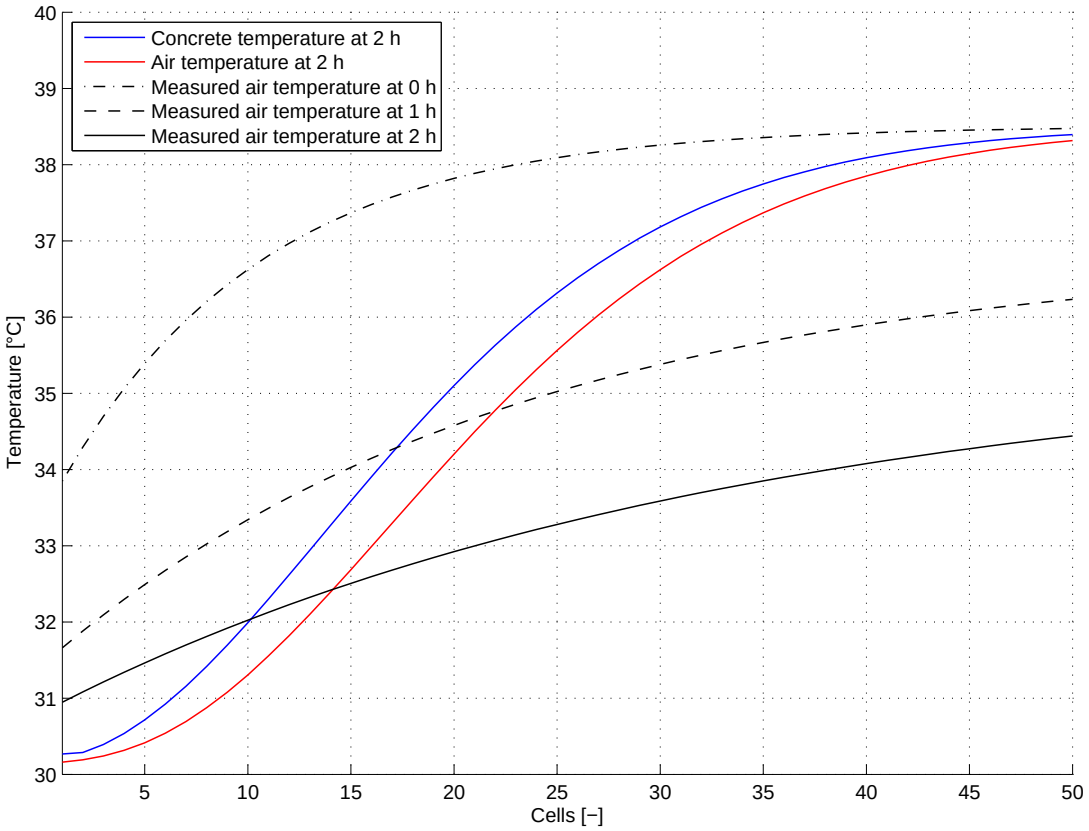

Fig. 15.1. Results of numerical model after 2 h compared to measured values.

It is clear that the model does not fit with the measured logarithmic temperature after 2 h. As can be seen, the outlet temperature is not changing before after 2 h for the model, whereas the measured value is dropped 4 °C. In the measurement the outlet temperature is starting to drop right after the experiment is started. The inlet temperature drops to approximately 30.1 °C in the model, which creates a large difference in the first 2 h in relation to the measurement. In fact, after 2 h the concrete at the inlet is almost completely discharged according to the model, whereas that takes 10-11 h in the measurement.

Looking at the result after 6 h for the model, there are still large differences between

temperatures. The result is shown in figure 15.2.

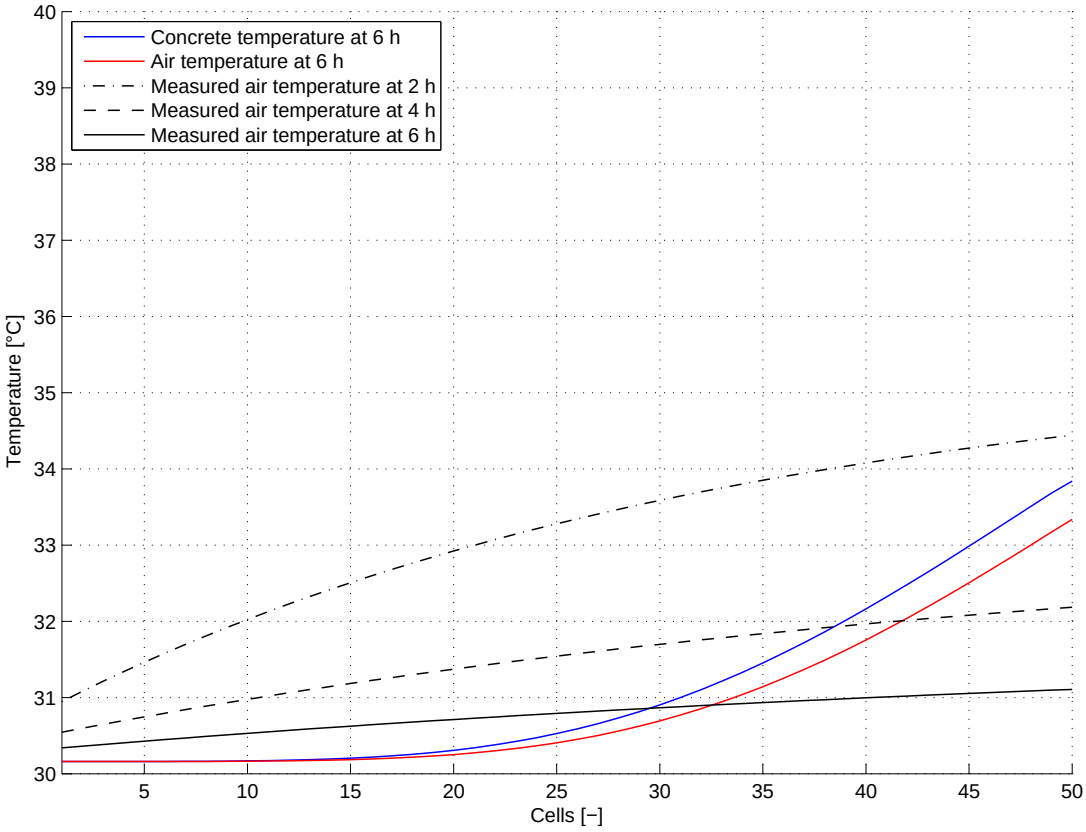

Fig. 15.2. Results of numerical model after 6 h compared to measured values.

After 6 h approximately 1/4 of the specimen has reached inlet temperature using the numerical model, where no parts is totally discharged yet according to the measurement. But at the outlet the temperature for the model is a little more than 2 °C higher. The areas under the two temperature curves (red and black) are approximately the same, stating that the same discharge of the concrete has taken place. This means that the same amount of energy is transferred to the air through the 6 h, confirming that the iterated convective heat transfer coefficient fits.

In the end the temperature in the model and the measurements fit. Both agree that the concrete specimen is discharged all the way through, which can be seen in figure 15.3.

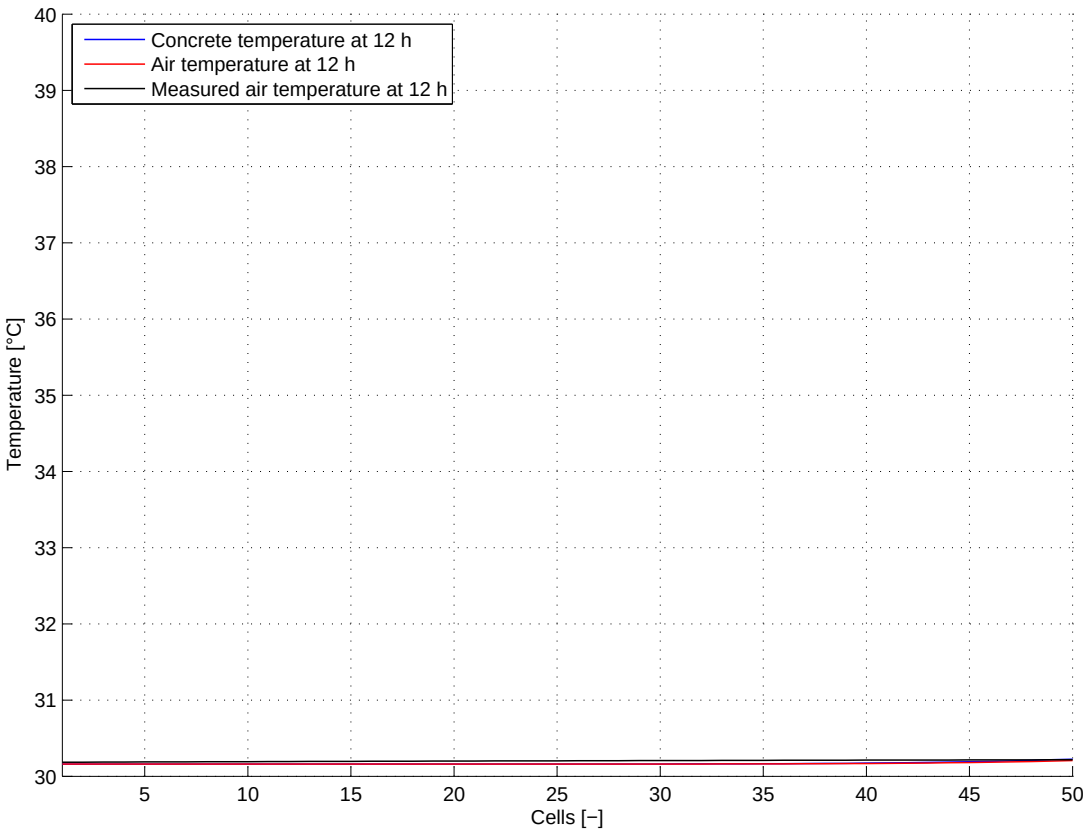

Fig. 15.3. Results of numerical model after 12 h compared measured values after 12 h.

As an experiment another iteration of the convective heat transfer is conducted, where the outlet air temperature in the model fits the measured. This result is shown in figure 15.4. The value for the coefficient is here set to 0.12 W/K, which is 1.38 W/K smaller than the scenario which fits with the discharge.

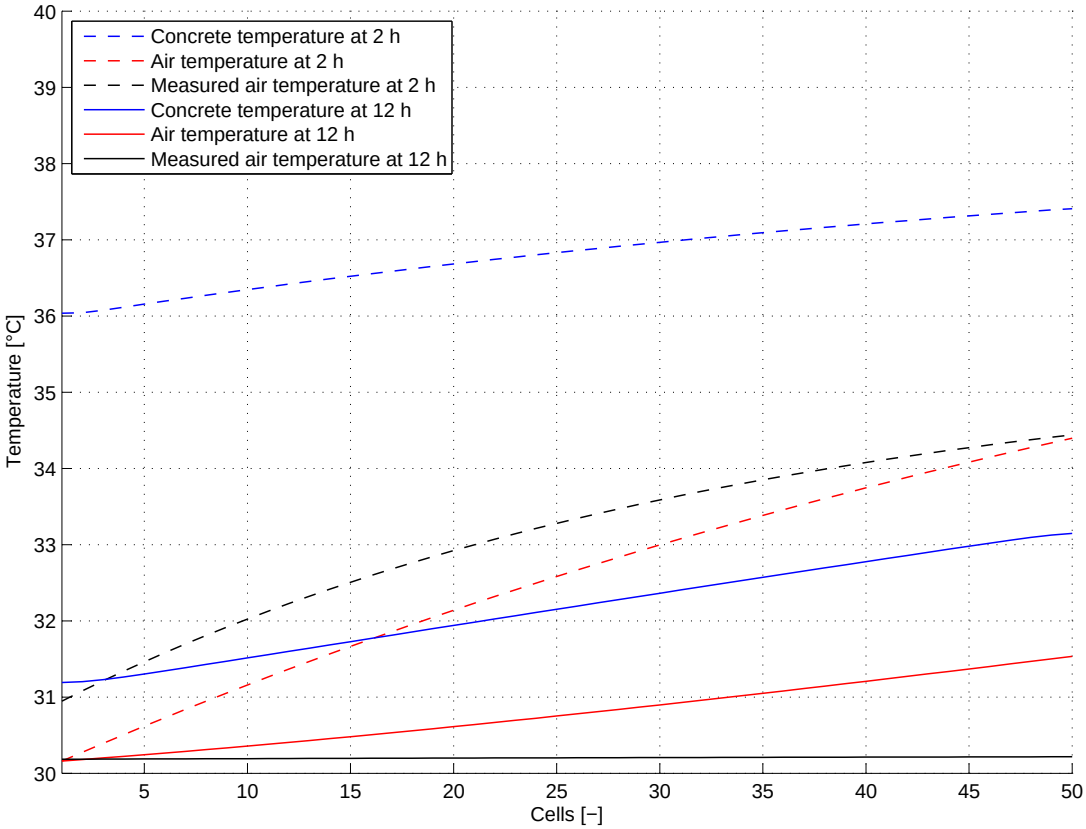

Fig. 15.4. Results of numerical model with an adjusted convective heat transfer coefficient to fit the measured air temperature.

In this scenario the outlet temperature is the same after 2 h, where it is approximately 1.5 °C higher in the model after 12 h. This, together with the concrete temperature after 12 h, states that the specimen is not discharged indicating the energy balance does not fit. After the 2 h the measurement temperatures drop faster than in the model, indicating that using this new value as heat transfer coefficient does not fit the temperatures well all the way through the 12 h period.

The conclusion is that due to the energy contributions from the surroundings to both inlet air and the specimen in the measurement, the model does not fit with both energy balance and air temperature. When the energy balance is adjusted correctly (convective heat transfer coefficient of 1.5 W/K for the model) the discharge of the concrete fits with the experimental observed result. As a comparison to both the initial performance calculation and the measured value, the dynamic heat capacity is calculated using the numerical model. The result is 309 kJ/m^2 K, which is satisfactory close to the 281 kJ/m^2 K from the initial performance calculation. For the measurement the result was 115 kJ/m^2 K, only approximately 40 % of the result from the numerical model. The reason for this is the constant lower temperature difference between the inlet and outlet temperature in the measurement compared to the calculated temperatures in the numerical model.

If the dynamic heat capacity calculated from the model is to fit with the value calculated from the measurements, the heat transfer coefficient is adjusted to a value of 0.025 W/K.

This is a very low value, which results in the air temperature, in the numerical model, not being near the concrete temperature at any time. The air temperatures fit with each other after 5 h, but this is the only time they correlate.

Values of the heat transfer coefficient for all the models are shown in table 15.2.

Case	Air flow [l/min]	Convective heat transfer coefficient [W/K]
7	4	1.8
7	6	0.9
8	4	1.8
8	6	1.5

Table 15.2. Iterated values of the heat transfer coefficient used in the numerical models.

In both cases for the air flow of 4 l/min, the heat tranfer coefficient is set as high as possible (before the model becomes unstable) because the model has difficulties with cooling the concrete within the period of 12 h.

Part V

Study closure

Conclusion 16

A series of air permeable concrete specimens has been cast and measured for both material and permeability properties. Casting processes and methods had to be developed as well as a method for measuring the air permeability of the concrete and heat exchanger efficiency. The findings of these measurements will be presented.

Casting an air permeable concrete proved to have more adjustable factors than first expected. In theory it is only the degree of filling, which controls the expected outcome of permeability, however, also the vibration frequency and time had an influence. The rheology of the cement paste and vibration factors must match in order to cast a consistent concrete corresponding to the recipe, thereby making it possible to calculate the concrete properties. Curing in a water bath revealed problems with deposits of calcium hydroxide, for which reason the method of curing in air tight plastic bags was used.

Given the gained experience it is possible to cast highly air permeable concrete, which also proves to have a relatively high compressive strength. Compressive strengths of 5-22 MPa was found, where the corresponding permeability is 0.60-0.18 m^2/Pa h. Good correlations between density, strength and permeability were found, resulting in functions predicting the permeability and compressive strength from density, although it is likely that these equations only can be used for data within this study.

The characteristics of the air flow through the specimens vary from laminar to slightly turbulent. The value of the pressure exponent varies from 0.853 to 0.995, where the low values correspond to the lowest values of the permeability measured. From these observations it can be concluded that with the low air velocities through the concrete, the air flow will be nearly laminar.

Adding PCM (2 % by weight concrete in this study) to the concrete, reveals a decrease of the compressive strength from 17.6 MPa to 15.3 MPa whereas the permeability increased from 0.23 m^2/Pa h to 0.29 m^2/Pa h, for the same w/c ratio and degree of filling. The recipe for casting concrete with PCM is different because the PCM changes the rheology of the cement paste surface, for which reason more SPA had to be added. The reason for the increase in permeability is unknown, but it might be the roughness of the cement paste which is changed generating less resistance through the permeation channels.

The thermal conductivity was measured on three chosen samples for the energy part of the study. Expectations of this parameter being lower than for traditional concrete were met and a 3 % increase in the thermal conductivity was observed when the only parameter changed in the recipe was the degree of filling by 0.1. This could be a singular instance for the measurements conducted in this study due to the small population, for which

reason this should not be seen as a conclusive finding. The results, around a temperature of 20 °C, are for case 7 1206 mW/m K, for case 8 1243 mW/m K and for case 8 with PCM 1377 mW/m K. The increase of thermal conductivity when adding PCM was not expected, as literature and other measurements suggest the opposite.

The same samples have been measured for specific heat capacity, where the results were 987 J/kg K for case 7, 1019 J/kg K for case 8 and 1021 J/kg K for case 8 with PCM, which is within the expectations for this measurement. For case 8 with PCM a higher value of 1045 J/kg K was expected, though, as the added PCM should have a larger influence. The measured values for case 7 and 8 are in the high end of the range given for traditional concrete (800-1000 J/kg K).

Measurements of the heat exchanger efficiency (η_e) proved that this type of concrete is suitable in a daily cycle, which means, from an energy perspective, it can be utilised in an office building. For all cases tested, the η_e is reduced to between 0.1 and 0.2 after 6 h of cooling the concrete and after 12 h reduced to near 0. The outlet air temperature drops just after having started all experiments, indicating an η_e different from 1.0. It is possible that the value is lower than 1.0, as it takes time for the inlet air to cool the measurement setup, delaying the effect. The η_e results from the four conducted experiments show that more energy is discharged using higher air flows and using higher degrees of filling.

As the concrete temperature could not be measured, it is difficult to conclude anything about the heat storage effectiveness, however, as the concrete seems to be discharged in the 12 h cooling period, it must reach 1.0. More specific conclusions about the discharge time are not possible to make, due to the large energy contributions from the surroundings to the specimen in the small scale setup.

The COP-value is calculated for all time steps of the measurements, where a peak value of around 380 was observed, although for other samples and air flows it was around 230, 170 and 140. These peak values were in every case achieved after 0.5 h of measurement, corresponding to the largest temperature difference between inlet and outlet air. In all cases it took 9-11 h for the COP to drop to approximately 5.0, which is the comparable value given for good heat pumps. It is better to use a low air flow because it has proven to generate a higher COP, as well as higher permeabilities generate higher COP-values.

A numerical model has been built to be able to calculate the temperature profiles of both the concrete specimen and the air. The model is also able to calculate a dynamic heat capacity. Results of using the model are compared with case 8 in the main study. An initial estimate of the convective heat transfer coefficient in the concrete is made and this value is then iterated until the outlet temperature at 12 h fits with the measured (energy balance fits). Using a convective heat transfer coefficient of 1.5 W/K fits with the measured values for case 8 with 6 l/min.

The measured temperatures are used to create a logarithmic temperature profile for the air, which is used in the comparison. With the iterated convective heat transfer coefficient the temperatures fit at 12 h, but not in all previous time steps. For the temperatures to fit, the convective heat transfer coefficient has to change to 0.12 W/K where it fits after 2 h. The conclusion is that this value changes in relation to the temperature, as the energy contribution from the surroundings increase when the temperature of the concrete

decreases. This is the case, because the ideal temperature in chamber 2 is based on an energy balance calculation, for which reason the temperatures will not fit with the model's prediction. Furthermore the calculated dynamic heat capacity is much larger than the calculated value from the measurements. This is due to the temperature difference between the inlet and outlet, which is much higher at all time steps through the 12 h period in the numerical model. The temperature profile does not fit very well with the measured values.

Discussion and future work 17

The heat exchanger efficiency is currently being investigated in a small scale setup, with cylindrical specimens of dimension 100 mm in diameter and 200 mm in length. When maintaining a stable environment around the specimen, the energy contribution to the specimen and inlet air becomes relatively large when the temperature difference is introduced by the cold inlet air. To overcome this problem large scale measurements are necessary, where these energy contributions become small and the inlet air flow much larger. If going from the cylindrical specimens to a wall of $100 \times 100 \times 20\,\mathrm{cm}^3$, the air flow will increase from 6 l/min to 764 l/min or 12.7 l/s. Then small contributions will have minimum influence and become negligible. In order to make a large scale setup it will be necessary to build a pressure chamber on each side of the wall to ensure an equally distributed air flow through the entire wall.

Even though it has been difficult to conduct measurements in a fashion, which would yield conlusive results of adding PCM to air permeable concrete, it is still believed to have a large potential. The problems in this study will also be solved with a large scale setup, where temperatures are easier to control.

In this study the energy measurements have been conducted on only three specimens. From this population it is hard to conclude much about the relation between various recipe parameters. To draw these conclusions it is necessary to conduct measurements on many different samples (recipes), which is very time consuming. Furthermore specimens of different shapes and sizes have been used in this study in the different measurement setups, where it might save time if setups were developed to measure on the same dimensions.

During the data treatment in this study and given the problems with casting the concrete, it would be advisable to utilise the porosity instead of density as the independent variable in mathematical models. The porosity will, even if some specimens are cast improper, serve as a better variable because it does not depend on weight, which will change even with a change in w/c ratio. This should in theory not change the permeability.

Casting consistent specimens from two separate mixtures has proven to be very difficult. Small changes in the casting process, together with a mixer which crushes some of the aggregates (recently discovered), can make large differences in the concrete and thereby also in the measured results. Thus, the use of another mixer is advised.

Given a time factor it has not been possible to make a thorough study of the rheology of the concrete when PCM is added. In order to be able to cast consistent and reproducable specimens this will be a necessity. The adding of PCM demands more SPA in the mixture and a study of this relation together with a new study of vibration time, frequency and

technique will be necessary.

In the setup for measuring specific heat capacity, the logged temperature in the water is a local temperature. During the data treatment it was discovered that logging this local temperature might induce a problem due to lack of circulation of the water. The results obtained in this study is believed to be valid, though it would increase the accuracy to circulate the water.

The aggregate grain size distribution is for this study found in the patent by Imbabi et al. [1]. They state that the grain fraction preferably should be 2-3 mm, where 2-3.55 mm has been used in this study. Preliminary tests with aggregate sizes lower than 2-3 mm showed changes in the properties for the concrete, where 2-3 mm were more promising with regard to wanted properties of compressive strength and permeability. Later in the study it was discovered, that the grain size used by Imbabi et al. in their study of thermal conductivity of air permeable concrete specimens was different than the preferred value from the patent [10]. Unfortunately this was discovered too late in this study to conduct further investigation of the influences of using larger size grains. It is advisable to make more experiments with this parameter, to find the limits and property changes, possibly making the concrete easier to cast with wanted values of permeability and compressive strength.

Bibliography

[1] Imbabi M. S, Glasser F. P, and Wong J. M. *A concrete mixture and method of forming the same.* Number International publication number: WO 2010/007400 A1. Patent cooperation treaty, 2010.

[2] Lechtenböhmer S and Schüring A. *The potential for large-scale savings from insulating residential buildings in the EU.* Energy Efficiency, pages 1–14, 2010.

[3] Artmann N. *Cooling of the building structure by night-time ventilation.* Number ISSN 1901-7294 in DCE Thesis No. 16. Aalborg University, 2008.

[4] Artmann N, Mainz H, and Heiselberg P. *Climatic potential for passive cooling of buildings by night-time ventilation in Europe.* Applied Energy, 84:187–201, 2007.

[5] Jensen J. M and Lund H. *Design Reference Year, DRY.* Number ISBN: 1395-0266 in Meddelelse nr. 281. Danmarks Tekniske Universitet, 1995.

[6] Artmann N, Mainz H, and Heiselberg P. *Potential for passive cooling of buildings by night-time ventilation in present and future climates in Europe.* PLEA2006 - The 23rd Conference on Passive and Low Energy Architecture, Geneva, Switzerland, 2006.

[7] Artmann N, Mainz H, and Heiselberg P. *Parametric study on the dynamic heat storage capacity of building elements.* 2nd PALENC Conference and 28th AIVC Conference on Building Low Energy Cooling and Advanced Ventilation Technologies in the 21st Century, Crete Island, Greece, 2007.

[8] BASF . *Micronal PCM product catalogue.* URL: `http://www.micronal.de/portal/basf/ide/dt.jsp?setCursor=1_290224`, 2011. Downloaded: 25-05-2011.

[9] Imbabi M. S, Glasser F. P, and Wong J. M. *Breathable concrete for low energy buildings.* World renewable energy congress, pages 850–855, 2005.

[10] Imbabi M. S, Glasser F. P, and Wong J. M. *Evaluation of thermal conductivity in air permeable concrete for dynamic breathing wall construction.* ScienceDirect, Cement & Concrete Composites 29:647–655, 2007.

[11] Taylor B. J, Cawthorne D. A, and Imbabi M. S. *Analytical investigation of the steady-state behaviour of dynamic and diffusive building envelopes.* Building and environment, 31(6):519–525, 1996.

[12] Taylor B. J and Imbabi M. S. *The application of dynamic insulation in buildings.* Renewable energy, 15:377–382, 1998.

[13] Imbabi M. S. *Modular breathing panels for energy efficient, healthy building construction.* Renewable Energy, 31:729–738, 2005.

[14] Khedari J, Hirunlabh J, and Fabre B. *Theoretical management of the deferred heat supplied by a composite Trombe wall using a porous concrete.* Energy and Buildings, 17:201–211, 1991.

[15] Traynor M. *Porous concrete replaces traditional drainage systems.* Engineering News-Record, 263:17–17, 2009.

[16] Taylor B. J and Imbabi M. S. *Passive ventilation system that incorporates a pitched roof construction of breathing walls for use in a passive solar house.* Solar energy, 64:189–195, 1998.

[17] Stone M. K. *"Breathing walls" for office buildings.* Whole Earth, 97:56, 1999.

[18] Kim K.-H, Jeon S.-E, Kim J.-K, and Yang S. *An experimental study on thermal conductivity of concrete.* Cement and Concrete Research, 33:363–371, 2003.

[19] Ruppersberger J. S. *Concrete blocks' adverse effects on indoor air and recommended solutions.* Environmental engineering, 121(4):No. 4265, 1995.

[20] Günther E, Hiebler S, and Mehling H. *Determination of the heat storage capacity of PCM and PCM-objects as a function of temperature.* 2005.

[21] Cabeza L. F, Castellón C, Nogués M, Medrano M, Leppers R, and Zubillaga O. *Use of microencapsulated PCM in concrete walls for energy savings.* Energy and Buildings, 39:113–119, 2007.

[22] Athienitis A. K, Liu C, Hawes D, Banu D, and Feldman D. *Investigation of the thermal performance of a passive solar test-room with wall latent heat storage.* Building and Environment, 32(5):405–410, 1997.

[23] Zhang Y, Zhou G, Lin K, Zhang Q, and Di H. *Application of latent heat thermal energy storage in buildings: State-of-the-art and outlook.* Building and Environment, 42:2197–2209, 2007.

[24] Hawes D. W, Feldman D, and Banu D. *Latent heat storage in building materials.* Energy and Buildings, 20(1):77–86, 1993.

[25] Kaasinen H. *Absorption of phase change substances into commonly used building materials.* Solar Energy Materials and Solar Cells, 27(2):173–179, 1992.

[26] Schossig P, Henning H. M, Gschwander S, and Haussmann T. *Microencapsulated phase-change materials integrated into construction materials.* Solar Energy Materials and Solar Cells, 89(2-3):297–306, 2005.

[27] Khudhair A. M and Farid M. M. *A review on energy conservation in building applications with thermal storage by latent heat using phase change materials.* Energy Conversion and Management, 45(2):263–275, 2004.

[28] Darkwa K and Kim J. S. *Dynamics of energy storage in phase change drywall systems.* Energy Research, 29(4):335–343, 2005.

[29] Darkwa K and Kim J. S. *Heat transfer in neuron composite laminated phase-change drywall.* Power and Energy, 218(A2):83–88, 2004.

[30] Setterwall F. *Advanced Thermal Energy Storage through Application of Phase Change Materials and Chemical Reactions - Feasibility Studies and Demonstration Projects.* INTERNATIONAL ENERGY AGENCY (IEA) and ENERGY CONSERVATION THROUGH ENERGY STORAGE (ECES), Annex 17, 2002.

[31] Peippo K, Kauranen P, and Lund P. D. *Multicomponent PCM wall optimized for passive solar heating.* Energy and Buildings, 17(4):259–270, 1991.

[32] Feldman D, Banu D, Hawes D, and Ghanbari E. *Obtaining an energy storing building material by direct incorporation of an organic phase change material in gypsum wallboard.* Solar Energy Materials, 22(2-3):231–242, 1991.

[33] Heim D and Clarke J. A. *Numerical modeling and thermal simulation of PCM–gypsum composites with ESP-r.* Energy and Buildings, 36(8):795–805, 2004.

[34] Gambhir M. L. *Concrete technology.* Number ISBN 0-07-058374-9 in 3rd edition. Tata McGraw-Hill, 2004.

[35] Almeborg J, Bache H. H, Eriksen K, Herholdt A. D, Justesen C. F. P, Nepper-Christensen P, Nielsen A, Pedersen S, Poulsen E, and Trudsø E. *Beton-Bogen.* Number ISSN 87-980916-0-8 in 2nd edition. Aalborg Portland, 1985.

[36] Newman J and Choo B. S. *Advanced Concrete Technology.* Number ISBN 0-7506-5104-0. Butterworth-Heinemann, 2003.

[37] Ferrai L, Kaufmann J, Winnefeld F, and Plank J. *Interaction of cement model systems with superplasticizers investigated by atomic force microscopy, zeta potential, and adsorption measurements.* Journal of colloid and interface science, 347(1):15–24, 2010.

[38] Ramachandran V. S. *Concrete Admixtures Handbook – Properties, Science, and Technology.* Number ISBN 0815513739 in 2nd Edition. William Andrew Publishing, 1995.

[39] Hansen P. F. *Hærdeteknologi - 1.* Aalborg Portland og BKF-centralen, 1978.

[40] Dansand . *Data sheet and sieve analysis - Dansand no. 6.* URL: `http://www.dansand.dk/fileadmin/download/english/S_V_6_ENG.pdf`, 2011. Downloaded: 10-05-2010.

[41] Technical committee ISO/TC 163 . *Thermal performance of building components - Dynamic thermal characteristics - Calculation methods.* Number 2nd edition. European standards, 2007.

[42] Tavman I. H. *Effective thermal conductivity of granular porous materials.* Int Commun Heat Mass Transfer, 23(2):169–176, 1996.

[43] Bird R. B, Stewart W. E, and Lightfoot E. N. *Transport phenomena.* Number ISBN 0-471-41077-2 in 2nd edition. Chemical engineering department, University of Wisconsin-Madison, 2002.

[44] Artmann N, Vonbank R, and Jensen R. L. *Temperature measurements using type K thermocouples and the Fluke Helios Plus 2287A data logger.* Number ISSN 1901-726X in DCE Technical Report No. 052. Aalborg University, 2008.

[45] Chapman A. J. *Fundamentals of heat transfer.* Number ISBN 0-02-321600-X in 1st edition. Macmillan Publishing Company, 1987.

Part VI

Appendices

Concrete mixing, casting and procedures A

In this appendix mixing of concrete, casting methods, developed procedures and applied equipment will be presented. The subsequent appendix deals with the comprehensive measurements of the various concrete specimens. In common, the descriptions are thorough corresponding to the long process in the laboratory, where large amounts of time has been spent with casting and measuring. A collection of measurement setups, processes and corresponding experiences can be found. Hopefully this can assist others with similar challenges in experimental and/or concrete studies. All data sheets for materials used can be seen on the [Enclosures-CD, Data sheets folder].

A.1 Parameters of casting concrete

There are many different parameters to consider when casting concrete. These can both be components in the concrete which are added during the mixing process and factors influencing the casting process. The parameters which are considered important for this project are listed below.

- w/c ratio
- Superplasticiser (SPA)
- Aggregate
- Degree of filling
- Vibration frequency and time
- Procedure

Based on theory, these parameters have different influences on both the fresh and hardened concrete. The parameters which are components in the concrete recipe are described in chapter 2 and vibration and procedure are described in the following sections.

A.1.1 Vibration frequency and time

In order to ensure a certain level of consistency when casting the concrete, reducing random variations and operator influence, all specimens are vibrated. The frequency used for vibrating this specific type of concrete can both be too low and too high. If it is set to be too low the concrete will not form a sufficiently dense substance resulting in a weak but very air permeable concrete. A high vibration frequency combined with a too viscous cement paste could possibly result in settling, where most of the paste are located in the

bottom of the sample. This means that every cement paste viscosity will have a different vibration level.

The time of vibration have the same effect. Longer vibration time yields a denser concrete specimen. These two factors of frequency and time are inversely proportional, meaning that a high frequency and short vibration time could lead to the same result as low frequency and long vibration time. In this study it attempted to maintain the same rheology, using different amounts of SPA, for which reason the same vibration frequency (50 Hz) and time (2×15 s) is used in all final cases.

A.1.2 Procedure

The procedure used for casting concrete specimens must be the same every time. This is essential due to the fact, that a change in procedure might change the properties of the concrete. Being fully consistent while mixing and casting many concrete specimens is not possible, because a human factor or level of error will occur. The vibration of each specimen is a step towards decreasing this factor.

A.2 Concrete mixing

As previously described mixing many different recipes of concrete requires a consistent procedure to achieve the comparable results wanted in this project. Furthermore it is decided to utilise the same materials for all cases, though it has been necessary to modify the aggregate a little during the latest sample production of cases. This was a necessity because only Dansand A/S was able to deliver the wanted fraction.

The materials used in this study are listed below.

- Cement: Rapid Aalborg Cement, CEM I 52.5 N (MS/LA/$\leq$2).
- Water: Regular tap water.
- Superplasticiser: BASF Construction Chemicals Denmark A/S, Glenium SKY 680.
- Aggregate: Kroghs A/S, 1/4 gravel class A, 2-3 mm sea material.
- Aggregate: Dansand A/S, Dansand nr. 6, 2-3.55 mm filter sand.

These materials have been carefully selected from experience gained from the permeable concrete patent by Imbabi et al. [1]. The size of the aggregate is chosen from this patent, but the actual material is selected from what is obtainable in the right size. The cement and SPA used are recommendations by Eigil V. Sørensen and are in context with the recommendations in the patent [1].

A.3 Mixing procedure

A consistent procedure has been conducted every time a concrete batch has been mixed. When working with small quantities of concrete, small changes from time to time can

generate relatively visible and significant alterations. Therefore it is important to, as far as possible, have the same procedure and it can be an advantage that the same person does the same things. The procedure is shown as a step by step list below.

1. Put aggregate in the mixer with water for saturation.
2. Mix for 10 minutes.
3. Add cement.
4. Mix for 2 minutes.
5. Add water and SPA.
6. Mix for 10 minutes.

The first step is to ensure that the aggregate attains the state of saturated surface dry (SSD), so there will not be an unexpected water absorption from the cement paste. This could lead to a smaller w/c ratio closely around the aggregate particles, creating unwanted properties and weakening the mechanical strength of the concrete, depending on the size of the absorption. The amount of water needed to saturate the aggregate is in this study set to be 0.4 % of the aggregate weight, recommended by Kroghs A/S in the provided data sheet. Although the level of saturation can vary from 0.3-0.7 % this project does not include this topic. The value of saturation is used for both aggregates from Kroghs A/S and Dansand A/S, as this information was not available at Dansand A/S.

Aggregate is put into the mixer with 0.4 %, of the aggregate weight, water and mixed for 10 minutes. The mixer used for this saturation and for mixing the concrete is shown in figure A.1.

Fig. A.1. Mixer with timer used for mixing the concrete.

The mixer has an integrated timer, which is used to secure the same uniform schedule for all batches. After the saturation, cement is added to the aggregate in the mixer and mixed for 2 minutes. This step is conducted as a part to ensure an even distribution of the cement.

Afterwards the water and SPA is added and the mixture is mixed for 10 minutes. If PCM is included in the recipe, this is added together with the water and SPA, as it is in liquid form. Experience from initial tests with this type of SPA shows that the SPA needs 3-4 minutes to take its full effect. By mixing for 10 minutes a good distribution of cement paste and aggregate should be ensured and it is certain that the SPA is fully active. Due to the viscosity of the cement paste, the concrete is becoming a mixture of aggregate grains coated with a layer of cement paste, basically creating larger aggregates shown in figure A.2. After 10 minutes of mixing the concrete is ready to be cast. In figure A.2 an example is shown of how the concrete appears right after being mixed.

Fig. A.2. Mixed concrete of recipe 9.

This specific recipe has a degree of filling of 0.6, for which reason its appearance seems dense. All recipes are listed in section A.6.

A.4 Casting

Casting the concrete, like mixing it, requires a consistent procedure to make all specimens comparable. In the initial phase of the project tests of different parameters were conducted. These initial test specimens were cast in cylinder moulds of the size 60 mm × 120 mm. Later in the project larger moulds of the size 100 mm × 200 mm were used. With larger moulds, small changes or errors are less visible due to a smaller part of the specimen being near the edges.

Preparation of the moulds includes ensuring a level of cleanness inside where the concrete is cast and apply a thin layer of mould oil so the concrete will not stick.

A part of the procedure to ensure consistency is to vibrate every specimen. This is done on the vibrating table shown in figure A.3 and in figure A.4 where a 100x200 mm mould is attached.

Fig. A.3. Vibration table.

Fig. A.4. Cylinder fastened on vibration table.

The procedure is to fill the mould with concrete to the top edge and then vibrate for 15 seconds with a frequency of 50 Hz. The 15 seconds is a result of initial tests conducted with the vibrating table regulating frequency and time. In figure A.5 the first filling of the mould is shown.

Fig. A.5. Cylinder filled with concrete before vibration.

Fig. A.6. Vibrated cylinder of concrete.

After vibrating for 15 seconds the concrete has compacted to a lower level, shown in figure A.6. At this point more concrete is needed to fill the mould and an amount of concrete is added so the mould is ample filled.

Vibrating concrete in this fashion could facilitate a larger density in the bottom of the mould because of the concretes self-weight. To counteract this, a counterweight is put on top of the concrete in the mould with a weight of approximately 0.5 kg. In figure A.7 it is shown how the counterweight is placed on top of the concrete.

Fig. A.7. Counterweight used when vibrating the concrete.

With the counterweight on top the mould is vibrated for another 15 seconds. Depending on how much the concrete has settled after this vibration, the mould is filled again for the last time. The top of the specimen is then closed with the lid of the mould in a distinct way: While pressure is applied to the lid, it is sheered until a firm and plane surface is achieved. This surface is shown in figure A.8.

Fig. A.8. Filled vibrated cylinder ready to close.

Fig. A.9. Closed cylinder with air permeable concrete.

At this stage the mould is ready to be closed, shown in figure A.9, and must now rest 24 hours before the specimen can be ejected. This must be done very carefully in order to preserve the specimens intact as they have very fragile edges.

A.5 Curing

Curing of the concrete after being ejected from the moulds, must happen without water exchange with the environment. The options are curing the specimens in water or in a sealed plastic bags. Both methods have been investigated in order to determine which

is more suitable for this type of concrete. In figure A.10 a water bath is shown where specimens are curing for the wanted amount of time.

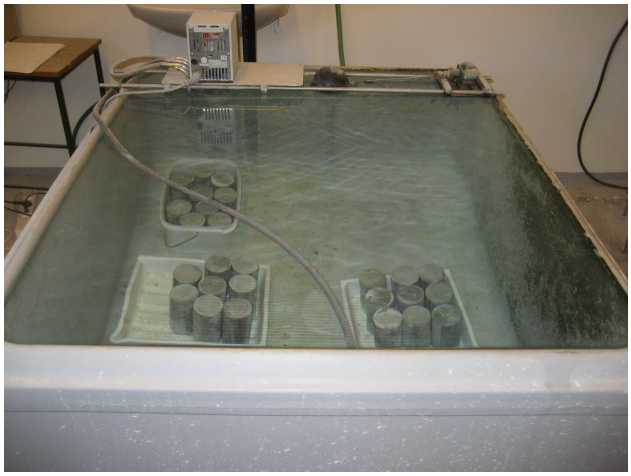

Fig. A.10. Water bath used for curing concrete specimens.

Unfortunately this method leads to a large deposit of salt on the surface of the specimen, which is shown in figure A.11. This is believed to be calcium hydroxide created from the hydration of the calcium silicates, which account for a large fraction of the cement. The salt is dissolved in the water and locally the saturation point is exceeded in already saturated water, resulting in a deposit on the large surface area characterising permeable concrete. Measurement of the water bath pH-value confirms the probability of a saturated calcium hydroxide solution. The deposit is unfortunate as it could interfere with subsequent measurements, where the pores intended for air transport might be blocked. The calcium hydroxide could possibly be removed with acid, however there is no guarantee that everything is removed from inside the specimen and the interconnected channels.

Fig. A.11. Concrete specimen with large amounts of salts.

The second method of curing, which is conducted in sealed plastic bags revealed no down sides. There is no deposit of calcium hydroxide and this method keeps the specimens free of water, which is positive given that no wet specimens can be tested for air permeability or density.

The method of curing in plastic bags was used for all samples. In the end of the curing stage all samples had the top 3-4 cm cut off. This minimises the variation in density that might occur during the vibration, filling and closing of moulds. Especially the final sheering with the lid can create a top more dense and possibly also close the interconnected channels. The saw used to cut off the ends is shown in figure A.12.

Fig. A.12. Concrete saw used to cut of ends of specimens.

The concrete specimens must cure for at least five days before the ends are cut off and the specimens are used for measurements. This is a rough estimate of how long the specimen needs to cure to obtain the necessary strength before they are used for measurements. The compressive strength of interest is the 28-day strength, because that is the reference maturity used for the structural design. Measuring mechanical strength must then be done either at the age of 28 days or measured 3-4 times during a sequence of days to be able to predict the 28-day strength.

A.6 Recipes cast

The variety of specimen recipes cast in this study is listed in table A.1.

Recipe	Aggregate size	W/c ratio	Degree of filling	SPA	NP**
1-1 S*	1-4 mm	0.25	0.5	0.50	0.399
1-2 S*	1-4 mm	0.25	0.5	1.00	0.399
1-3 S*	1-4 mm	0.25	0.5	1.50	0.399
2-1 S*	1-4 mm	0.10	0.2	0.50	0.399
2-2 S*	1-4 mm	0.15	0.2	1.00	0.399
2-3 S*	1-4 mm	0.20	0.6	1.00	0.399
3 S*	1-4 mm	0.30	0.6	1.00	0.399
4 S*	1-4 mm	0.35	0.6	1.00	0.399
5 S	2-3 mm	0.25	0.5	1.00	0.421
6 S	2-3 mm	0.25	0.5	1.00	0.421
7 S	2-3 mm	0.25	0.5	1.00	0.421
1 L	2-3.55 mm	0.20	0.4	1.00	0.402
2 L	2-3.55 mm	0.20	0.5	1.00	0.402
3 L	2-3.55 mm	0.20	0.6	1.00	0.402
4 L	2-3.55 mm	0.25	0.4	0.75	0.402
5 L	2-3.55 mm	0.25	0.5	0.75	0.402
6 L	2-3.55 mm	0.25	0.6	0.75	0.402
7 L	2-3.55 mm	0.30	0.4	0.50	0.402
8 L	2-3.55 mm	0.30	0.5	0.50	0.402
8 PCM L	2-3.55 mm	0.30	0.5	0.50	0.402
9 L	2-3.55 mm	0.30	0.6	0.50	0.402

Table A.1. Recipes used in this study's parameter variation. S - Moulds of size 60-120 mm, L - Moulds of size 100-200 mm. *Specimens cured in water. **Natural porosity of aggregate.

Looking through this list shows that several recipes have the same parameters in the preliminary specimen list. This is the case due to tests regarding vibration and procedure techniques. Furthermore permeability measurements have not been conducted on the samples cured in water.

Measurement setups B

This appendix contains detailed descriptions of the various measurements carried out in this study, which have formed the basis of the results and conclusions presented in the report. This is obviously a matter of setup, used instruments and procedures, but also (if any) evaluation of the process, adjustments along the way, advice for future work and suchlike. Measurements of the following parameters are described:

- Density
- Compressive strength
- Porosity
- Permeability
- Thermal conductivity
- Specific heat capacity
- Dynamic heat capacity

B.1 Density measurements

The density of the different concrete samples is an important parameter, because it is used as a variable for mathematical models in this study. When using the same cement, aggregate and SPA, a relatively small density would indicate a relatively large permeability and vice versa. In this case the degree of filling will have the largest effect on the density, where a small value will generate larger voids in the concrete.

The measurements used for calculating the density includes height, width and weight of the cylinder specimens. The dimensions are measured with a vernier caliper, three places for diameter and one place for length. The weight is measured right after the specimens are done curing in plastic bags, so the measured density includes the gel water. These measurements are conducted both before and after the end is cut off. Using this method creates a control sequence, testing if the density is the same for the specimens after the end has been cut off. The terms original and reduced density are used, respectively.

B.2 Compressive strength measurements

Measuring the compressive strength of the concrete specimens is essential to be able to evaluate the results of this study. Making concrete air permeable means removing a part

of the cement paste, which will have a negative effect on the strength in comparison with traditional concrete.

When testing compressive strength of the concrete specimens, the output is generated on the basis that the test specimens have a height-width ratio of 2:1, which is the standard ratio used [35]. This parameter, together with the diameter of the cylinder specimens, can adjust the true value of the compressive strength both up and down. The relations are shown in figure B.1 and figure B.2.

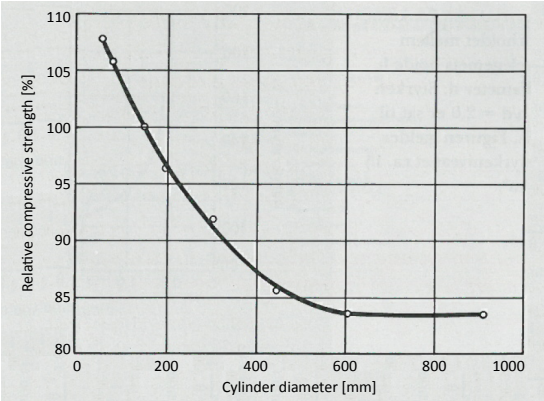

Fig. B.1. Compressive strength varying with the diameter of the specimens [35].

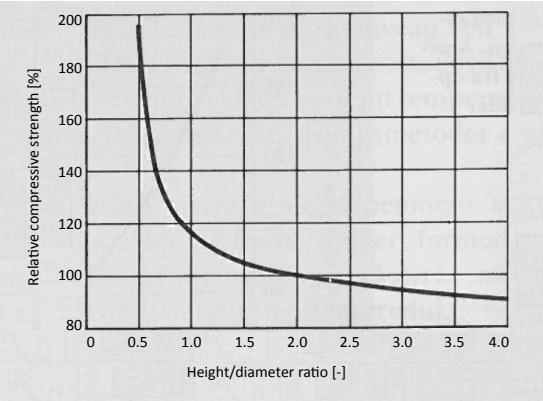

Fig. B.2. Compressive strength as a function of the specimens' height/diameter ratio [35].

The instrument used to test the specimens' compressive strength is shown in figure B.3. Additionally a multimeter is used to measure the voltage output, which can be converted to a compressive strength.

Fig. B.3. Tonipact 3000 compressive strength tester.

The multimeter is set to measure the maximum voltage output, representing the maximum compressive strength of the specimens.

Normally the machine stops when a drop in the oil pressure is registrered. This occurs when the weakest part of the concrete cylinder gives in, and represents the compressive strength of the concrete, at the top of the stress-strain curve. This is different working with permeable concrete because of the structure of the concrete. Applying a large pressure on air permeable concrete could loosen a particle on the surface due to an air pocket under it. The machine is highly sensitive and the loosening of one particle will provoke the oil pressure to drop, but this does not necessarily represent the maximum compressive strength. Therefore it is necessary to keep applying pressure until the specimen breaks. The multimeter will then show the highest voltage achieved corresponding to the highest oil pressure.

Crushing regular concrete usually creates a v-shaped fracture, but this is not the case with most of the air permeable specimens. The relatively weak and different structure in the concrete generates other shapes, of which one is shown in figure B.4.

Fig. B.4. Fracture lines in specimen 2-5.

In the figure it is visible how the fracture lines go straight down through the specimen and how the disintegrated aggregate with a layer of cement paste is laying all around the specimen. Specimen 2-5 had a compressive strength of 3.7 MPa which is very weak. The more stronger specimens revealed the characteristic v-shape.

The output from the machine is a voltage, where 1 V roughly equals 300 kN. The loading rate on the specimens has through all tests been 1 kN/s. From this output the force and thereby the stress can be calculated. In the next section the calibration for the compression tester can be found.

B.2.1 Calibration

The Tonipact 3000 compressive strength tester has a digital display which shows the force. The display is calibrated by Force Technology. In this study the voltage output is used and the calibration for this output is shown in figure B.5.

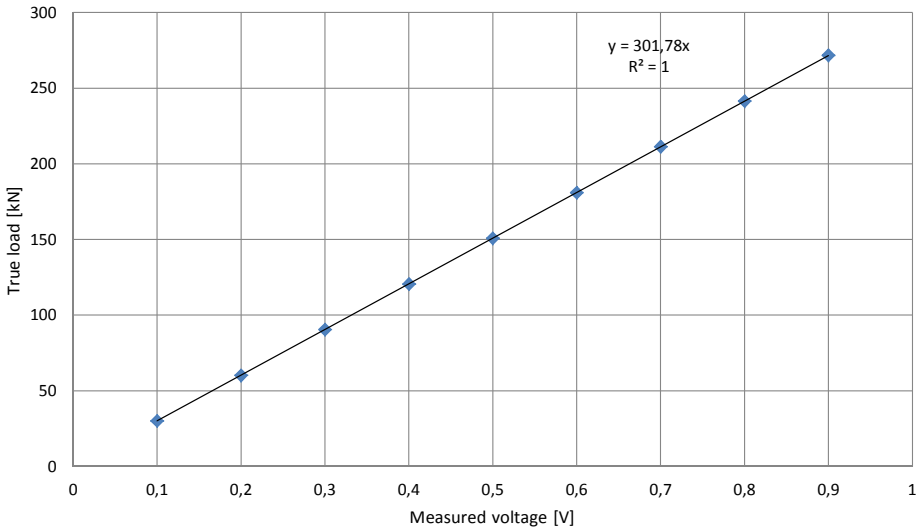

Fig. B.5. Calibration of digital output on Tonipact 3000 compression tester.

This calibration is conducted by setting up the multimeter side by side with the digital display on the Tonipact 3000 and filming these while testing a very strong element. In this way is it possible to take the matching values from both and make a calibration curve.

The display also has a small error in relation to the true value, for which reason it is calibrated. The calibration from Force Technology is shown in figure B.6.

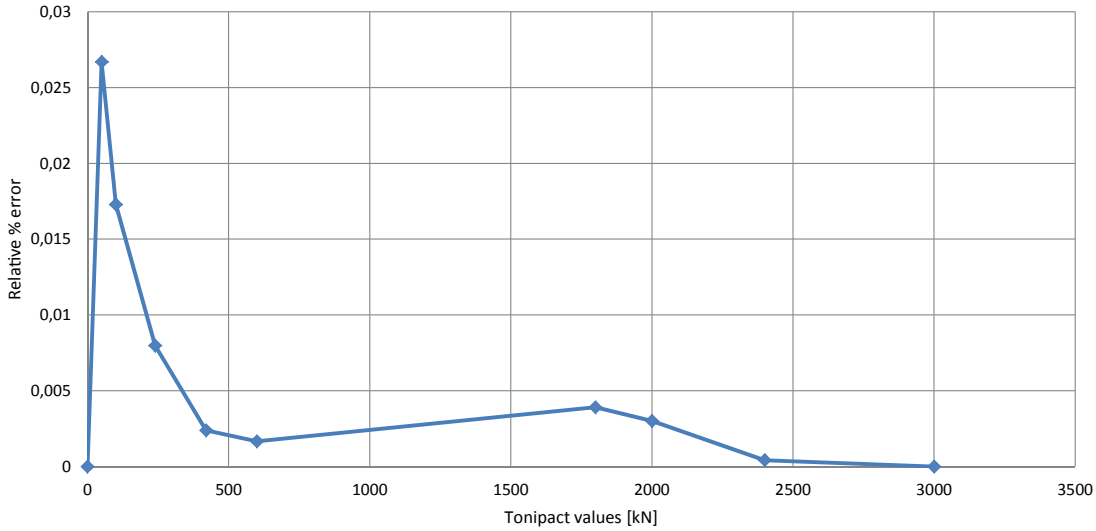

Fig. B.6. Relative error for Tonipact 3000 readings.

The calibration comes with an expression to calculate true values based on the readings of the display on the instrument. This expression is shown in equation B.1.

$$F_{true} = A0 + A1 \cdot V + A2 \cdot V^2 + A3 \cdot V^3 \tag{B.1}$$

$$A0 = -1.337682529873780$$
$$A1 = 1.001142367131900$$
$$A2 = -4.883396031350590\ 10^{-6}$$
$$A3 = 1.568936823852750\ 10^{-9}$$

B.3 Porosity measurements

There are a number of different methods to measure the porosity of the concrete specimens. In this study two methods are used to determine which is more accurate working with air permeable concrete. In theory there could be several problems with measuring the porosity of permeable concrete because there is a large void fraction. Also there might be closed air gaps, which are difficult to include in the measurements. The results of the two methods will be compared with the calculated porosity.

The two methods used are; weighing the specimens filled with and without water in the original mould and weighing the specimens under water. For both methods boiled water (water without air) is used in order to ensure a higher accuracy.

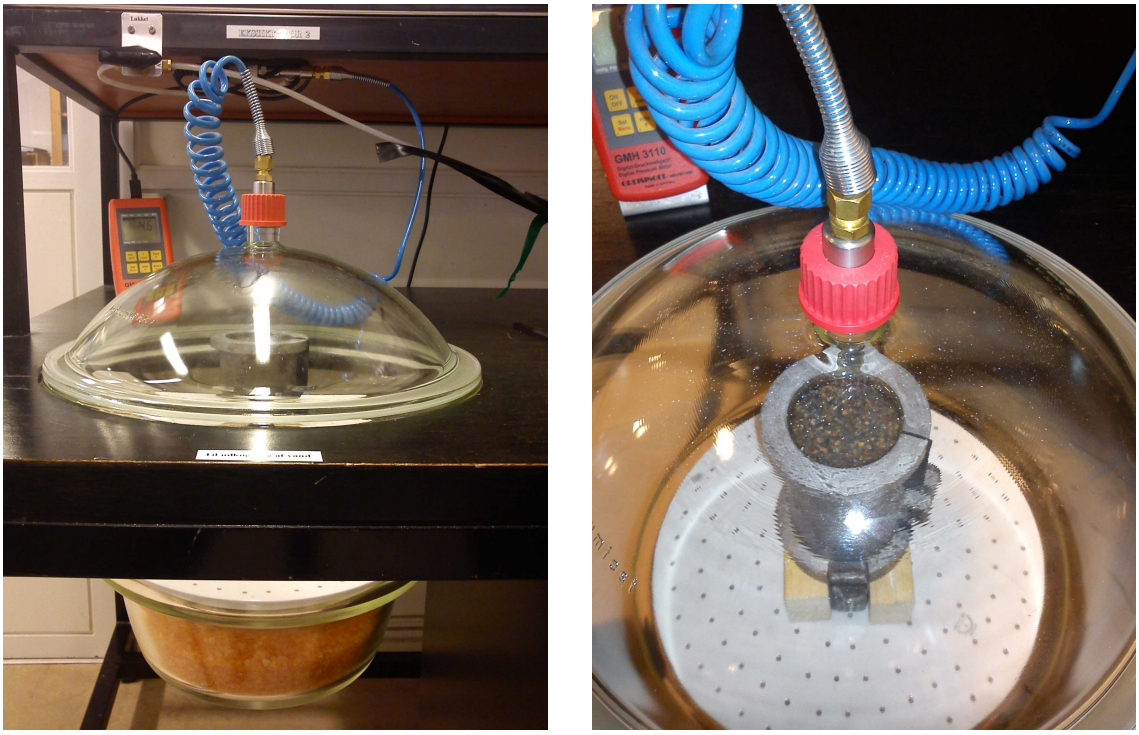

Fig. B.7. Specimen in casting mould, filled with boiled water without air, in desiccator.

The setup for the method of weighing the specimens with and without boiled water in the original moulds is shown in figure B.7. After the specimen is put back into the mould and filled with water it is placed in a desiccator to suck vacuum and remove air bubbles from within the specimen.

After the specimen has been in the desiccator for about one hour the water level in the mould have sunk as a result of the removed air. Water is added again until the water level is the same height as the specimen in the mould. At this point it is assumed that there are only concrete and water in the mould and the final mass can be measured. The added weight of the water can be directly transformed into a volume, because the density of boiled water is 1 kg/L. The equation for calculating the porosity is shown in equation B.2.

$$\epsilon = \frac{V_w}{V_s} \tag{B.2}$$

Where:

ϵ	Porosity of the specimen [-]
V_w	Volume of the added boiled water [cm^3]
V_s	Volume of the specimen [cm^3]

The second method, where the specimens are weighed under water, uses Archimedes' principle: Any object, wholly or partially immersed in a fluid, is buoyed up by a force equal to the weight of the fluid displaced by the object. The setup is shown in figure B.8.

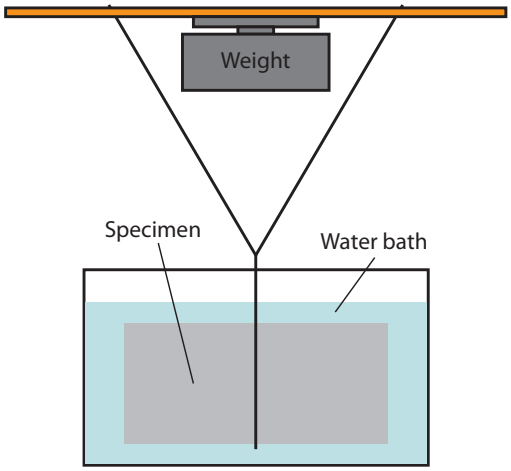

Fig. B.8. Sketch of how the specimens are weighed under water to calculate the porosity.

Before the specimen is weighed under water, it is placed in water in the desiccator to remove the presence of air. It is important that the specimen is not raised from the water before it is weighed, or the effect from the desiccator is removed. Once the weight of the specimen under water is obtained, equation B.3 can be used to calculate the porosity.

$$\epsilon = 1 - \left(\frac{m_d - m_w}{\rho_w \cdot V_s} \right) \tag{B.3}$$

Where:

m_d	Dry weight of the specimen [g]
m_w	Weight of the specimen under water [g]
ρ_w	Density of the water [g/cm^3]

Using this equation it is assumed that the density of the water is 1 kg/L.

B.4 Permeability measurements

Measuring permeability means measuring at which pressure a certain air flow occurs. In this project the air permeable elements are concrete cylinders. It has not been possible to find a well described method for measuring permeability and therefore a method had to be developed.

In order to measure the permeability, the pressure difference across a concrete cylinder and the air flow through the cylinder must be measured. Other parameters are also needed - partly to determine if the flow through the cylinder is laminar or turbulent and partly to calculate the specific air permeability. These are the dimensions of the cylinder and the dynamic viscosity of the air. To be able to relate the measurements with theory, theory from Transport Phenomena [43] is included where friction factors in packed columns are treated. To use this theory on the later obtained measurement data the absolute pressure before and after the specimen is needed. The calculation of permeability and the mentioned theory are described in sections 7.3 and chapter 11.

B.4.1 Measurement development process

Throughout the process of developing a method for measuring the permeability, different setups and strategies have been tested. These will be explained to illustrate the whole process and the improvements made on the setup during this process.

Initially a fan was used to provide the air flow through the specimen, but during calibration of the rotameter and initial tests it was realised that it could not generate a sufficient air flow or pressure through the rotameter to reach 10 l/min. This was a problem due to the very narrow fittings going in and out of the rotameter, creating huge pressure drops. Therefore the air supply was switched to pressurised air.

Early thoughts was to simply put some tape, normally used for sealing of ducts and suchlike. during blower door tests, around the cylinder specimen, to ensure that the air would not flow through the sides, and let air into one of the ends. When letting air through the specimen it is important that the entire surface is used to get credible results. Figure B.9 illustrates this idea.

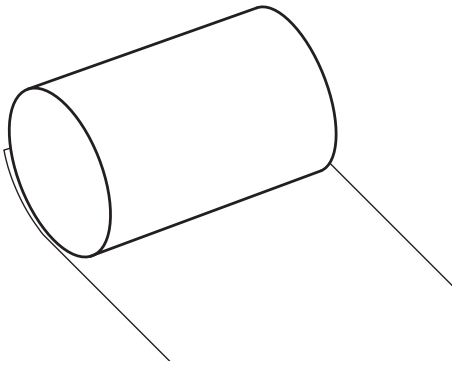

Fig. B.9. Specimen rolled in tape.

This solution generated a problem with the air flow. The tape was not strong enough to hold the air which resulted in the air going along the cylinder side under the tape instead of through the specimen. Because of this problem the measurements would not be reliable and the idea needed improvements to function. To resolve the problem a setup was needed which could put pressure on the side of the cylinder or hold the tape fixed. Given the minor add in diameter caused by the tape, it was reasonable to believe that the mould the specimens were cast in could be used. Unfortunately this was not the case and the added width did moreover cause the mould to destroy the specimen. When the mould was tightened with tape around the specimen it created a gap in the tape, which formed a path for the air down the side of the specimen. This problem is graphically shown in figure B.10.

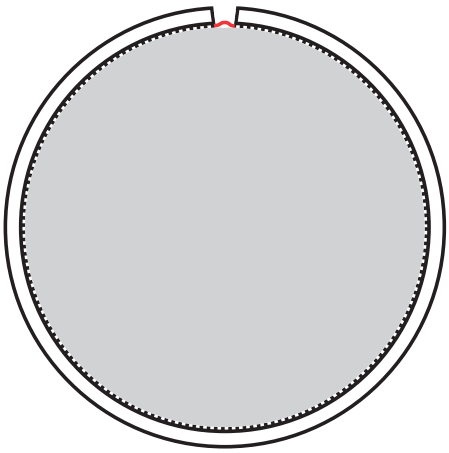

Fig. B.10. Cross section of cylinder in original mould showing the tape folding in mould crack.

In order to use the mould a substitute for the tape was necessary, which would have to be thinner and airtight. When this was not possible the mould was rejected and a new application to put pressure on the cylinder side was created. The new application consisted of a metal plate bend to fit around the cylinder. The tape was replaced with black foam in solid form which is thicker and sufficiently airtight. This black foam would have the properties to restrict the air from flowing down the side and sparing the specimen keeping it intact after the measurement. Three hose clamps were then distributed on the

metal plate, one in each end and one in the middle, to generate the necessary pressure. The setup is shown in figure B.11.

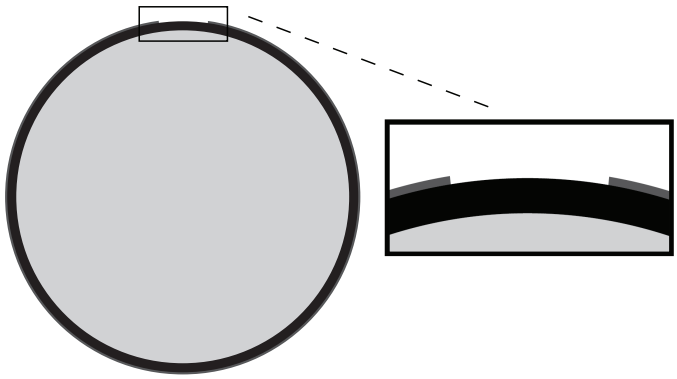

Fig. B.11. Cross section of cylinder rapped in black foam, pressed by metal plate.

Trying this setup showed a similar problem with the black foam as with the tape, though it was less significant. It might have been possible to make this method work, but it would be very difficult to get consistency in the measurements and considering the application it would be very time consuming to change to a new specimen after ended measurements.

Every time an application had to tighten either tape or other things around the cylinder there seemed to be a problem. Therefore another concept was thought of where the necessary pressure could be generated without such an application. If a setup was put in a pressure-box this problem would not occur. The pressure in the pressure-box would have to be higher than in the specimen, being able to retain the tape around the specimen in place. Furthermore the pressure-box must be a closed system to avoid interference with the measurement of permeability of the specimen. This setup worked and is described further in the following section.

B.4.2 Measurement setup

The setup consists of a pressure-box containing a specimen rolled in tape with fittings and external air supply and exhaust. Outside the box there is a rotameter to measure the air flow and two manometers and a barometer to measure pressure differences in the setup and to regulate the pressurised air for the box. In figure B.12 the setup is illustrated.

Before the air enters the pressure-box and the specimen the air flow is measured using the rotameter. A total of two manometers and a barometer are used to acquire the necessary information. One of the manometers measures the pressure difference over the specimen (green squares), returning the Δp required to calculate the permeability. The barometer measures the absolute pressure in the pressure-box (blue triangle), which is the same as chamber 1. From this and the result from the first manometer, the pressure in chamber 2 can be found. The last manometer is used to regulate the pressure in the pressure-box to be equal to the pressure in chamber 1 (red circles). This is important in order to ensure that no leakage is present between the pressure-box and chamber 1. This problem occurs

by the O-rings. If a leakage is present the measurements are not be trustworthy. Theory regarding leakage and pressure can be found in section B.4.3.

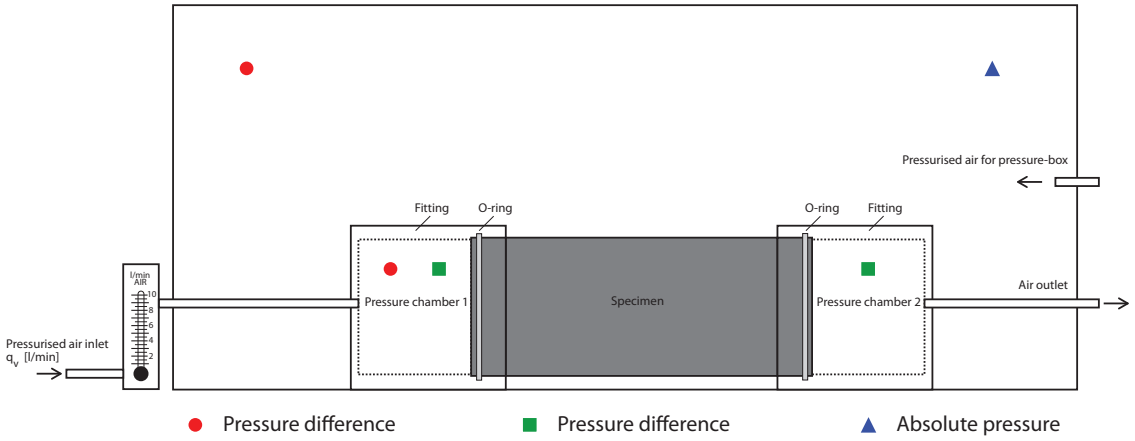

Fig. B.12. Permeability measurement setup.

One of the large challenges was to make fittings that would fit perfectly on the specimens making the setup airtight. The result was a fitting with a mounted O-ring in one end and a plug for pressurised air in the other end. Between these two connectors there is a pressure chamber, whose function is to ensure equal air flow over the surface of the specimen. Furthermore a plug is installed in the normal direction of the air flow in the pressure chamber to be able to measure the pressure, both before and after the specimen. Figures B.13 and B.14 show this application.

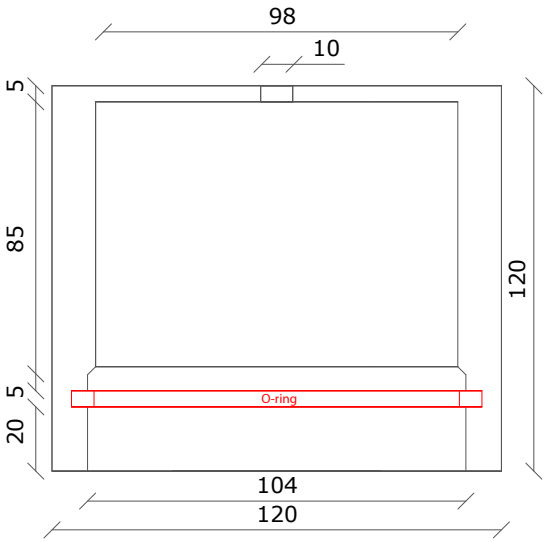

Fig. B.13. 2D sketch of fitting. Dimensions are in mm. The red ring is the O-ring.

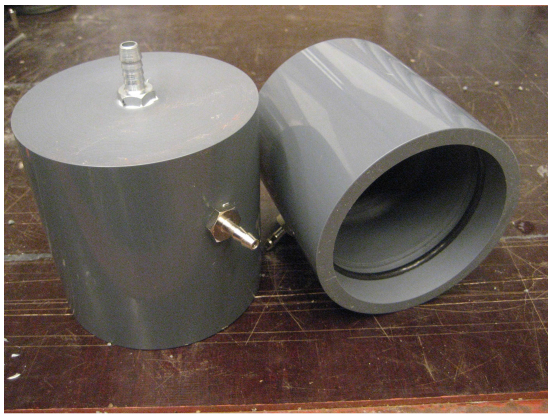

Fig. B.14. The two fittings for specimens with 100 mm in diameter.

Before the fittings are placed on the individual specimens, tape is rolled on the specimens to prevent the air from flowing through the side. Moreover the tape ensures a better

effectiveness of the O-rings when these are not in direct contact with the very rough and porous concrete material.

B.4.3 Leakage and pressure

In order to trust the measurement of air flow going into the specimen it is necessary to eliminate possible leakage between chamber 1 and the pressure-box. During initial tests using the fittings it was discovered that the O-rings did not seal tightly around the specimen. The reason for this is that this type of concrete do not form a perfect cylinder when cast. Figure B.15 shows this problem.

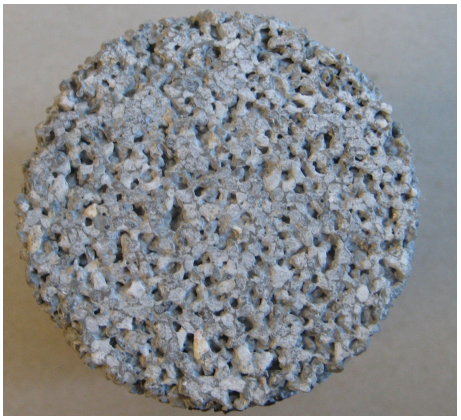

Fig. B.15. Cut air permeable concrete cylinder. Edges are very rough, not forming a perfect circle.

To solve this problem it is necessary to regulate the pressure in the pressure-box to be equal to the pressure in chamber 1. When this equilibrium is achieved, and the pressure-box is a closed system, air flow between chamber 1 and the pressure-box should be non-existing given Darcy's law, which states that a fluid will flow if there exists a pressure difference. In this case it will be through the specimen. A small leakage between chamber 2 and the pressure-box is not important as the air already has passed through the specimen and air flow has been measured beforehand.

By achieving a pressure equilibrium between chamber 1 and the pressure-box, the pressure difference between the inside of the specimen and the pressure-box will be approximately the same at the end going in chamber 1. The pressure difference going through the specimen from chamber 1 to chamber 2 will increase as the pressure decreases inside the specimen. The first idea was to obtain a pressure in the pressure-box of 1.5 times the pressure inside the specimen to retain the tape, but the practical solution showed that this was not possible due to the leakage by the O-rings.

The argument of the leakage being non-existent when the pressure in chamber 1 is equal to the pressure in the pressure-box is derived from Darcy's law, shown in equation B.4.

$$q = \frac{\kappa \cdot A}{\mu \cdot L} \left(\frac{\partial p}{\partial L} \right) \tag{B.4}$$

Where:

q	Flowrate [m^3/h]
κ	Relative permeability [D]
A	Cross-sectional area [m^2]
μ	Dynamic viscosity [Pa s]
L	Length [m]
p	Pressure [Pa]

If the last term of the equation, which is the change in pressure over a length, is equal to zero, Darcy's law concludes that there is no flow through the porous medium. This equation can also be solved for permeability, allowing this to be calculated by forcing a fluid through a specimen of a known length and area and measuring the pressure drop across the specimen. This is further processed in section 7.3.

B.4.4 Equipment and calibration

When conducting experiments and measurements it is important that the equipment makes very precise measurements. To ensure this all equipment is calibrated. In this section each instrument used is presented with its corresponding calibrations. The calibration of the flowmeter is described with setup and calibration procedure because this is not a digital instrument, for which reason there can be more factors of error involved.

Furness micro manometer FCO510

The Furness micro manometer FCO510 measures pressure difference. In this project it is used for measuring the pressure difference across the concrete specimens. Its high reading accuracy of 0.01 Pa is important as the results are used to calculate the permeability. In figure B.16 the equipment is shown.

Fig. B.16. Furness micromanometer FCO510. Range: 0-200 Pa. Reading accuracy: 0.01 Pa.

The calibration for this device is conducted by the danish Technological Institute 19-08-2009 and can be seen in figure B.17. The instrument has an uncertainty of less than 0.1 % of the reading.

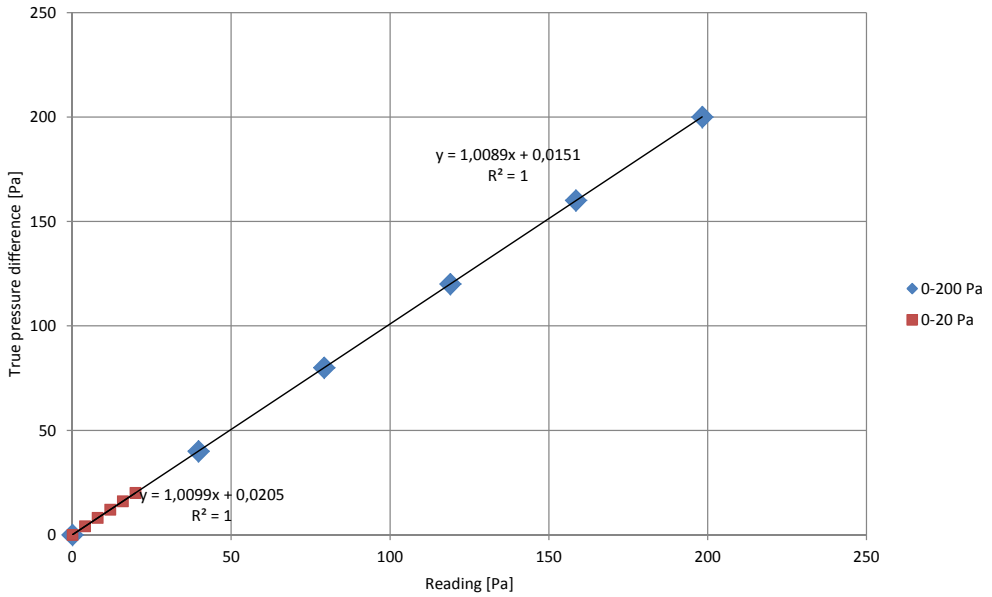

Fig. B.17. Furness micromanometer FCO510 calibration curve.

The figure holds two functions which correspond to two different settings on the device. The two settings are the two ranges that the device is able to switch between automatically(0-20 Pa and 0-200 Pa). The lower range has a higher accuracy. The calibration for the second setting is used to cover all measurements to maintain the same level of detail.

Mensor barometer 2104

The Mensor barometer 2104 is used to measure the pressure in the pressure chamber before the air enters the concrete specimen. In the calculations where this measurement is used it is not the absolute pressure, but the pressure difference between the chamber and outside the pressure-box. This means that before each measurement it is necessary to measure the absolute pressure outside the pressure-box and then subtract this value from the pressure in the chamber. The instrument is shown in figure B.18.

Fig. B.18. Mensor barometer 2104. Range: 900-1100 kPa. Reading accuracy: 1 Pa.

The calibration for this instrument is performed by Arepa Test og Kalibrering A/S 22-06-2005 and is shown in figure B.19.

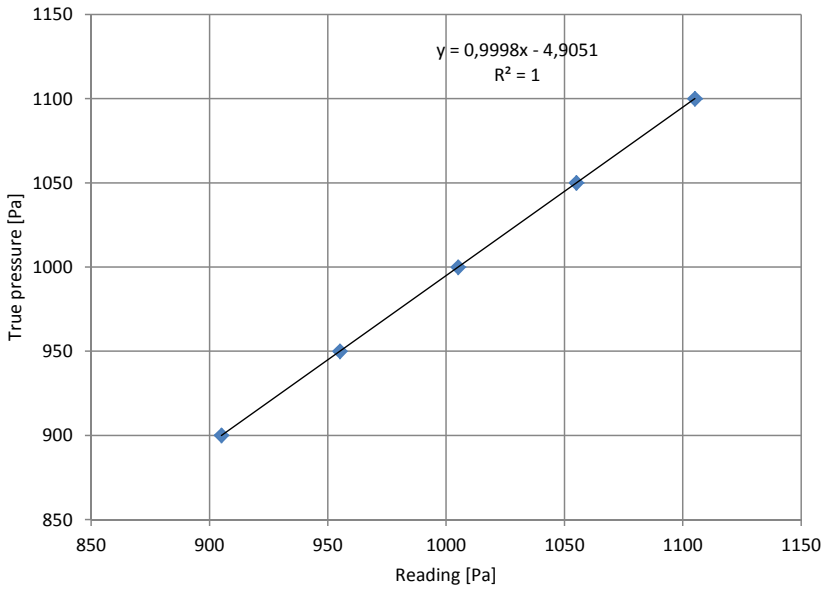

Fig. B.19. Mensor barometer 2104 calibration curve.

Due to the linear correlation in the calibration and the function of the instrument in this study, the old calibration date is not considered crucial.

Debro micro manometer 43701

This piece of equipment is in this study used as a guide to regulate the pressure in the pressure-box to be the same as in the pressure chamber 1 before the air enters the specimen. The reason for this regulation is explained in section B.4.2. The instrument has an uncertainty of ±0.7 Pa. The Debro micro manometer can be seen in figure B.20.

Fig. B.20. Debro micro manometer 43701. Range: 0-2000 Pa. Reading accuracy: 0.1 Pa.

Dwyer rotameter

A rotameter from Dwyer is used to measure the air flow through the specimen. The flowmeter can measure up to 10 l/min and has a scale of 0.5 l/min.

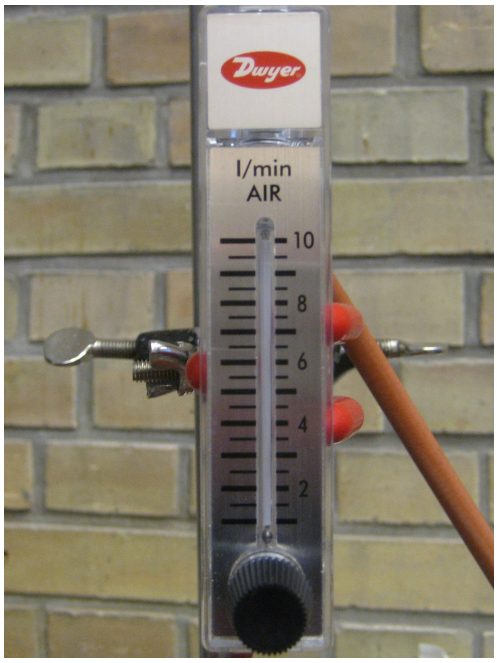

Fig. B.21. Dwyer rotameter used for measuring air flows between 0-10 l/min.

Fig. B.22. Calibration device for calibrating flow meters.

Calibration of the rotameter is done by providing a constant air flow, measuring the amount of air flowing through the instrument and the time it takes. The flowmeter can be seen in figure B.21. The Rate-master RMA series has an accuracy of $\pm 4\,\%$ of full scale. The device used to calibrate the flowmeter is shown in figure B.22.

The procedure is to let air through the flowmeter and then into one of the openings in the bottom of the device. The other opening must be closed so the air is trapped inside the device making it possible to measure the amount of air flowing in. In the top of the device there is a scale measuring the amount of air inside the device. Held in relation to the measured amount of time it takes, yields the air flow. The entire setup is illustrated in figure B.23.

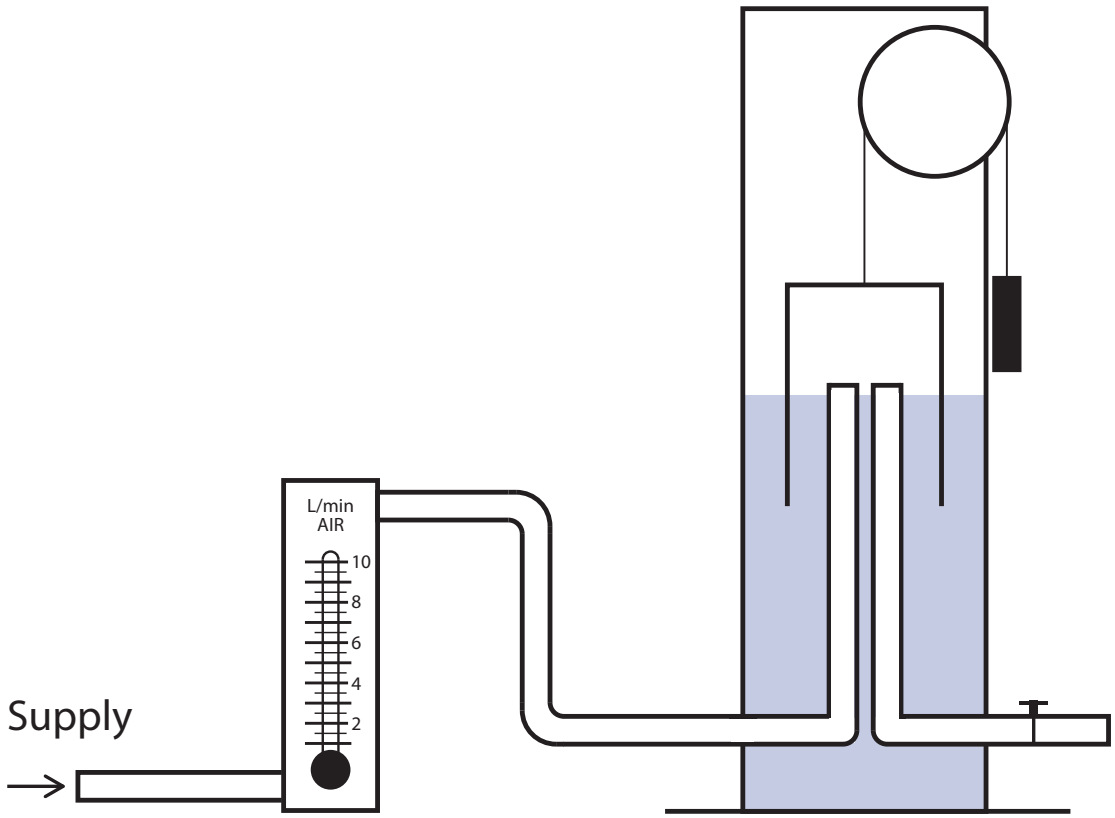

Fig. B.23. Calibration setup for rotameter.

This is done for flows covering the whole scale on the flowmeter and afterwards plotted. Doing this makes it possible to create a function $q(x)$ where x is the measured flow value on the flowmeter and the function returns the actual flow value. The plot and function is shown in figure B.24.

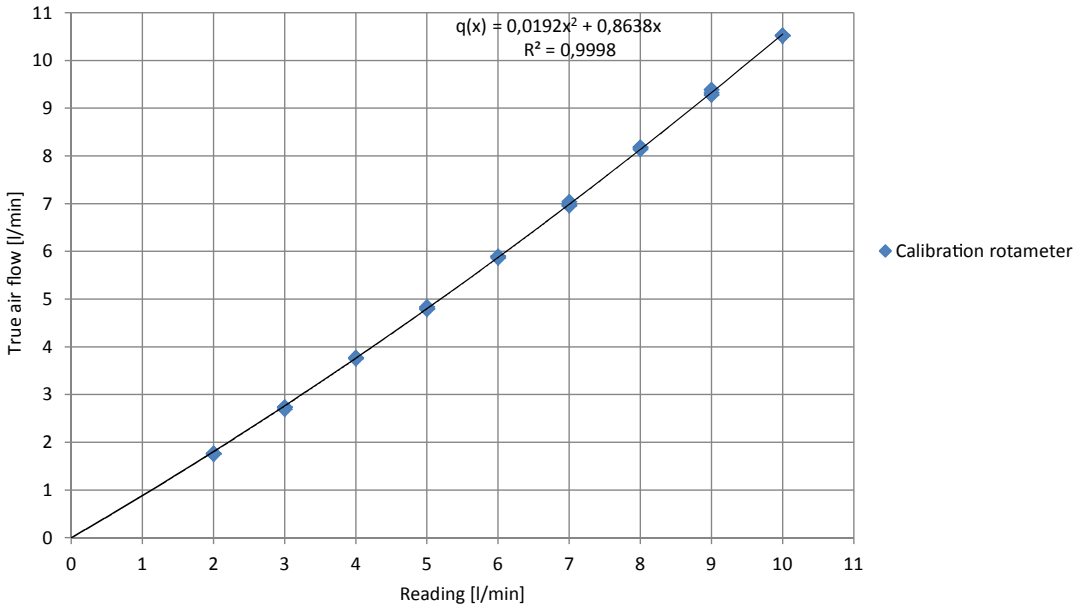

Fig. B.24. Calibration plot for flowmeter 10 l/min.

B.5 Thermal conductivity measurements

As part of the material properties investigation conducted in this study, the thermal conductivity (λ) for the concrete specimens have to be measured. This is done by using a guarded hot plate apparatus λ-meter EP500, which have been modified and also able to measure specific heat capacity. Due to complications with specimens of this special type of concrete, this instrument is only used for measuring λ values.

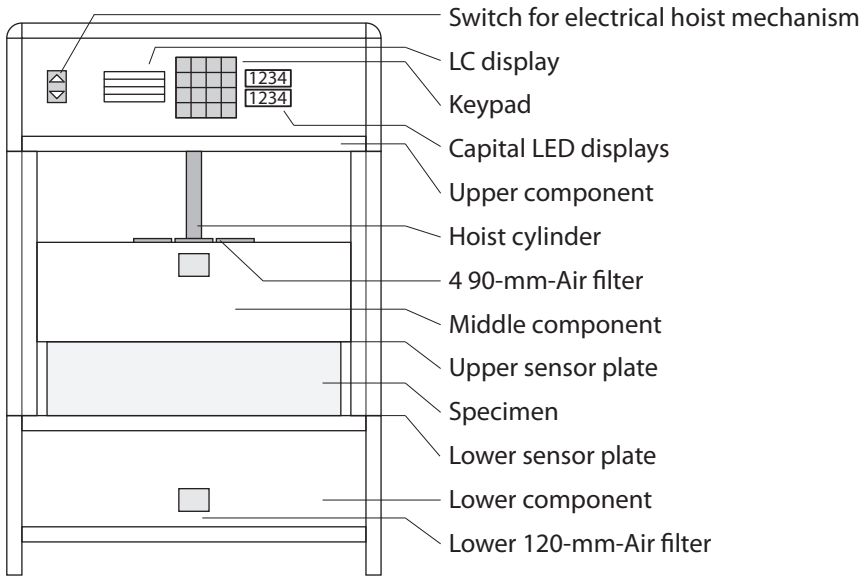

Fig. B.25. Illustration of λ-Meter EP 500.

The advanced control algorithm of the instrument calculates the optimum measurement parameters, thereby also reducing the measurement time to a minimum. An electronic hoist mechanism is responsible for controlling the middle component, thereby controlling the sensor plate's pressure on the surface of the specimen and ensuring good contact, depending on the specimen sides to be fully parallel. This mechanism will at the same time measure the specimen thickness. In figure B.25 is an illustration of the apparatus shown.

Concentric sensor plates are located in the lower and middle components and the centerpiece of these plates are 40 mm aluminium units necessary to maintain an isothermal temperature. Peltier coolers controls the temperatures of the sensor plates and can apply any temperature between 0 °C and 50 °C. Measurements can be conducted within the temperature range of 10 °C and 40 °C or a difference range of 5 and 15 K.

In this study λ-values are measured with a temperature difference of 15 K, at three different temperatures. This is 10, 20 and 40 °C where the sensor plates have temperatures of ± 7.5 K.

The warmest sensor plate is always the upper plate in the instrument. Above the upper sensor plate there is an additional heating plate, which provides a thermal barrier making sure that all heat from the upper sensor plate will dissipate into the specimen. Between these two heaters, there is a highly sensitive heat flux plate used to detect if there are any heat convection present. Deflection of transverse heat between the measurement zone and the protective ring are measured with more than 100 thermocouples, which are evenly spread over the measuring zone, forming a chain. These will detect the smallest temperature differences and the protective ring will then compensate for this and ensuring precise thermal sealing. The protective ring is surrounded by another heating ring and again by a cooling ring and heat flow between these is measured with thermocouple chains.

The absolute temperature is measured at various locations and together with the specimen's thickness and room temperature, the PC software is able to calculate the thermal conductivity. The criteria for when a stationary case is obtained is having a deviation of the calculated λ-value $< 1\,\%$ for 150 minutes in this study.

There are several constraints using the guarded hot plate apparatus λ-meter EP500, where different dimensions excludes options of temperature ranges. Valid in this study, with the used dimensions, is that λ values between 0.18 and 2.00 W/m K can be measured for which the error rate is $< 2.5\,\%$.

The specimens have to be dry before being measured and if this is not the case, drying is necessary. After drying the specimens must be prevented from high humidity and tempered to room temperature. This procedure is important because a high content of water will generate false results.

According to the device manual the ideal dimensions are $500 \times 500\,\mathrm{mm}^2$, however this is not a necessity. The actual measurement zone of the instrument is a central square of $150 \times 150\,\mathrm{mm}^2$, shown in figure B.26. The specimens cast in this study for the measurements have the dimensions of $15 \times 15 \times 8\,\mathrm{cm}^3$.

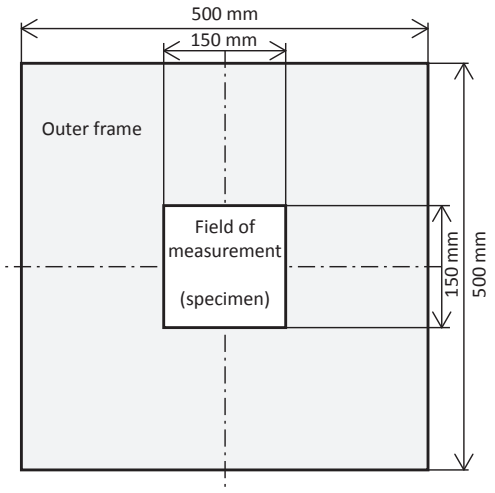

Fig. B.26. Specimen placement including outer frame.

Values outside of this zone are of no interest, but this 'outer frame' is important for creation and maintenance of the thermal conditions required in the measurement zone. This refers to an adiabatic environment with one-dimensional heat transfer and stationary conditions. For the instrument to be operational, if dimensions are less than $500 \times 500\,\mathrm{mm}^2$, the outer frame must be filled by an identical or similar medium or by a material with a very low thermal conductivity. In this study a square of foam with a hole in the middle was used.

For specimens with uneven or rough surfaces (top and bottom $15 \times 15\,\mathrm{cm}^2$), which is the case measuring on air permeable concrete, a certain procedure must be conducted before measuring. To avoid test errors these two surfaces must connect firmly with the sensor plates, without air gaps. In order to even the surfaces to a perfect parallel a thermal interface is attached, like ultrasonic gel with a very good thermal conductivity. In cases where this procedure is not conducted sufficiently the instrument will measure smaller values without giving errors, which would be an undetectable error.

The procedure is to wrap the specimen in thin film to keep the gel from going in to the concrete. After this a thin layer of ultrasonic gel is applied evenly. Then the gel is covered with another layer of thin film, where air pockets must be avoided to obtain the best results. With this applied gel the surfaces should connect firmly with the sensor plates when these are pressed against the specimen and the outer frame which must be slightly thicker than the specimen with gel in order to ensure that there are no air gaps present.

In figure B.27 a reading is shown where the criteria of a deviation of 1 % is shown. As the λ-value is within the criteria for 150 min the criteria is met and the thermal conductivity is found.

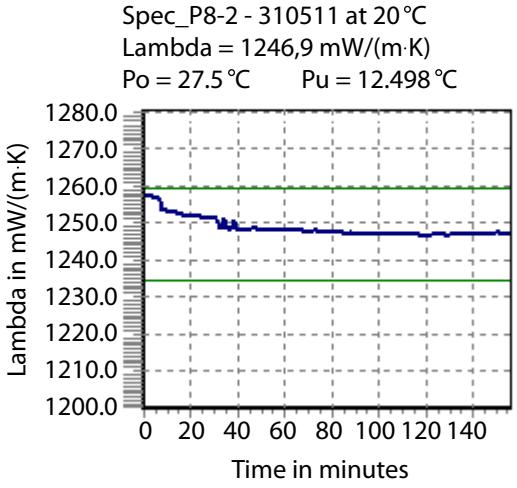

Fig. B.27. Plot from the λ-measurement software, viewing a measurement around 20 °C

B.6 Specific heat capacity measurements

Measuring the specific heat capacity for a material can be done in several different ways. The requirements are that the energy content of the material is changing over time, due to a temperature change in the material. In this study the measurements are conducted with air permeable concrete and water in a good insulated environment. Shortly explained, a warmer concrete element is put into cold water where these will exchange energy. After a while a state of equilibrium will occur, both materials will have the same temperature and the specific heat capacity can be calculated by calorimetric principles.

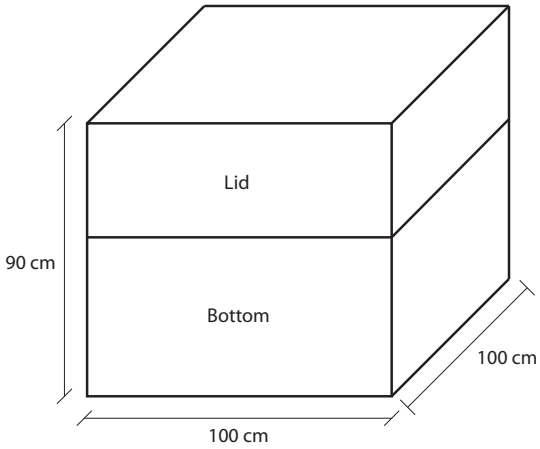

Fig. B.28. Outer dimensions of the polystyrene setup.

The specimens used for this experiment are once again square concrete blocks of $15 \times 15 \times 8\,\mathrm{cm}^3$. As water is going to be in and around the specimen a waterproof container is necessary. This container is placed in the middle of a well insulated environment made of polystyrene. The dimensions of the setup are presented in figure B.28.

The lid is removed when samples are put in the setup or taken out. In figures B.29 and B.30 vertical and horizontal cross sections are shown with dimensions and position of sample and container.

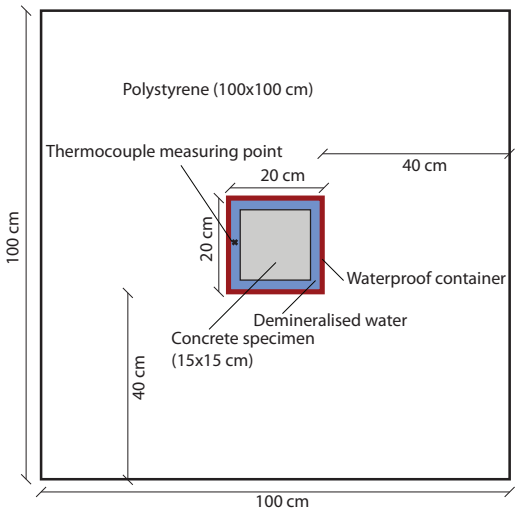

Fig. B.29. Horisontal cut at the center of the setup, including concrete specimen and container.

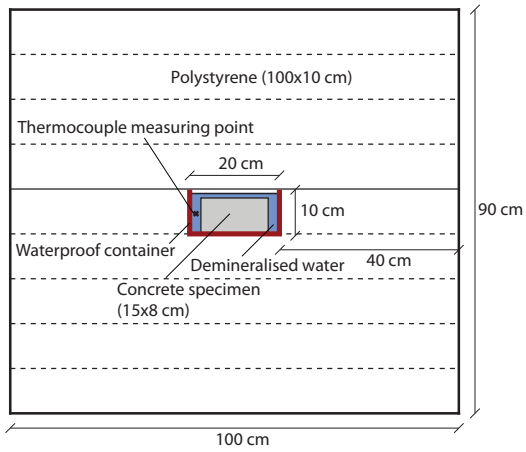

Fig. B.30. Vertical cut at the center of the setup, including concrete specimen and container.

The procedure of measuring the specific heat capacity starts with putting cold water in the container and closing the lid again. At all times there is a thermocouple placed in the water to log the temperature, and this initial test with only water is conducted to quantify the heat transfer through the polystyrene. This heat transfer is then taken into account when calculating the specific heat capacity.

A measurement starts in the same fashion, where water is put into the setup for 30 minutes to stabilise the setup and equilise the temperature of the water and container. Afterwards the lid is opened and a concrete specimen is put in the water. The amount of water in the container is adjusted to almost fill the container and make sure the whole concrete specimen is submerged. Then the lid is closed again and the temperature is logged until the system has achieved an equilibrium. From this temperature log and the initial temperatures of the water and the concrete sample the specific heat capacity can be found, when the contribution from the surroundings is taken into account.

B.7 Heat exchanger efficiency measurements

The heat exchanger efficiency of permeable concrete, η_e, the dynamic heat capacity and COP-value will be calculated from a series of temperature measurements of air inlet and outlet over a half cycle period.

B.7.1 Measurement setup

An advanced setup is used to measure temperatures, from which the objective is to send cold air through a warm specimen in a warm, stable environment and measure the cooling of the specimen over a period of time. The setup is illustrated in figure B.31.

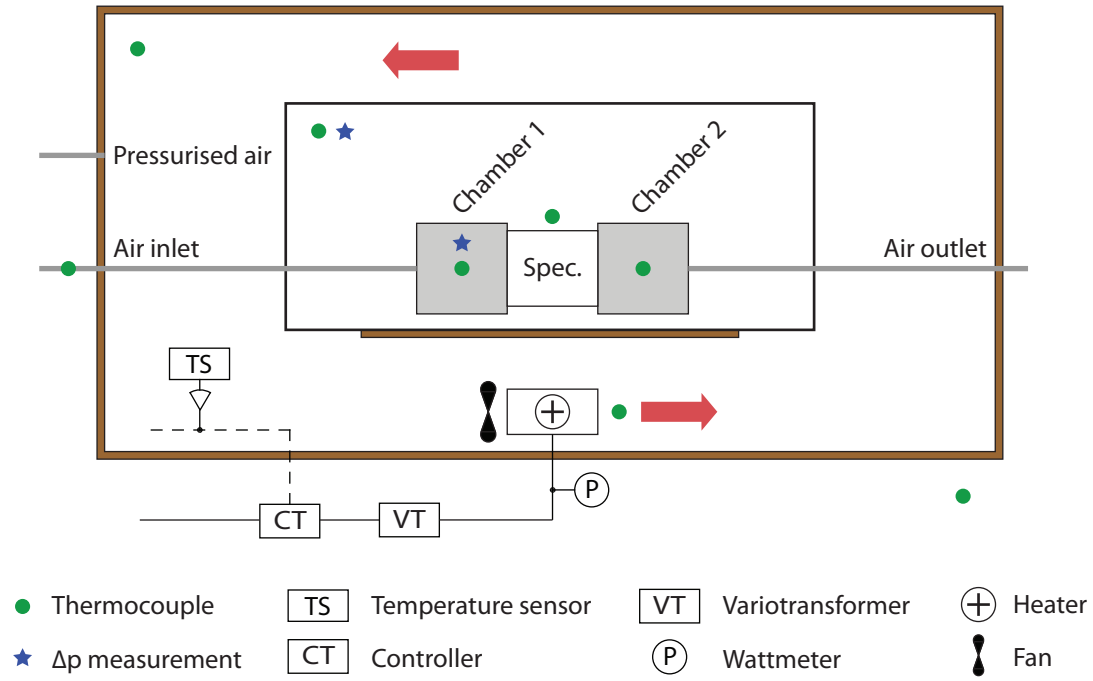

Fig. B.31. Setup to measure η_e, dynamic heat capacity and COP.

The setup is an extended version of the pressure-box used for permeability measurements. The fittings are still needed to enclose the specimen ends and distribute air and pressurised air is still needed to eliminate leakage from chamber 1. The small pressure-box (denoted small box) is now placed in a larger box, which functions as a heating environment. The heater is connected to a vario-transformer, enabling adjustment of the supplied wattage according to the wattmeter. The whole system is controlled by a Danfoss regulator. It functions as a simple on/off control with a temperature sensor and a set point as reference. This method has proven to ensure a stable temperature in the small box, compared to a solution with a heater and temperature reference placed in the small box. To circulate the air a number of fans are used.

To control and secure an equal pressure between chamber 1 and the small box (marked with stars) the Furness manometer is used. The small box is sufficiently leaky, so the pressurised air can enter. In order to measure temperatures over time thermocouples connected to a data logger are used. The points of interest for temperature measurements are displayed as green circles in figure B.31.

B.7.2 Thermocouples

Thermocouple wires consist of two dissimilar metal alloys between which an electric potential is produced in proportion to the temperature gradient exposed to the ends (thermoelectric effect). Because the temperature difference between two points is measured, one of the junctions is typically maintained at a known reference temperature. An obvious reference is 0 °C, which then is equivalent to measuring absolute temperature. This can be achieved with an ice point reference, which upholds an ice bath made of finely crushed ice and air saturated water. The configuration is illustrated in figure B.32.

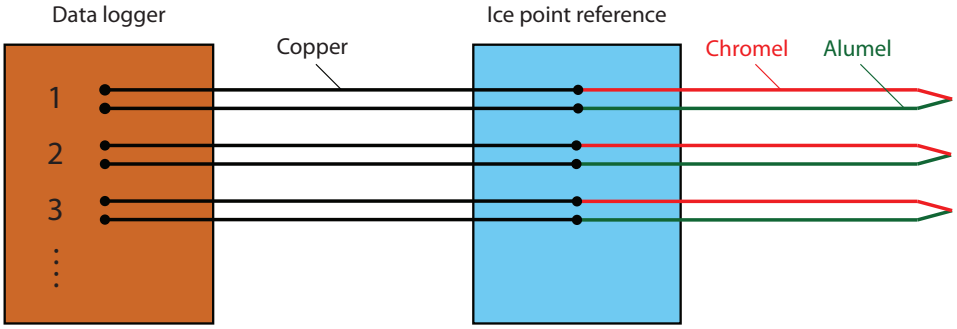

Fig. B.32. Configuration of thermocouples with use of ice point reference.

Collection of data is done with a Fluke Helios Plus 2287A data logger. The log interval is 30 s. The used thermocouples are of type K consisting of two nickel alloys, chromel (90 % nickel and 10 % chromium) and alumel (95 % nickel, 2 % manganese, 2 % aluminium and 1 % silicon) with a sensitivity of approximately 41 µV/K. Deviations in the alloys can affect the accuracy of thermocouples. For type K thermocouples the tolerance class one is given as ±1.5 K. However, deviations between thermocouples coming from the same production are very small and a much higher accuracy can be achieved by individual calibration. After calibration the absolute uncertainty of thermocouples is 0.083 K [44]. This covers contributions from the voltage measurement of the data logger, the cell temperature of the ice point reference and the composition of the thermocouple alloys. Calibration is done at three temperatures with a precision thermometer and calibration curves are made for direct conversion from the signal (mV) to absolute temperature. Additional information on temperature measurements using type K thermocouples can be found in [44].

B.7.3 Grounding and noise problems

The small voltage signals picked up by the data logger are very sensible to noise from different sources. In order to prevent noise it is important that all measurement devices including the computers and monitors used for data logging are properly grounded. To prevent ground loops each device needs to be connected to the ground at only one point and not through several individual connections (for example power cables). If radiation from external noise sources penetrates the setup, currents can be generated in the system and transferred into the signal lines. This can come from the 230 V power cables as well, for which reason they must be separated from the thermocouple wires.

B.7.4 Procedure

Each measurement cycle takes approximately 24 h to complete. A specimen is preheated to a couple of degrees above the environment set point in an oven. By morning the heater and fans are turned on in order for the environment to reach a target of 39 °C. The pressurised air is also turned on at an estimated level to secure some level of air mixing.

After midday the specimen is taken out of the oven and the boxes are quickly opened to insert the specimen in the fittings and closed again. The whole system is now given 4-6 hours to achieve the state of equilibrium. At this time, around evening, the cold air inlet will be opened and the actual measurements can begin. To be precise the air is not cold, only colder than the environment and the specimen - it has approximately the same temperature as the laboratory. Starting by evening also holds the advantage that the laboratory is less affected by solar radiation, causing temperature fluctuations during the day. Furthermore the pressurised air is more stable when not in use by other setups and staff. After 12 h of measuring, corresponding to the planned discharge period, the measurements are stopped by morning.

The three cases subjected to energy performance measurements are each tested at air flows of 4 and 6 l/min. This gives a total of six planned measurements.

B.7.5 Adjustments

Reaching the final setup displayed in figure B.31 has been a long process of gaining experience and making adjustments. It was at an early stage clear that something had to be done to avoid the small amounts of inlet air getting heated by the surroundings before reaching the specimen. In fact this has been a consistent problem. Adding tube insulation only delayed the heating. The solution was partly to reduce the distance to a minimum and partly to maintain the temperature with a separate pressurised air system flowing along the inlet tube in a larger tube.

In the early design the pressurised air was also led to the small box. Between the two boxes it was sent through a copper spiral to get preheated. However, the small tube diameters could not handle the pressure needed to balance with the pressure of chamber 1. After learning that the small box was sufficiently leaky and the functional principle was unchanged, the pressurised air was moved to the large box.

To ensure a minimum of heat exchange with the surroundings and isolate the colder stream of air from the time the measurement is started some kind of complete insulation of the small box was needed. To avoid interference with cables, specimen and so on the box was filled with small spheres of EPS. The solution was flexible - the spheres distributed out among the cables and could be sucked back out. However, the spheres were unable to handle easily, so the solution was to use packing foam, which have the same properties, but are larger and more manageable. These were added to and filling the small box immediately after insertion of a warm specimen. This is shown in figure B.34. Also here the large box proved advantageous with the separation of the heating/circulation system and the small box as casing for the foam.

B.7.6 Adjustments for PCM measurements

For the specimen with PCM it was necessary to reduce the inlet temperature in order to ensure activation of the PCM. This was problematic as cooling cannot be extracted directly from electrical energy. Instead a solution with tap water as refrigerant was tested. In a large bucket with overflow the copper spiral was submerged to cool the large air flow flowing along the tube. The water supply was running to ensure constant capacity. However, the convective heat transfer was insufficient and the solution did not work.

Instead a condenser was obtained. It was placed in the small box and used to circulate cold water around a glass spiral with large surface area where the air flows within. After shielding the condenser with insulation to avoid cooling the entire content of the small box and adding more tube insulation, the inlet air temperature was satisfactory low. The complete setup and condenser is shown in figure B.33 and figure B.34 shows the small box filled with packing foam.

Fig. B.33. Complete setup with condenser.

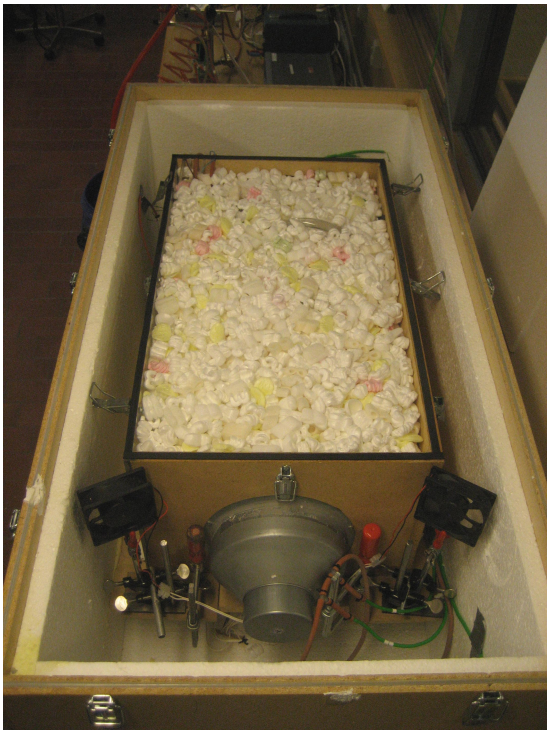

Fig. B.34. Packing foam added to the small box before measurement.

However, the temperature of the outlet air still turned out to be too high. The conclusion is that the air flow through the specimen is simply too small, absorbing the heat exchanged with the surroundings through the surface of the fittings and the specimen. The solution was to increase the air flow to 20 l/min even though the pressure between chamber 1 and the small box could not be balanced due to technical limitations.

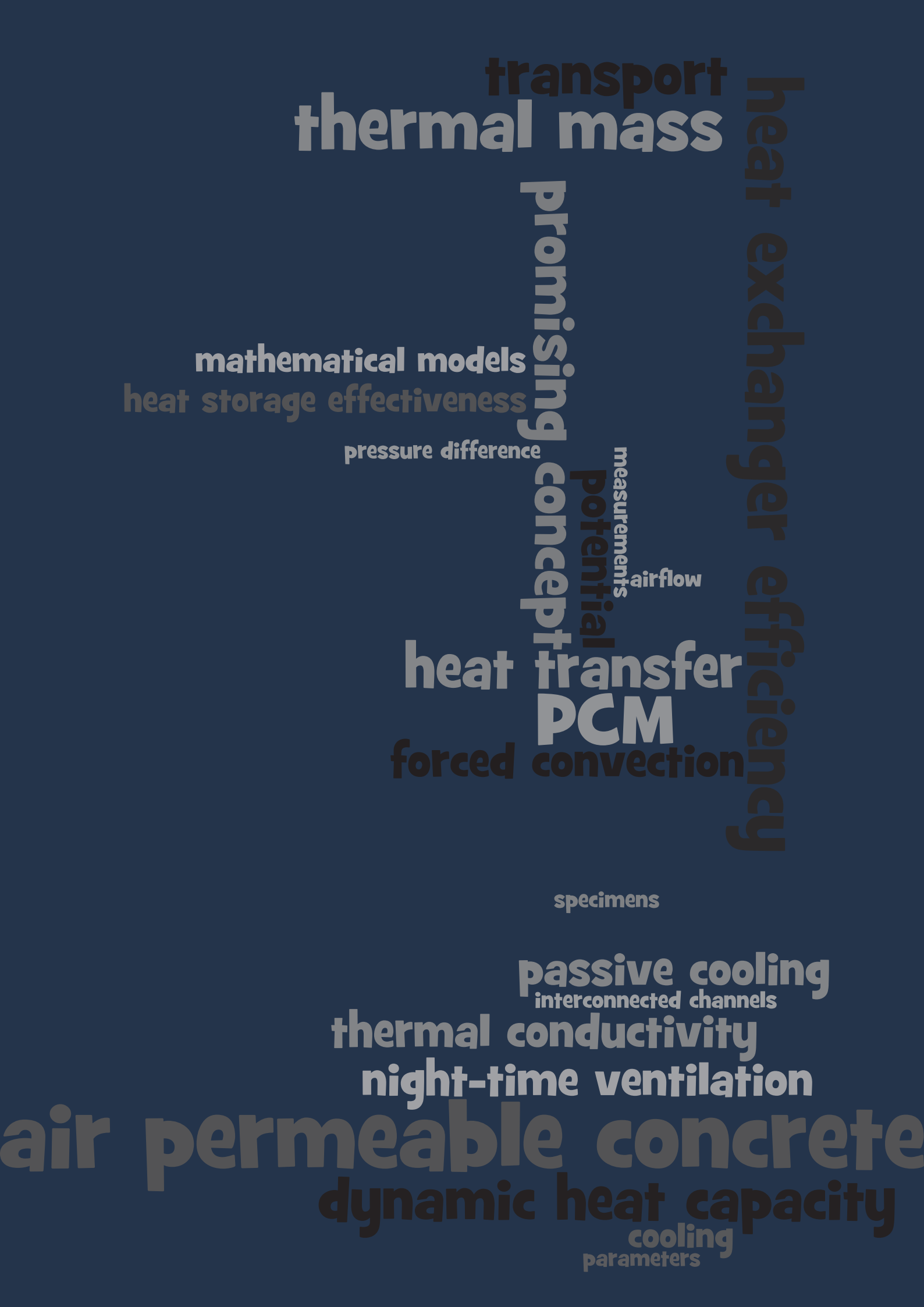
transport
thermal mass
heat exchanger efficiency
promising concept
mathematical models
heat storage effectiveness
pressure difference
measurements
potential
airflow
heat transfer
PCM
forced convection
specimens
passive cooling
interconnected channels
thermal conductivity
night-time ventilation
air permeable concrete
dynamic heat capacity
cooling
parameters